

**Sensors Journal**  
(ISSN 1424-8220; [www.mdpi.net/sensors](http://www.mdpi.net/sensors))

**Special Issue**

**Sensors for Environmental Monitoring**

**Guest Editor:**

Clifford K. Ho  
Sandia National Laboratories  
Albuquerque, NM, U.S.A  
(505) 844-2384  
[ckho@sandia.gov](mailto:ckho@sandia.gov)

## Editor-in-Chief Introduction:

Dear readers, it is a pleasure for me, to introduce Clifford K. Ho as the guest editor for this special issue. Clifford K. Ho finished his PhD at the University of California at Berkeley in 1993. His research topics cover:

- Development of microchemical sensor systems and novel characterization methods for real-time, continuous, in-situ sensing of volatile organic compounds.
- Performance of numerical simulations and analytical analyses of problems related to environmental restoration and nuclear waste management.
- Predicting of flow and transport of groundwater and contaminants in heterogeneous and fractured porous media in thermally perturbed systems.
- Validating mathematical models of heat and mass transfer processes in porous media through combined experimental and numerical studies.

At the moment, he is working at Sandia National Laboratories in Albuquerque, New Mexico, where he is a distinguished member of the technical staff. He also serves as an adjunct professor at the University of New Mexico in Albuquerque.

I am very pleased to win Clifford K. Ho over as an expert and guest editor for this special issue. Furthermore, I would like to thank him for his work and his contribution to *Sensors*.



Michael J. Schöning, Editor-in-Chief  
University of Applied Sciences Aachen, Jülich Campus, Germany  
Department of Applied Sciences and Technology,  
Biomedical Engineering Division  
and  
Research Centre Juelich GmbH  
Institute of Thin Films and Interfaces (ISG-2)  
January 28, 2005

## Preface

Monitoring air, soil, and water for hazardous contaminants has traditionally been motivated by the need to protect our environment from industrial pollutants such as volatile organic compounds, pesticides, heavy metals, and radionuclides. Typical environmental sampling methods for these contaminants employ manual grab samples that are collected on site and then transported to a laboratory for analysis. These sampling methods can be very costly and time consuming, and ongoing research has focused on the development of sensors that can replace traditional sampling methods to monitor contaminants in the environment. More recently, the threat of chemical, biological, and radiological agents introduced into our air or water supplies has also stimulated the demand for continuous, real-time, in-situ sensors.

The scope of this special issue focuses on sensors that are designed to detect hazardous substances that could potentially pollute the air, water, or subsurface. Laboratory and field investigations of new and emerging sensors are presented, and data analysis methods are also described. Eight papers from five different countries are included in this special issue that represent global research in the area of sensing for the environment. My hope is that this special issue will provide the reader with a broad overview and sampling of the innovative research that is occurring to improve our capabilities for real-time, continuous sensors for the environment.



Clifford K. Ho, Guest Editor

Sandia National Laboratories Albuquerque, New Mexico, U.S.A.

January 20, 2005

© 2005 by MDPI (<http://www.mdpi.org>). Reproduction is permitted for non-commercial purposes.

## **Overview of Sensors and Needs for Environmental Monitoring**

**Clifford K. Ho<sup>\*</sup>, Alex Robinson, David R. Miller and Mary J. Davis**

Sandia National Laboratories, P.O. Box 5800, Albuquerque, NM 87185, USA. Tel: (505) 844-2384, Fax: (505) 844-7354.

\* Author to whom correspondence should be addressed. E-mail: [ckho@sandia.gov](mailto:ckho@sandia.gov)

*Received: 31 August 2004 / Accepted: 01 December 2004 / Published: 28 February 2005*

---

**Abstract:** This paper surveys the needs associated with environmental monitoring and long-term environmental stewardship. Emerging sensor technologies are reviewed to identify compatible technologies for various environmental monitoring applications. The contaminants that are considered in this report are grouped into the following categories: (1) metals, (2) radioisotopes, (3) volatile organic compounds, and (4) biological contaminants. United States regulatory drivers are evaluated for different applications (e.g., drinking water, storm water, pretreatment, and air emissions), and sensor requirements are derived from these regulatory metrics. Sensor capabilities are then summarized according to contaminant type, and the applicability of the different sensors to various environmental monitoring applications is discussed.

**Keywords:** environmental monitoring, sensors, regulatory standards.

---

## Introduction

Environmental monitoring is required to protect the public and the environment from toxic contaminants and pathogens that can be released into a variety of media including air, soil, and water. Air pollutants include sulfur dioxide, carbon monoxide, nitrogen dioxide, and volatile organic compounds, which originate from sources such as vehicle emissions, power plants, refineries, and industrial and laboratory processes. Soil and water contaminants can be classified as microbiological (e.g., coliform), radioactive (e.g., tritium), inorganic (e.g., arsenic), synthetic organic (e.g., pesticides), and volatile organic compounds (e.g., benzene). Pesticide and herbicides are applied directly to plants and soils, and incidental releases of other contaminants can originate from spills, leaking pipes, underground storage tanks, waste dumps, and waste repositories. Some of these contaminants can persist for many years and migrate through large regions of soil until they reach water resources, where they may present an ecological or human-health threat.

The United States Environmental Protection Agency (U.S. EPA) has imposed strict regulations on the concentrations of many environmental contaminants in air and water. However, current monitoring methods are costly and time-intensive, and limitations in sampling and analytical techniques exist. For example, Looney and Falta [1] report that the Department of Energy (DOE) Savannah River Site requires manual collection of nearly 40,000 groundwater samples per year, which can cost between \$100 to \$1,000 per sample for off-site analysis. Wilson et al. [2] report that as much as 80% of the costs associated with site characterization and cleanup of a Superfund site can be attributed to laboratory analyses. In addition, the integrity of the off-site laboratory analyses can be compromised during sample collection, transport, storage, and analysis, which can span several days or more. Clearly, a need exists for accurate, inexpensive, long-term monitoring of environmental contaminants using sensors that can be operated on site or *in situ*. However, the ability to deploy and use emerging sensors for these applications is uncertain due to both cultural and technological barriers.

The purpose of this report is to assess the needs of long-term environmental monitoring applications in the U.S. and to summarize the capabilities of emerging sensor technologies (with an emphasis on Sandia-developed sensor technologies). A market survey is presented that elucidates the costs, drivers, and potential benefits of using in-situ sensors for long-term environmental monitoring. Regulatory metrics for different environmental monitoring applications are then presented to provide requirements for the sensor technologies. Emerging sensor technologies that are being developed at Sandia National Laboratories are then evaluated that can be used to monitor environmental contaminants, particularly for long-term environmental stewardship. We limit our focus to four categories of contaminants: (1) metals, (2) radioisotopes, (3) volatile organic compounds, and (4) biological contaminants. For each contaminant, we seek portable sensors that can provide rapid responses (relative to current methods and technologies), ease of operation (for field use), and sufficient detection limits.

## Market survey

In 2001, U.S. companies generated \$213 billion in environmental industry revenue, with a growth of 2.1% and exports representing 11% of this figure [3]. Overall, the environmental industry is in a state of evolution. The U.S. environmental remediation/industrial services markets have topped out

and are projected to decline. A decline in hazardous waste management funding continues with a trend that began in 1993. Returns on investment in hazardous waste remediation technologies have been low for some time and the DOE continues to be the largest funding source within the U.S. for the site remediation market.

A 15% growth in the overall environmental industry is forecasted as the combination of two major groups. The first group is comprised of energy and water that is projected to experience growth ranging from 19% to over 250% during the first decade of the 21<sup>st</sup> century [3]. The second group consists of compliance, remediation and waste management that are projected to decline 13% to 49% during the same timeframe. The first group is driven by economics and basic human needs while the second group is driven by regulations and enforcement.

The two best performing environmental industry segments are also the best performers over the past decade: clean energy systems/power (+16%) and process/pollution prevention technology (+9%). Clean energy systems/power (\$10.0 b) accounted for 65% of the overall market growth in dollars. Process and pollution prevention technology have annual revenues of \$1.3 billion. Continued growth of clean energy/power and process/pollution prevention technologies are projected.

Instrument technology is a \$3.8 billion dollar industry and has experienced an annual growth rate of approximately 4%. The U.S. water industry – made up of water utilities (\$30.9 b), wastewater treatment works (\$28.8 b), and water equipment/chemicals (\$20.3 b) accounts for 38% of the environmental industry revenues. Solid waste management (\$40.8 b), air pollution control equipment (\$18.3 b) and consulting/engineering (\$18.0 b) are also major contributors to the environmental industry revenue stream.

In the present DOE Environmental Management (EM) market, technology investments are not occurring on a scale that is likely to make major cost and schedule differences. EM is focusing its resources on actual clean-ups and site closures and not on technology innovations. Low interest in technologies increases the difficulty in finding willing investors. Investors are likely to be wary of any growth potential in a market that has an environmental connotation. However, technologies that have a specific need that saves money can be successful. Technological improvements in excavation, transportation, disposal, analytical services, robotics, sample preparation, field sampling, and monitoring are examples of areas where technological improvements could be successful [4].

Data Quality Objectives (DQOs) must be considered as part of technology development and a focus should be made on the most urgent problems, such as situations where contaminants are in contact with groundwater. Regulator involvement in new technology development and acceptance of technologies is also very important [4].

Science and technology needs include methods of detection, analysis, remote sensing, and data transmission. A technology-needs analysis determined that the most important needs for analytical capabilities were the use of fieldable instrumentation for organic compounds in water/soil/air and for Resource Conservation and Recovery Act (RCRA) metals in water/soil [4]. It was further noted that a leap in technology would occur when the performance of the field instruments more closely approaches that of laboratory-based instruments. A potential application in long-term monitoring and stewardship is in the area of performance monitoring of water to address current technical uncertainties [5]. Additionally, information is needed to determine if ambient conditions change significantly enough over the long term to diminish the effectiveness of the remedy.

Based on information gathered in equipment user surveys, an analysis of the market for environmental field instrumentation determined that field instrumentation has been expanding due to cost savings from on-site analysis and improved regulatory and customer acceptance of on-site methods [6]. The environmental field instrument market is expected to enjoy an average growth of 7% annually for the foreseeable future. The market will expand with technology developments and increasing regulatory acceptance. However, given the current regulatory environment, field instruments may never completely replace laboratory analysis, and therefore never realize its maximum market potential.

Remediation opportunities will wane and be replaced with smaller, longer-term opportunities related to post-closure monitoring and long-term stewardship. This should open doors to new instruments and measurement technologies and remote information management systems. The market consists of many niche applications, which are met by a number of different technologies. The long-term nature of post-closure monitoring and surveillance will be required at a wide variety of nuclear sites, uranium mill tailing sites, low-level and mixed-waste burial grounds, and hazardous waste sites that may create new areas for application. This market overlaps with other markets, such as for chemical industry process monitoring. Technology developments that can crosscut multiple areas within the environmental industry have a greater potential for success within the industry.

Long-term stewardship is not unique to the DOE. The EPA is currently determining its stewardship responsibilities through its Federal Facilities Restoration and Reuse Office. Both EPA Region IV and X have released policy documents on the use of institutional controls at Federal facilities. However, the specific ways in which long-term institutional control issues are implemented vary considerably at state and local offices. The Department of Defense (DoD) conducts cleanup activities at more than 10,000 sites, nearly 2,000 military installations and more than 9,000 formerly used defense properties. The Department of Interior (DoI) is responsible for overseeing approximately 13,000 former mining sites, some of which have been abandoned by the original owners. The nation's commitment is also not limited to federal properties. For example, sanitary and hazardous landfills, industrial facilities, and former waste management operations likely require long-term monitoring that will be funded by state and local governments.

The DOE conducts its stewardship activities in compliance with applicable laws, regulations, and inter-agency agreements. In general the DOE is required to implement some land-use controls at waste disposal facilities in perpetuity. Groundwater-monitoring timeframes are expected to be 30 years or greater. Costs of post-cleanup stewardship activities are currently unknown. However, a DOE Office of Inspector General audit found that the "DOE groundwater monitoring activities were not being conducted economically as they could have been since some sites had not adopted innovative technologies and approaches to well installations, sampling operations, and laboratory analysis." The report concluded that in part this occurred because innovative groundwater monitoring techniques were either unavailable or had not been effectively disseminated, evaluated for applicability at other sites and implemented" [7]. In summary, the development of sensors for long-term groundwater monitoring may fill a niche that could have a wide-ranging application for long-term environmental monitoring.

## Regulatory requirements, standards and policies

### Drinking water

National Primary Drinking Water Regulations apply to public water systems and are legally enforceable standards. These primary standards are intended to protect public health by limiting the levels of contaminants that can be found in drinking water. Although these standards are applicable to public water systems (i.e., at the tap), they are often applied by remediation regulators in the aquifer (i.e., at the monitoring wellhead). The following tables (Tab. 1 to Tab. 6) summarize the drinking water standards imposed by the U.S. Environmental Protection Agency (EPA). Additional information regarding potential health impacts and sources of contamination can also be found at their web site (<http://www.epa.gov/safewater/mcl.html>).

**Table 1.** EPA national primary drinking water standards for microorganisms.

Contaminant	Maximum Contaminant Level Goal (mg/L)	Maximum Contaminant Level (mg/L)
<i>Cryptosporidium</i>	zero	See footnote*
<i>Giardia lamblia</i>	zero	See footnote*
Heterotrophic plate count	n/a	See footnote*
<i>Legionella</i>	zero	See footnote*
Total Coliforms (including fecal coliform and <i>E. Coli</i> )	zero	5.0%**
Turbidity	n/a	See footnote*
Viruses (enteric)	zero	See footnote*

\*EPA's surface water treatment rules require systems using surface water or ground water under the direct influence of surface water to (1) disinfect their water, and (2) filter their water or meet criteria for avoiding filtration so that the following contaminants are controlled at the following levels:

- *Cryptosporidium* (as of 1/1/02 for systems serving >10,000 and 1/14/05 for systems serving <10,000) 99% removal.
- *Giardia lamblia*: 99.9% removal/inactivation.
- Viruses: 99.99% removal/inactivation.
- *Legionella*: No limit, but EPA believes that if *Giardia* and viruses are removed/inactivated, *Legionella* will also be controlled.
- Turbidity: At no time can turbidity (cloudiness of water) go above 5 nephelometric turbidity units (NTU); systems that filter must ensure that the turbidity go no higher than 1 NTU (0.5 NTU for conventional or direct filtration) in at least 95% of the daily samples in any month. As of January 1, 2002, turbidity may never exceed 1 NTU, and must not exceed 0.3 NTU in 95% of daily samples in any month.
- HPC: No more than 500 bacterial colonies per milliliter.
- Long Term Enhanced Surface Water Treatment (Effective Date: January 14, 2005): Surface water systems or (GWUDI) systems serving fewer than 10,000 people must comply with the applicable Long Term 1 Enhanced Surface Water Treatment Rule provisions (e.g., turbidity standards, individual filter monitoring, *Cryptosporidium* removal requirements, updated watershed control requirements for unfiltered systems).
- Filter Backwash Recycling: The Filter Backwash Recycling Rule requires systems that recycle to return specific recycle flows through all processes of the system's existing conventional or direct filtration system or at an alternate location approved by the state.
- \*\*More than 5.0% samples total coliform-positive in a month. (For water systems that collect fewer than 40 routine samples per month, no more than one sample can be total coliform-positive per month.) Every sample that has total coliform must be analyzed for either fecal coliforms or *E. coli* if two consecutive TC-positive samples, and one is also positive for *E. coli* fecal coliforms, system has an acute MCL violation.

**Table 2.** EPA national primary drinking water standards for disinfectants.

Contaminant	Maximum Contaminant Level Goal (mg/L)	Maximum Contaminant Level (mg/L)
Chloramines (as Cl <sub>2</sub> )	MRDLG=4*	MRDL=4.0**
Chlorine (as Cl <sub>2</sub> )	MRDLG=4*	MRDL=4.0**
Chlorine dioxide (as ClO <sub>2</sub> )	MRDLG=0.8*	MRDL=0.8**

\*Maximum Residual Disinfectant Level Goal (MRDLG) - The level of a drinking water disinfectant below which there is no known or expected risk to health. MRDLGs do not reflect the benefits of the use of disinfectants to control microbial contaminants.

\*\*Maximum Residual Disinfectant Level (MRDL) - The highest level of a disinfectant allowed in drinking water. There is convincing evidence that addition of a disinfectant is necessary for control of microbial contaminants.

**Table 3.** EPA national primary drinking water standards for disinfection byproducts.

Contaminant	Maximum Contaminant Level Goal (mg/L)	Maximum Contaminant Level (mg/L)
Chlorite	0.8	1.0
Haloacetic acids (HAA5)	n/a*	0.060
Total Trihalomethanes (TTHMs)	n/a*	.08

\*Although there is no collective MCLG for this contaminant group, there are individual MCLGs for some of the individual contaminants:

- Trihalomethanes: bromodichloromethane (zero); bromoform (zero); dibromochloromethane (0.06 mg/L). Chloroform is regulated with this group but has no MCLG.
- Haloacetic acids: dichloroacetic acid (zero); trichloroacetic acid (0.3 mg/L). Monochloroacetic acid, bromoacetic acid, and dibromoacetic acid are regulated with this group but have no MCLGs.

**Table 4.** EPA national primary drinking water standards for inorganic chemicals.

Contaminant	Max. Contaminant Level Goal (mg/L)	Max. Contaminant Level (mg/L)
Antimony	0.006	0.006
Arsenic	0*	0.010 (as of 01/23/06)
Asbestos (fiber >10 micrometers)	7 million fibers per liter	7 million fibers per liter
Barium	2	2
Beryllium	0.004	0.004
Cadmium	0.005	0.005
Chromium (total)	0.1	0.1
Copper	1.3	Action Level=1.3**
Cyanide (as free cyanide)	0.2	0.2
Fluoride	4.0	4.0
Lead	zero	Action Level=1.3**
Mercury (inorganic)	0.002	0.002
Nitrate (measured as Nitrogen)	10	10
Nitrite (measured as Nitrogen)	1	1
Selenium	0.05	0.05
Thallium	0.0005	0.002

\*MCLGs were not established before the 1986 Amendments to the Safe Drinking Water Act. Therefore, there is no MCLG for this contaminant.

\*\*Lead and copper are regulated by a Treatment Technique that requires systems to control the corrosiveness of their water. If more than 10% of tap water samples exceed the action level, water systems must take additional steps. For copper, the action level is 1.3 mg/L, and for lead is 0.015 mg/L.

**Table 5.** EPA national primary drinking water standards for organic chemicals.

Contaminant	Max. Contaminant Level Goal (mg/L)	Max. Contaminant Level (mg/L)
Acrylamide	zero	Treatment Technology*
Alachlor	zero	0.002
Atrazine	0.003	0.003
Benzene	zero	0.005
Benzo(a)pyrene (PAHs)	zero	0.0002
Carbofuran	0.04	0.04
Carbon tetrachloride	zero	0.005
Chlordane	zero	0.002
Chlorobenzene	0.1	0.1
2,4-D	0.07	0.07
Dalapon	0.2	0.2
1,2-Dibromo-3-chloropropane (DBCP)	zero	0.0002
o-Dichlorobenzene	0.6	0.6
p-Dichlorobenzene	0.075	0.075
1,2-Dichloroethane	zero	0.005
1,1-Dichloroethylene	0.007	0.007
cis-1,2-Dichloroethylene	0.07	0.07
trans-1,2-Dichloroethylene	0.1	0.1
Dichloromethane	zero	0.005
1,2-Dichloropropane	zero	0.005
Di(2-ethylhexyl) adipate	0.4	0.4
Di(2-ethylhexyl) phthalate	zero	0.006
Dinoseb	0.007	0.007
Dioxin (2,3,7,8-TCDD)	zero	0.00000003
Diquat	0.02	0.02
Endothall	0.1	0.1
Endrin	0.002	0.002
Epichlorohydrin	zero	Treatment Technology*
Ethylbenzene	0.7	0.7
Ethylene dibromide	zero	0.00005
Glyphosate	0.7	0.7
Heptachlor	zero	0.0004
Heptachlor epoxide	zero	0.0002
Hexachlorobenzene	zero	0.001
Hexachlorocyclopentadiene	0.05	0.05
Lindane	0.0002	0.0002
Methoxychlor	0.04	0.04
Oxamyl (Vydate)	0.2	0.2
Polychlorinated biphenyls (PCBs)	zero	0.0005
Pentachlorophenol	zero	0.001
Picloram	0.5	0.5
Simazine	0.004	0.004
Styrene	0.1	0.1

Contaminant	Max. Contaminant Level Goal (mg/L)	Max. Contaminant Level (mg/L)
Tetrachloroethylene	zero	0.005
Toluene	1	1
Toxaphene	zero	0.003
2,4,5-TP (Silvex)	0.05	0.05
1,2,4-Trichlorobenzene	0.07	0.07
1,1,1-Trichloroethane	0.20	0.2
1,1,2-Trichloroethane	0.003	0.005
Trichloroethylene	zero	0.005
Vinyl chloride	zero	0.002
Xylenes (total)	10	10

\*Each water system must certify, in writing, to the state (using third-party or manufacturer's certification) that when acrylamide and epichlorohydrin are used in drinking water systems, the combination (or product) of dose and monomer level does not exceed the levels specified, as follows:

- Acrylamide = 0.05% dosed at 1 mg/L (or equivalent).
- Epichlorohydrin = 0.01% dosed at 20 mg/L (or equivalent).

**Table 6.** EPA national primary drinking water standards for radionuclides.

Contaminant	Max. Contaminant Level Goal	Max. Contaminant Level
Alpha particles	zero	15 picocuries per Liter (pCi/L)
Beta particles and photon emitters	zero	4 millirems per year
Radium 226 and Radium 228 (combined)	zero	5 pCi/L
Tritium	zero	20,000 pCi/L
Uranium	zero	30 ug/L (as of 12/08/03)

### *Storm water monitoring*

Under the National Pollutant Discharge Elimination System (NPDES) regulations, all facilities which discharge pollutants from any point source into waters of the United States (US) are required to obtain a permit. The NPDES storm water regulations cover the following classes of storm water dischargers: operators of municipal separate storm sewer systems (MS4s); industrial facilities in any of eleven identified categories that discharge to an MS4 or to a water of the US; and operators of certain construction activities. Storm water regulations are implemented by the EPA or authorized states.

NPDES permits may be issued as individual or general permits. In either case, NPDES permits generally require the development of a storm water pollution prevention plan, implementation of best management practices, and monitoring and reporting of storm water discharge data. Most industrial facilities elect coverage under a general permit because the permitting process is designed to be more efficient.

EPA has developed a multi-sector general permit (MSGP) for storm water dischargers, providing both general requirements and sector-specific requirements. The specific requirements apply to each of 30 industrial sectors and their associated subsectors. The current MSGP was published in the Federal Register on October 30, 2000 [8]. Authorized states may use alternative permits and/or may impose additional requirements.

Three types of monitoring may be required under the MSGP: visual examination, analytical monitoring, and compliance monitoring. Visual examinations are intended to provide a simple, inexpensive evaluation of storm water quality. Analytical monitoring is required for only specified

subsectors, those which EPA has determined have a high potential to discharge a pollutant at concentrations of concern. For each of the identified subsectors, EPA has defined the parameters to be monitored and has established benchmark concentrations for each parameter. Analytical monitoring is required on a quarterly basis in year two of the permit; if these results exceed a benchmark value, a second round of analytical monitoring is required in year. Any time a benchmark concentration is exceeded, the facility must review their storm water pollution prevention plan to reduce pollutant loads.

Compliance monitoring is performed on an annual basis for certain storm water discharges subject to effluent guidelines. Some EPA regions require quarterly monitoring. The applicability of compliance monitoring is limited to the following discharges: landfill discharges; coal pile runoff; contaminated runoff from phosphate fertilizer manufacturing facilities; runoff from asphalt paving and roofing emulsion production areas; material storage pile runoff from cement manufacturing facilities; and mine dewatering discharges from crushed stone, construction sand and gravel, and industrial sand mines.

The MSGP analytical and compliance monitoring requirements are limited to discrete sampling events at specified intervals. Grab sampling is required. Authorized states may impose more extensive monitoring requirements.

#### *National pretreatment program monitoring*

Under the NPDES permitting program, EPA established the National Pretreatment Program to address “indirect discharges” into waters of the United States. Indirect discharges are discharges from industrial facilities to publicly owned treatment works (POTWs). The National Pretreatment Program requires dischargers to treat or control pollutants in their wastewater prior to discharge to the POTW. (The POTW is required to obtain an NPDES permit as a direct discharger.)

Under the General Pretreatment Regulations [9], all large POTWs, and some smaller POTWs with significant industrial discharges, must establish local pretreatment programs. The local pretreatment programs impose national pretreatment standards and requirements, as well as any more stringent local requirements.

EPA has established two general requirements for industrial dischargers prohibiting “interference” and “pass through.” These requirements are designed to prevent damage to the treatment works and environmental harm downstream. In addition, EPA controls the discharge of 126 “priority pollutants,” including metals and toxic organics.

Categorical pretreatment standards limit the discharge of specific pollutants; they are national standards for indirect dischargers in specific industrial categories. These standards are further categorized into pretreatment standards for existing sources (PSES) and pretreatment standards for new sources (PSNS). Currently, 32 industrial categories are subject to pretreatment standards. The standards may be expressed as concentration-based or mass-based, or both, depending upon the operational characteristics of the industry. Significant industrial users (SIUs) are required to monitor, at a minimum, on a semi-annual basis. Confirmatory sampling by the regulatory authority is required annually. Depending upon factors such as effluent variability, effluent impacts, and compliance history, the SIU may be required to sample more frequently.

**Table 7.** Pretreatment standards for manufacturers of organic chemicals, plastics, and synthetic fibers [10].**Environmental Protection Agency**

Effluent characteristics	BAT effluent limitations and NSPS <sup>1</sup>	
	Maximum for any one day	Maximum for monthly average
Anthracene .....	47	19
Benzene .....	134	57
Benzo(a)anthracene .....	47	19
3,4-Benzofluoranthene .....	48	20
Benzo(k)fluoranthene .....	47	19
Benzo(a)pyrene .....	48	20
Bis(2-ethylhexyl) phthalate .....	258	95
Carbon Tetrachloride .....	380	142
Chlorobenzene .....	380	142
Chloroethane .....	295	110
Chloroform .....	325	111
Chrysene .....	47	19
Di-n-butyl phthalate .....	43	20
1,2-Dichlorobenzene .....	794	196
1,3-Dichlorobenzene .....	380	142
1,4-Dichlorobenzene .....	380	142
1,1-Dichloroethane .....	59	22
1,2-Dichloroethane .....	574	180
1,1-Dichloroethylene .....	60	22
1,2-trans-Dichloroethylene .....	66	25
1,2-Dichloropropane .....	794	196
1,3-Dichloropropylene .....	794	196
Diethyl phthalate .....	113	46
2,4-Dimethylphenol .....	47	19
Dimethyl phthalate .....	47	19
4,6-Dinitro-o-cresol .....	277	78
2,4-Dinitrophenol .....	4,291	1,207
Ethylbenzene .....	380	142
Fluoranthene .....	54	22
Fluorene .....	47	19
Hexachlorobenzene .....	794	196
Hexachlorobutadiene .....	380	142
Hexachloroethane .....	794	196
Methyl Chloride .....	295	110
Methylene Chloride .....	170	36
Naphthalene .....	47	19
Nitrobenzene .....	6,402	2,237
2-Nitrophenol .....	231	65
4-Nitrophenol .....	576	162
Phenanthrene .....	47	19
Phenol .....	47	19
Pyrene .....	48	20
Tetrachloroethylene .....	164	52
Toluene .....	74	28
Total Chromium .....	2,770	1,110
Total Copper .....	3,380	1,450
Total Cyanide .....	1,200	420
Total Lead .....	690	320
Total Nickel .....	3,680	1,690
Total Zinc <sup>2</sup> .....	2,610	1,050
1,2,4-Trichlorobenzene .....	794	196
1,1,1-Trichloroethane .....	59	22
1,1,2-Trichloroethane .....	127	32
Trichloroethylene .....	69	26
Vinyl Chloride .....	172	97

<sup>1</sup> All units are micrograms per liter.

<sup>2</sup> Total Zinc for Rayon Fiber Manufacture that uses the viscose process and Acrylic Fibers Manufacture that uses the zinc chloride/solvent process is 6,796 µg/l and 3,325 µg/l for maximum for any one day and maximum for monthly average, respectively.

The type of industry regulated under the pretreatment program is wide-ranging, including grain mills, feedlots, electroplating facilities, iron and steel manufacturers, and fertilizer manufacturers. For many industries, the monitoring required is limited to several effluent characteristics, such as biological effluent demand, total suspended solids, and pH. For other industries monitoring of a select set of priority pollutants, such as a specified subset of metals, is required. In a few instances, monitoring of all priority pollutants is required. Pretreatment standards for indirect discharges from manufacturers of organic chemicals, plastics, and synthetic fibers are provided in Table 7.

*Ambient air quality*

A number of substances are identified as hazardous air pollutants (now termed “toxic air pollutants” by EPA) under the Clean Air Act and are regulated under the National Emission Standards for Hazardous Air Pollutants program. The American Conference of Governmental Industrial Hygienists (ACGIH) established airborne concentration limits called Threshold Limit Values (TLV) of various hazardous air pollutants. The TLVs are believed to represent conditions under which nearly all workers could be exposed day after day without adverse health effects. The TLVs are based on information from industrial experience and experimental studies on humans and animals. Table 8 lists a few hazardous air pollutants (HAP) and the associated ACGIH TLVs. Additional information on these compounds can be found from the following web sites:

- [www.epa.gov/ttn/atw/hlthef/benzene.html](http://www.epa.gov/ttn/atw/hlthef/benzene.html)
- [www.epa.gov/ttn/atw/hlthef/xylenes.html](http://www.epa.gov/ttn/atw/hlthef/xylenes.html)
- [www.epa.gov/ttn/atw/hlthef/tri-ethy.html](http://www.epa.gov/ttn/atw/hlthef/tri-ethy.html)

**Table 8.** Threshold Limit Values for several hazardous air pollutants [11].

Hazardous Air Pollutant	Threshold Limit Value (ppm)	
	8-Hour Time Weighted Average	15-Minute Short-Term Exposure Limit
Benzene	0.5	2.5
Xylenes	100	150
Trichloroethylene	50	100

In 1998, the City of Albuquerque adopted a policy for regulating emissions from industries. An analysis for each relevant HAP at a site is performed to determine if the emissions from the stack result in an exceedance of the ACGIH TLV for any of the relevant substances. If the ACGIH TLV at the stack is exceeded, the concentration of that substance must be analyzed at the “fence line” (i.e., property boundary). The concentration at the fence line should not exceed 1/100<sup>th</sup> the ACGIH TLV. For any HAP that has uncontrolled emissions which result in an exceedance of the ACGIH TLV at the stack and 1/100<sup>th</sup> of the ACGIH TLV at the fence line, air-pollution controls will be required to reduce the concentrations to 1/100<sup>th</sup> the TLV at the fence line. An air quality permit will also be required to ensure proper operation of the control equipment.

Additional air quality standards have been compiled from 20.11.1 NMAC - Title 20, Environmental Protection - Chapter 11, Albuquerque/Bernalillo county Air Quality Control Board - Part 1 General Provisions (see Table 9).

**Table 9.** Enforceable standards for various air pollutants.

Pollutant	Goals	Enforceable Standards		
	Albuquerque	New Mexico State	Federal Primary	Federal Secondary
<b>Carbon Monoxide (CO)</b>				
8-hour average	---	8.7 ppm	9.0 ppm	9.0 ppm
1-hour average	13 ppm	13.1 ppm	35 ppm	35 ppm
<b>Nitrogen Dioxide (NO<sub>2</sub>)</b>				
24-hour average	.062 ppm	10 ppm	---	---
Annual arithmetic mean	.053 ppm	.05 ppm	.053ppm	.053 ppm
<b>Ozone (O<sub>3</sub>)</b>				
1-hour average	.120 ppm	---	.120 ppm	.120 ppm
<b>Sulfur Dioxide (SO<sub>2</sub>)</b>				
24-hour average	.10 ppm	.10 ppm	---	.140 ppm
3-hour average	---	---	---	.5 ppm
Annual arithmetic mean	.004 ppm	.02 ppm	.03 ppm	---
<b>Particulate Matter (PM<sub>10</sub>)</b>				
24-hour average	150 µg/m <sup>3</sup>	---	150 µg/m <sup>3</sup>	---
Annual arithmetic mean	---	---	---	50 µg/m <sup>3</sup>
<b>Lead (Pb)</b>				
Quarterly arithmetic mean	1.5 µg/m <sup>3</sup>	---	1.5 µg/m <sup>3</sup>	1.5 µg/m <sup>3</sup>
<b>Hydrogen Sulfide</b>				
1-hour average	.003 ppm	.010 ppm	---	---
<b>Total Reduced Sulfur</b>				
½ hour average	---	.003 ppm	---	---
1-hour average	.003 ppm	---	---	---
<b>Particulate Matter (TSP)</b>				
24-hour average	150 µg/m <sup>3</sup>	150 µg/m <sup>3</sup>	---	---
7-day average	---	110 µg/m <sup>3</sup>	---	---
30-day average	---	90 µg/m <sup>3</sup>	---	---
Annual geometric mean	60 µg/m <sup>3</sup>	60 µg/m <sup>3</sup>	---	---

### Sensor technologies for environmental monitoring

The purpose of this section is to identify and describe sensor technologies (with an emphasis on Sandia-developed technologies) that may be applicable to monitoring various contaminants described in the previous sections. The technologies are organized according to analyte, which include trace metals, radioisotopes, volatile organic compounds, and biological pathogens. The sensor technologies are described briefly, and then tables summarizing features and specifications (e.g., sensitivity, size, speed, etc.) of each sensor technology are presented in Table 10 through Table 13 in the section "Summary and specifications of sensor technologies".

### Trace metal sensors

#### -Nanoelectrode array

Nanoelectrode arrays have been fabricated to identify and quantify dissolved metals [12-13]. Signals from the electrodes are obtained by monitoring current and voltage during application of an electrical potential. Approximately 1 million individual electrodes can be placed on a 1 square inch substrate using electron-beam lithography or chemical vapor deposition. The sensing electrodes are integrated with the reference electrode, eliminating the need for buffers and permitting non-contaminating sensing in ultra-pure water. The small electrode size coupled with a very high density produces a signal with up to  $10^3$  times better signal-to-noise ratio than standard electrodes. Using multiple electrodes, coatings, and electrochemical techniques, target analytes can include toxic industrial chemicals and metals, such as trichloroethylene, methyl-t-butyl ether, arsenic, lead, and chromium.

#### -Laser-induced breakdown spectroscopy (LIBS)

As its name implies, LIBS uses a laser to rapidly heat a very small area (usually solid or liquid), generating a plasma from the atomic constituents present at the focal point. Radiative relaxation of the plasma is then observed using sensitive spectroscopic instrumentation (see Figure 1). LIBS is also known as Laser Spark Spectroscopy (LASS).

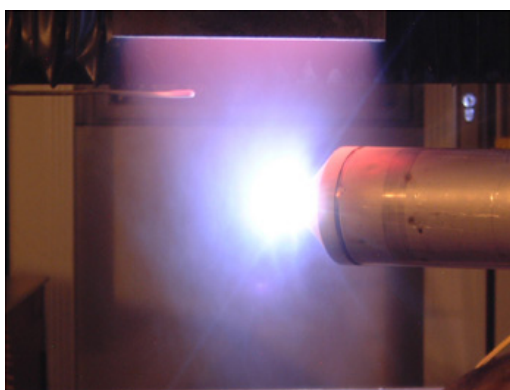


**Figure 1.** Stand-off LIBS probe head. Laser ablation energy and spectroscopic collection occurs through fiber optics.

LIBS can be used for rapid analysis of hazardous metals and other inorganic contaminants in water, soil, and mixed waste sites [14-15]. It can be used to detect almost all elements, though certain metals exhibit orders of magnitude greater emission. Detection limits are a function of each specific metal, and the spectroscopic and detector hardware. Low ppb levels are typical. Contaminants targeted in Sandia projects include As, Be, Hg, Se, Pb, Cd, Cu, Zn, Ag, Cr, Fe, and Mn. Recently, a LIBS system was set up for measuring metal emissions in the waste streams of a thermal treatment facility [16]. Currently, a field deployable LIBS system is configured at Sandia-Livermore employing an image intensified CCD array, which provides sufficient signal intensity for single laser pulse LIBS. Delivery of the laser light to remote location via a fiber-optic cable has been performed. Spectral emission

likewise can be readily be transported over hundreds of feet for analysis [15]. LIBS can be extended to biodetection by looking for rapid, temporal increases in the presence and/or ratios of Ca, Na, K.

#### -Miniature chemical flow probe sensor

The miniature chemical flow-probe sensor can detect metals, especially copper. See “Miniature chemical flow probe sensor” below for details (page 19).

#### Radioisotope sensors

##### RadFET (Radiation field-effect transistor)

The RadFET concept for measuring gamma radiation dose has been around for many years. It is based on ionizing radiation permanently promoting high mobility electrons into low mobility holes. This creates an irreversible shift in the FET’s threshold voltage. Sandia has microfabricated miniature RadFETs [17]. Sensitivities depend in part upon fabrication structure, and range from 0.01 to 5 mV per rad. An energy spectrometer can be made by fabricating filters of varying threshold energies on RadFET arrays (Figure 2). With consideration of threshold barriers, RadFETs are universal ionizing radiation detectors. The sensitivity of RadFETs increases with application of increasing bias voltage. However Sandia has fabricated designs that are moderately sensitive with no voltage source.

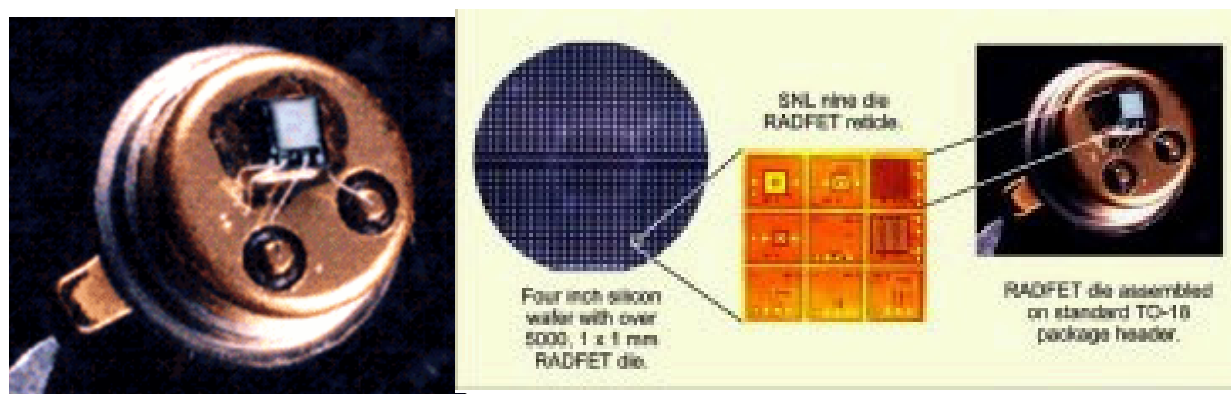


**Figure 2.** The 1 mm<sup>2</sup> RadFET element fits on a standard TO-18 package header. Over 5000 RadFETs can be microfabricated on a single 4 inch wafer.

#### Cadmium zinc telluride (CZT) detectors

CZTs are semiconductor gamma and neutron radiation detectors, producing current flow under the influence of a gate voltage, upon exposure to high energy radiation. They can be fabricated in arrays to perform imaging or spectroscopy [18] (see Figure 3). While these are promising and sensitive sensors, their performance, and thus calibration, degrades with cumulative exposure. Long term performance is hard to track, as damage may be progressive with radiation energy levels [19]. Sandia performed experiments to improve the fabrication process for industry (see also Figure 3). Commercial sensors and spectrometers are available from EV Products or AmpTek.

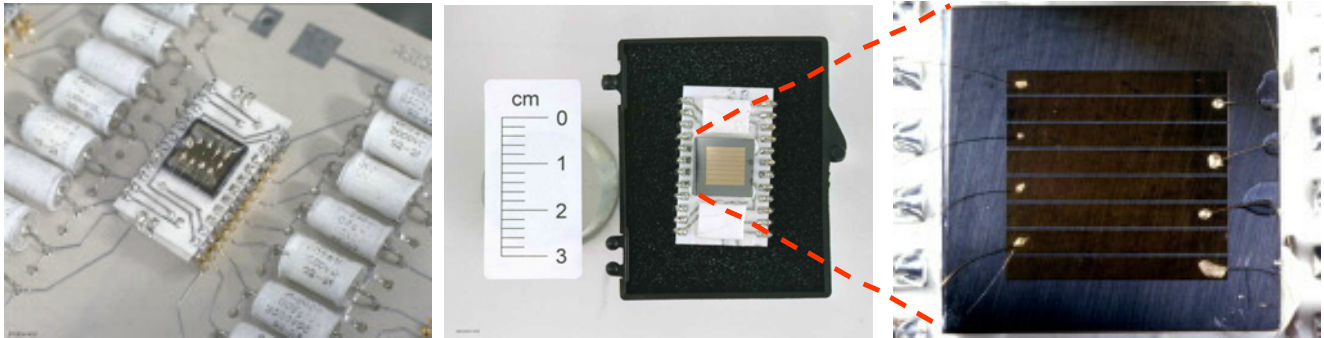


**Figure 3.** The 1 cm<sup>2</sup> CZT array sits on a dip package on a circuit board for a handheld gamma radiation spectrometer.

#### -Low-energy pin diodes beta spectrometer

A handheld low-energy beta spectrometer was assembled at Sandia for detecting tritium contamination using commercially available pin photodiodes from Hamamatsu [20]. The system works by measuring current pulses generated in the diode when beta particles strike. Electronic circuits convert each signal to a voltage pulse whose amplitude is proportional to the energy of the particle.

#### -Thermoluminescent dosimeter (TLD)

A thermoluminescent dosimeter is a crystal that absorbs energy from radiological exposure, semi-permanently promoting electrons into semiconductor holes. Upon heating the crystal, the trapped energy is released in the form of light. A TLD reader uses a photodetector to convert the signal into a radiation dose reading. Commonly used crystals are calcium fluoride-manganese and lithium fluoride. Sandia has fabricated TLDs with crystals implanted in Teflon to improve sensitivity [21-22]. Thin crystals can be used to measure low energy radiation, while thick crystals measure total exposure. Filters and different crystal types can also be used for energy discrimination.

#### -Isotope identification gamma detector

An isotope identification gamma detector was developed in conjunction with the Defense Threat Reduction Agency, Northrup Grumman, Applied Research Associates, and DOE/NNSA laboratories. This was designed as a portal instrument to find and identify unconventionally transported nuclear weapons and radiological dispersal devices.

#### -Neutron generator for nuclear material detection

A small neutron generator is being developed for use in probing for the presence of nearby nuclear materials [23]. The meter-tall instrument interrogates nuclear material by "pinging" it with neutrons to incite the release of secondary particles. These particles, which are indicative of their atomic source, are then detected. The smaller prototype will be tested soon.

#### -Non-sandia radiation detectors

Commonly used gamma radiation detectors include high purity germanium (require liquid nitrogen), and scintillation crystals such as thallium-doped sodium iodide (low energy resolution).

Geiger counters were one of the first radiation detectors available, and the first to provide quantitative measurements of radiation. They use very simple electronics and cover a wide radiation range, but they are bulky compared to some of the sensors described above.

Commercial options: Radiation Experiments and Monitors (REM) makes a commercial radiation FET sensor with a sensitivity of  $-10$  mV/rad when biased to  $+20$ V. TLDs can be purchased from Teledyne Isotopes. CZT detectors can be purchased from Mitsubishi Electric and Communication Electronics, Inc. (Ann Arbor, MI). Geiger counters can be purchased from Mineralab (Prescott, AZ).

#### *Volatile organic compound sensors*

##### -Evanescent fiber-optic chemical sensor

An evanescent wave is the energy that penetrates a dielectric interface when electromagnetic radiation undergoes total internal reflection. This wave can interact with matter within the penetration depth. By using specialized coatings as the fiber-optic cladding, chemical species can be preferentially concentrated from a matrix into the evanescent interaction zone. Polymer optical wave guides have been used for sensing organic compounds in aqueous solutions at low ppm levels [24]. pH measurements can be made using sol-gel coatings. For sensing applications, near infrared (NIR) spectroscopy is used for quantitative measurements. With excellent light transmission in this region, sensing can be performed over great distances. However, the spectroscopic signal from mixtures must be deconvolved using multivariate analysis.

##### -Grating light reflection spectroelectrochemistry

Grating light reflection spectroscopy (GLRS) is a technique for spectroscopic analysis and sensing. A transmission diffraction grating is placed in contact with a liquid sample to be analyzed, and an incident light beam is directed onto the grating. At certain angles of incidence, some of the diffracted orders are transformed from traveling waves to evanescent waves. This occurs at a specific wavelength that is a function of the grating period and the complex index of refraction of the sample. The intensity of a diffracted order is also dependent upon the sample's complex index of refraction. The real part of the theoretical equations correspond to the speed of light in the material, and the imaginary part corresponds to light absorption. This technique was used at Sandia in combination with electrochemical modulation of a gold-coated metallic spectroscopic grating for the detection of trace amounts of aromatic hydrocarbons [25]. The grating was configured as the working electrode in an electrochemical cell containing water plus trace amounts of TNT and a dye. Cyclic electrochemical modulation produced lower limits of detection, 50 parts per million and 50 parts per billion, respectively.

##### -Miniature chemical flow probe sensor

This down-hole probe is designed to measure organic analytes diffusing through a semi-permeable membrane [15]. The analytes react with a reagent, forming spectrally distinct products. Absorption bands from a flash lamp are then observed with a spectrometer system, using fiber-optics to carry the light in both directions. Target analytes can be volatile organic compounds in air or water (particularly chlorinated halocarbons), or dissolved metals (copper gives particularly strong response).

#### -SAW chemical sensor arrays

An acoustic sensor is typically used by measuring a decrease in its active resonant frequency that is related to trace mass loading on the active surface (Figure 4). Polymers, sol-gels, and high surface area coatings are often applied to enhance mass absorption/adsorption, and to provide a degree of chemical class selectivity. Acoustic sensors used at Sandia include flexural plate wave (FPW) sensors, quartz crystal microbalances (QCM), and surface acoustic wave (SAW) sensors. By placing coatings of various chemical properties on a 6-SAW array, chemical speciation and quantification of vapors have been performed [26]. In one test the responses of these materials to each of 14 different analytes, representing the classes of saturated alkane, aromatic hydrocarbon, chlorinated hydrocarbon, alcohol, ketone, organophosphonate, and water, was evaluated. The results revealed a qualitative "chemical orthogonality" of the films useful for pattern recognition analysis. SAWs are the most sensitive of the above-mentioned acoustic sensors, and a number of technological advances have been made to facilitate their use in other chemical systems. Perhaps the most important of these advances is an ASIC (application specific integrated circuit) that converts DC power to the required high frequency impulse, and a reverse conversion for monitoring the frequency shift as a proportional DC shift [27].

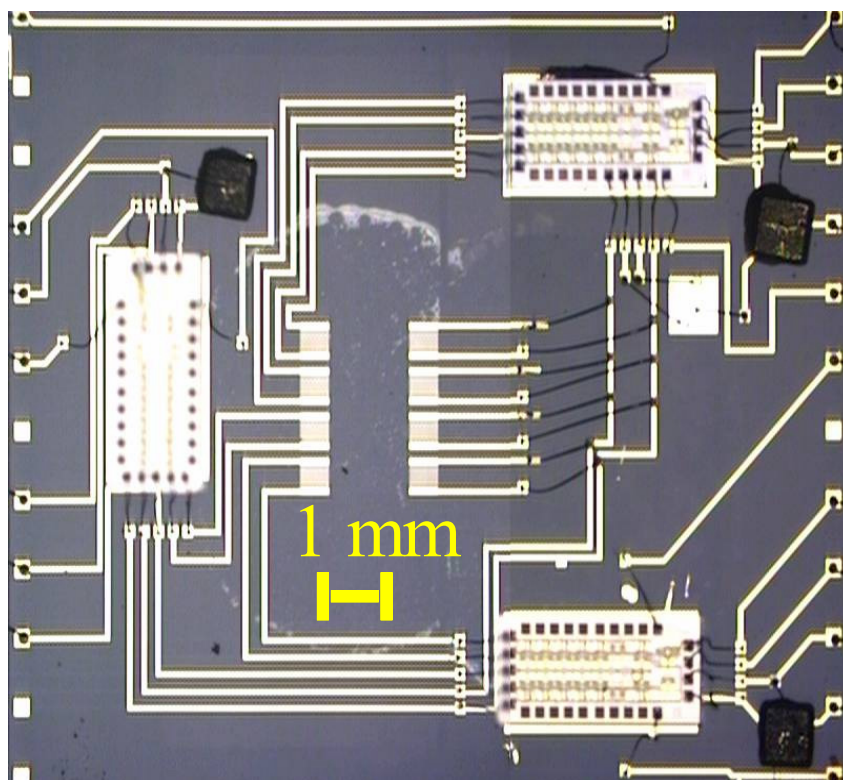


**Figure 4.** Four SAW sensor elements aligned vertically on an application specific integrated circuit. One delay line is left uncoated to compare frequency shifts of the other polymer or sol-gel coated lines.

#### -MicroChemLab (gas phase)

The gas phase MicroChemLab is a miniature gas chromatography (GC) system originally designed for chemical warfare agent detection for national security needs. Due to the high versatility of GC it has widespread utility. The MicroChemLab can likewise be configured for a variety of applications,

including quantification of organic compounds from natural gas to explosives to derivatized biological fatty acids. The main components typically consist of a microfabricated hotplate preconcentrator (PC), a micromachined silicon gas chromatography column ( $\mu$ GC), and a surface acoustic wave (SAW) sensor array [28]. The PC uses absorbent sol-gels, polymers, or a high surface area adsorbent solid phase. The low heat capacity membrane is then heated to hundreds of degrees in milliseconds to desorb collected analyte. This serves as the injection mechanism for the  $\mu$ GC. The  $\mu$ GC separates the injected chemicals in elution time through differing retention capacities with the polymer coated wall or solid packing materials. The chemicals are then detected in order by the SAW sensor.

To address the different nature of the various applications, several variations in components exist. For highly volatile compounds (methane, carbon dioxide) an injection loop is commonly used. A Sandia microfabricated version does not yet exist. A variety of sensors are also in various stages of development, each with advantages and disadvantages. These include a thermal conductivity detector, micro-pellistor array, gold nanowire sensor, and a nitrogen-phosphorous detector.

#### -Gold nanoparticle chemiresistors

Gold nanoparticle chemiresistors rely on the general ohmic sensing principles behind other chemiresistors with a few differences. In this sensor, the gold nanoparticles are electrically connected through conductive polymer linkages. While the conduction system is structurally bound in a second, nonconductive polymer, polymer swell minimally affects the resistive measurement. A more stable, reproducible, and sensitive signal is obtained from the direct interaction of analytes with the polarizable polymer links. Thus, films can be significantly thinner and detect lesser concentrations. To date, the sensors have measured pH and other ion concentrations in liquids (personal communication, D. Wheeler, Sandia National Laboratories, April 1, 2004). Outside researchers have primarily focused on gas phase VOCs, which is the next target of the Sandia sensor.

#### -Electrical impedance of tethered lipid bilayers on planar electrodes

This sensor consists of a very thin layer of lipid bilayers. VOCs adsorbing or absorbing into the layer changes ion mobility in the structure. This may offer orders of magnitude increase in sensitivity over existing polyelectrolyte coated capacitive chemiresistors. The large increase in sensitivity arises from molecular recognition elements, like antibodies that bind the analyte molecules.

#### -MicroHound

The MicroHound is a complete analytical system consisting of a chemical preconcentration system and a miniature Ion Mobility Spectrometer (IMS) [29]. Designed primarily for explosives, it can be modified for detecting semi-volatile organic compounds in air. The preconcentration system draws large volumes of air through a mesh screen that selectively adsorbs explosives. The screen is then rapidly heated to desorb the chemicals as a pulse into the inlet of the IMS. The IMS ionizes chemicals at the time-gated entrance of a drift tube. The ions are electrostatically driven against a counter-flowing inert gas to a sensing electrode. Ions are separated from each other in the drift tube according to size, with smaller chemicals arriving first. Identification and quantification are determined by drift time and peak size, respectively.

### -Hyperspectral imaging

Multiple infrared images of the same location (microscopic or macroscopic) are obtained using different filters. Thus, a color spectrum of each pixel is obtained. These multidimensional images can be processed for quantitative species mapping [30]. This is a stand-off method and could be used from a UAV or satellite for surface soil monitoring. These methods have also been used for biological and biomedical applications [31].

### -Chemiresistor array

The chemiresistor sensor is a chemically sensitive resistor comprised of a conductive polymer film deposited on a micro-fabricated circuit [32]. The chemically-sensitive insulating polymer is dissolved in a solvent and mixed with conductive carbon particles. The resulting ink is then deposited and dried onto thin-film, parallel, non-intersecting platinum traces on a solid substrate (chip). When chemical vapors come into contact with the polymers, the chemicals absorb into the polymers, causing them to swell. The swelling changes the physical conformation of the conductive particles in the polymer film, thereby changing the electrical resistance across the platinum-trace electrodes, which can be measured and recorded using a data logger or an ohmmeter. The swelling is reversible if the chemical vapors are removed, but some hysteresis can occur at high concentration exposures. The amount of swelling corresponds to the concentration of the chemical vapor in contact with the chemiresistor, so these devices can be calibrated by exposing the chemiresistors to known concentrations of target analytes.

The architecture of the microsensors integrates an array of chemiresistors with a temperature sensor and heating elements [33]. The chemiresistor array has been shown to detect a variety of VOCs including aromatic hydrocarbons (e.g., benzene), chlorinated solvents (e.g., trichloroethylene (TCE), carbon tetrachloride), aliphatic hydrocarbons (e.g., hexane, iso-octane), alcohols, and ketones (e.g., acetone). The on-board temperature sensor comprised of a thin-film platinum trace can be used to not only monitor the in-situ temperature, but it can also be used in a temperature control system. A feedback control system between the temperature sensor and on-board heating elements can allow the chemiresistors to be maintained at a fairly constant temperature, which can aid in the processing of data when comparing the responses to calibrated training sets. In addition, the chemiresistors can be maintained at a temperature above the ambient to prevent condensation of water, which may be detrimental to the wires and surfaces of the chemiresistor.

A robust package has been designed and fabricated to house the chemiresistor array [34]. This cylindrical package is small (~ 3 cm diameter) and is constructed of rugged, chemically-resistant material. Early designs have used PEEK (PolyEtherEtherKetone), a semi-crystalline, thermoplastic with excellent resistance to chemicals and fatigue. Newer package designs have been fabricated from stainless steel (Figure 5). The package design is modular and can be easily taken apart (unscrewed like a flashlight) to replace the chemiresistor sensor if desired. Fitted with Viton O-rings, the package is completely waterproof, but gas is allowed to diffuse through a GORE-TEX<sup>®</sup> membrane that covers a small window to the sensor. Like clothing made of GORE-TEX<sup>®</sup>, the membrane “breathes,” allowing vapors to diffuse through. Even in water, dissolved VOCs can partition across the membrane into the gas-phase headspace next to the chemiresistors to allow detection of aqueous-phase contaminants. The aqueous concentrations can be

determined from the measured gas-phase concentrations using Henry's Law. Mechanical protection is also provided via a perforated metal plate that covers the chemiresistors. The chemiresistors are situated on a 16-pin dual-in-line package that is connected to a weatherproof cable, which can be of any length because of the DC-resistance measurement. The cable can be connected to a hand-held multimeter for manual single-channel readings, or it can be connected to a multi-channel data logger for long-term, remote operation.

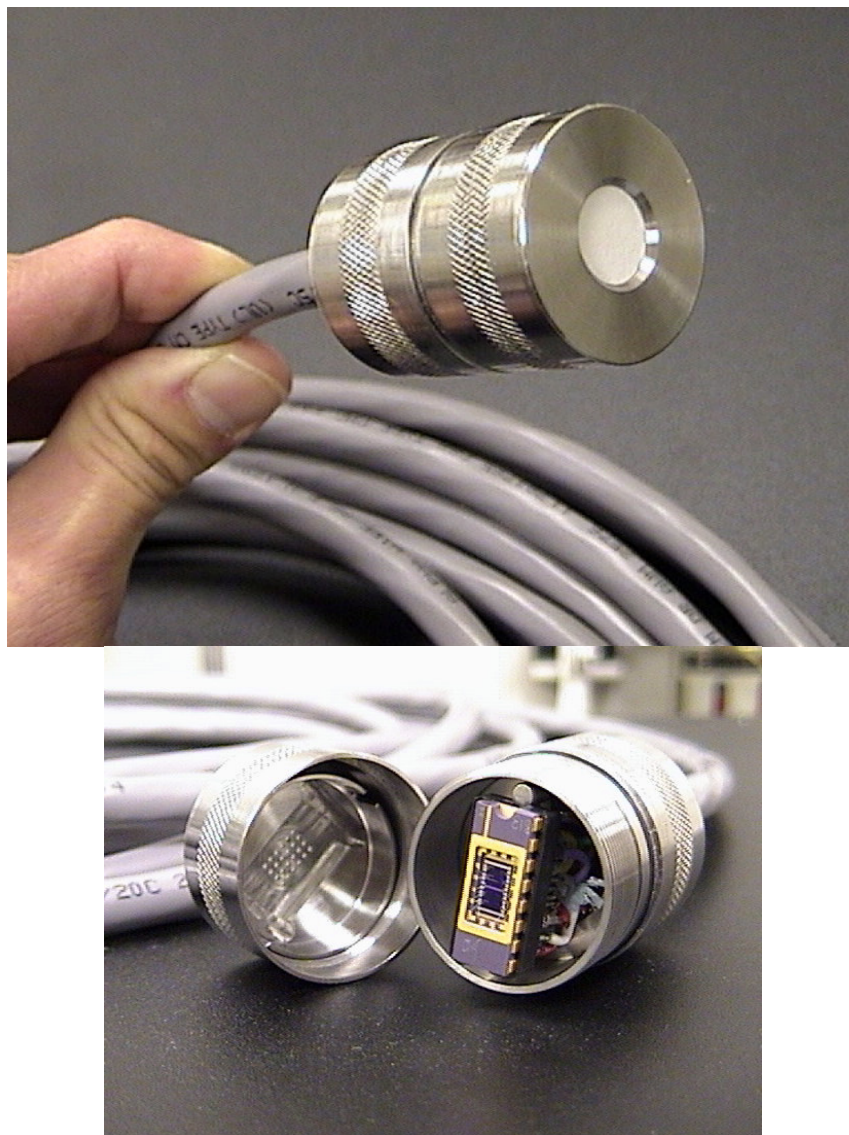


**Figure 5.** Stainless-steel waterproof package that houses the chemiresistor array. Left: GORE-TEX<sup>®</sup> membrane covers a small window over the chemiresistors. Right: Disassembled package exposing the 16-pin dual-in-line package and chemiresistor chip.

### *Biological sensors*

#### *-Fatty acid methyl esters (FAME) analyzer*

This method uses microhotplates and micro-chromatography columns ( $\mu$ GC) from the MicroChemLab to analyze whole biological cells [35]. A liquid sample is placed on the hotplate along with a methylating agent. When the hotplate is thermally ramped (to 500°C in tens of milliseconds) the

cells are lysed with proteins in the lipid bilayer forming semi-volatile FAMES. This also served as the injection mechanism into a  $\mu$ GC, where the FAMES were separated for identification and quantification. The ratios of the FAMES can be used to distinguish bacteria at the gram-type, genera, and even species level with high-resolution instrumentation. Sandia work aimed at miniaturizing half-million dollar bench scale instrumentation down to a handheld, battery-powered instrument with minimal sample preparation. Target analytes include biological warfare agents, food contaminants, and other toxic pathogens.

#### -iDEP (insulator-based dielectrophoresis)

This technique uses an electric field applied across a microfabricated array of insulating posts [36]. The polypropylene device selectively preconcentrates particles based on their polarizability and size (Figure 6). It can be used to preconcentrate proteins for analysis in the liquid MicroChemLab or other systems for fingerprint identification of pathogens.

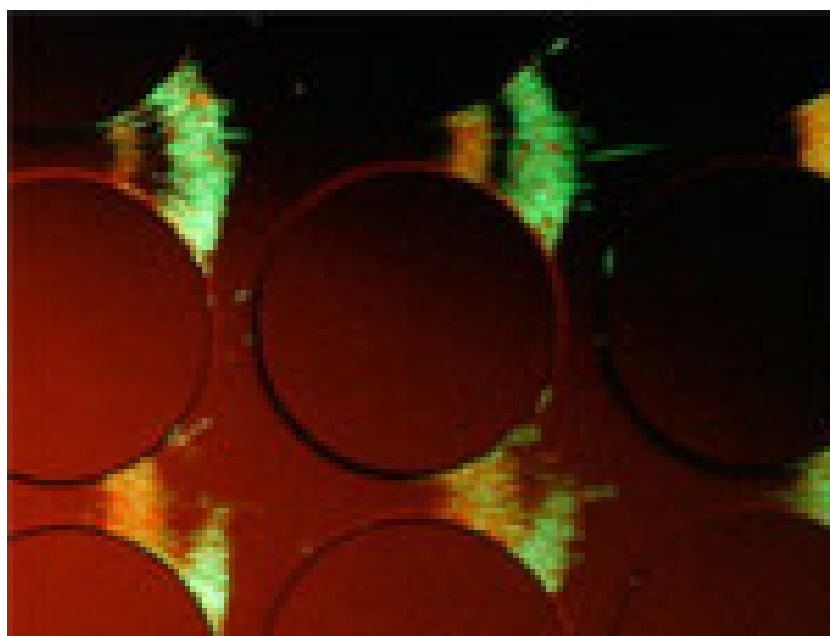


**Figure 6.** Electric field gradients created between microfabricated posts separate fluorescently tagged live and dead *E. coli* while dielectrophoretically concentrating them in zones.

#### -Bio-SAW sensor

Acoustic sensors are typically used by measuring a decrease in their resonant frequency that is related to mass loading. Biological detection can be performed by applying specific antibody coatings to the active surface of the acoustic device (Figure 7). Anthrax spores can be detected in a few minutes, and other biological threats can be detected using other antibody coatings [37]. An array of sensors with different coatings would provide increased versatility.

#### - $\mu$ ProLab

This LDRD Grand Challenge system is being designed for preconcentration and analysis of proteins and peptides using MIMS (molecular integrated microsystems) [38]. This architecture will

take the advantages inherent in system miniaturization to a higher level of performance. At the same time, simplicity of production is sought. Successes to date include cast-in-place fluidic structures and coatings, and the ability to preconcentrate protein and peptide signatures 1000 fold using programmable switchable polymers and electrokinetic trapping.

#### -MicroChemLab (Liquid)

The liquid MicroChemLab is the counterpart to the gas-phase MicroChemLab above [39]. It is a hand-portable, low-power instrument designed to detect a broad range of chemical and biological agents in less than five minutes. The detector uses capillary electrophoresis with three analysis trains: 1) DNA analysis to identify bacteria and viruses, 2) immunoassays to identify bacteria, viruses, toxins, and 3) protein signatures to identify toxins. Fluid handling is contained to micromachined channels on a single board, and driven by high voltage, but low power, electrokinetic forces. Sample preconcentration and injections occur through manipulation of the electrophoretic fields without the use of valves. Fluorescent detection occurs using a diode laser. The system has been designed to have manufacturable, replaceable modules with simplicity for a non-technical end-user.

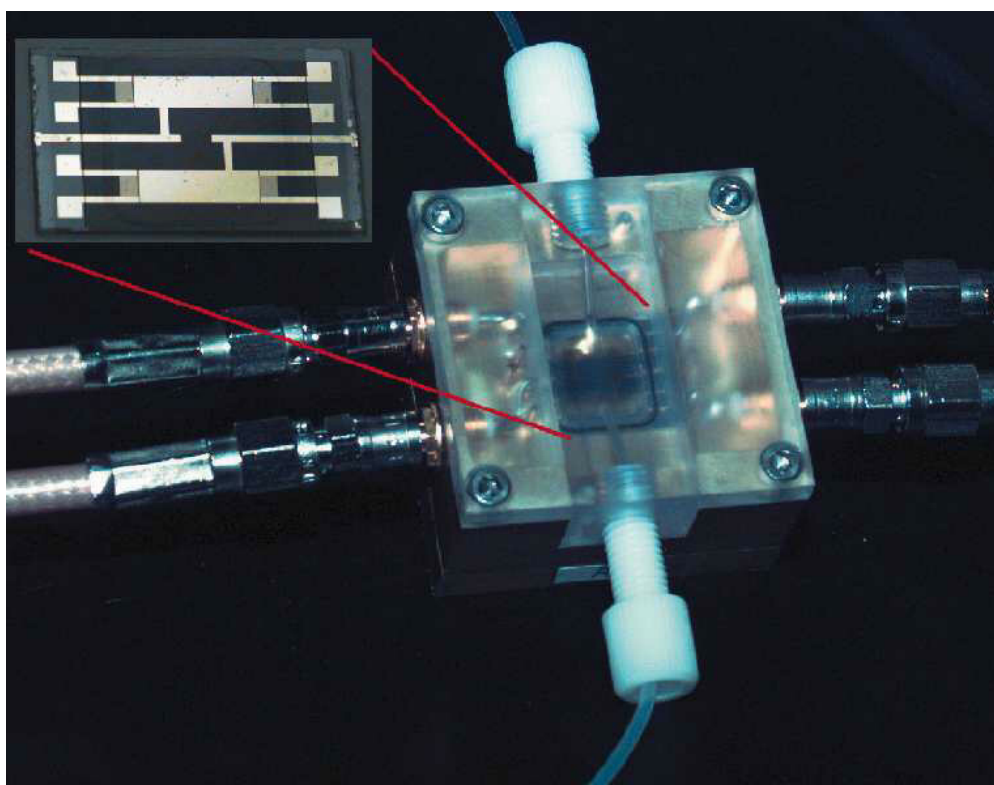


**Figure 7.** A miniaturized biosensor is shown consisting of a shear horizontal surface acoustic wave sensor coated with a molecular recognition layer. Highly specific coatings are used for biological warfare agent detection and medical diagnostics.

*Summary and specifications of sensor technologies*

The following tables (Tab. 10 to Tab 13) summarize specifications for the sensor technologies described in the previous sections. In many cases, rigorous specifications are not available because of limited studies. In these cases, estimates are provided based on the judgment of the principal investigators.

**Table 10.** Summary of specifications for **trace metal** sensors.

Sensor Technology	Specifications							
	Sensitivity	Selectivity	Stability	Speed	Size	Power	User Interface	Cost
A) Nanoelectrode Array	low ppb	elemental in non-complex mixtures	long-term	seconds	1 square inch dip probe		personal computer	sensor:
B) Laser-Induced Breakdown Spectroscopy	low ppb	elemental	long-term	ms with intensified-CCD, minutes with scanning spectrometers or signal averaging	fiber-optics; lengths of 100+ meters possible	mW per pulse	personal computer	system: \$50-150K

Table 11. Summary of specifications for radioisotope sensors.

Sensor Technology	Specifications									
	Sensitivity	Selectivity	Stability	Speed	Size	Power	User Interface	Cost		
A) RadFET	5 mV/rad	speciation with filters	> 1 year, 5% drift over 1000 hours after strong exposure	milliseconds, or cumulative expose can be read later	1/4" with ASIC and dip	passive or mW bias	sensitive digital multimeter	< \$1 in volume		
B) Cadmium Zinc Telluride detectors (CZT)	0.8 mV/keV	very selective with spectroscopy	long-term	microseconds	3 mm <sup>2</sup> plus electronics	< 1 Watt	hand held or personal computer	\$3000+ for system		
C) Low-energy Pin Diodes Beta Spectrometer	single events > 1.4 keV. Above background noise, LOD is 0.1 disintegrations/cm <sup>2</sup> /sec (3 rem/year)	very selective	long-term	20 ms	sensor: 13 mm <sup>2</sup> , plus electronics	passive or mW bias	hand held or personal computer	\$1000+ for photodiode		
D) Thermoluminescent Dosimeter (TLD)	1 micro-rad/hour	non-specific to radiation source, but can employ filters or different crystal thicknesses and types	long-term	cumulative dose; nanoseconds per event	5 mm <sup>2</sup>	passive	TLD Reader	low dollars for crystals; \$1000+ for reader		
E) Isotope Identification Gamma Detector	very high	very selective	long term	seconds	vehicle portal	110 AC	laptop			
F) Neutron Generator for Nuclear Material Detection	very high	very selective	long term	seconds	1 meter tall	110 AC	laptop			

**Table 12.** Summary of specifications for **volatile organic compound (VOC)** sensors.

<b>Specifications</b>									
<b>Sensor Technology</b>	<b>Sensitivity</b>	<b>Selectivity</b>	<b>Stability</b>	<b>Speed</b>	<b>Size</b>	<b>Power</b>	<b>User Interface</b>	<b>Cost</b>	
A) Fiber Optic Chemical Sensor	low ppm for hydrophobic organics	good selectivity with multivariate analysis in moderately complex environments; coating is non-specific for hydrophobic compounds	weekly calibration	20 minutes	fiber-optics; lengths up to kilometers possible	110 V, 5 amps	laptop	\$0.25/meter \$2500 for spectrometer	
B) Grating Light Reflection Spectro-electrochemistry	ppm to ppb	multivariate analysis required for simple mixtures	long term	seconds to minutes	dip probe	5 Watts	laptop	<\$500	
C) Miniature Chemical Flow Probe Sensor	low ppb to low ppm, depending on analyte	good selectivity in moderately complex matrix	flow cell and fresh reagents ensure high reproducibility	1-2 minutes	2" probe diameter, up to 150 feet long; spectrometer and PC in 2 suitcases	110 AC when built (1995)	laptop	\$10K for total system	
D) SAW Chemical Sensor Arrays	ppm to ppb	good with multivariate analysis of mixtures that are not too complex	slow drift over time	tens of seconds	< 1 square inch sensor	mW	laptop or digital display	<\$500	
E) MicroChemLab (gas phase)	ppb	very good	slow drift over time	1-5 minutes	handheld	< 1 Watt	laptop or digital display	\$10-20K	
F) Gold Nanoparticle Chemiresistors	ppb	may be tailored to chemical classes	TBD	seconds	< 1 square inch sensor	mW	laptop or digital display	<\$100	
G) Electrical Impedance of Tethered Lipid Bilayers on Planar Electrodes	ppm to ppb	very high with antibody coatings; lower for non-specific receptors	weeks	minutes	cm <sup>2</sup>	mW for sensor; 110 AC for whole instrument	laptop	<\$1 per sensor	
H) MicroHound	ppb	fairly high	days to weeks	seconds	handheld	battery	laptop or digital display	<\$5K	
I) Hyperspectral Imaging	ppm to ppb	good with multivariate analysis of mixtures that are not too complex	long term	seconds to minutes	handheld		laptop	\$10K to \$100K	
J) Chemiresistor Arrays	~typically tens to hundreds of ppm; 0.1% of saturated vapor pressure	arrays can discriminate different classes of VOCs	slow drift over time	seconds to minutes, depending on concentration	several mm; package is ~2.5 cm diameter x~6 cm long	mW; battery powered	laptop or computer	<\$100 for sensor array; package can be ~\$500	

**Table 13.** Summary of specifications for **biological** sensors.

Sensor Technology	Specifications									
	Sensitivity	Selectivity	Stability	Speed	Size	Power	User Interface	Cost		
A) Fatty Acid Methyl Esters (FAME) Analyzer	low nanograms	highly selective	SAW sensor can irreversibly load	< 10 min.	handheld	< 5 Watts per analysis	syringe and keypad or laptop	potentially < \$10K		
B) iDEP (insulator-based dielectrophoresis)	preconcentration method for other sensors	non-selective	expected to be high	milliseconds	millimeters	< 1 W	Is a module for larger systems	< \$1		
C) Bio-SAW Sensor	picograms of proteins	highly selective	SAW can drift over time; analyte binding can be irreversible	minutes	several square cm	mW	system display plus some liquid handling; laptop	<\$100 per sensor		
D) $\mu$ ProLab	picograms	expected to be highly selective	acoustic sensors tend to drift with time; optical systems will be more stable	minutes	handheld	< 5 W	minimal fluid handling, system display or laptop	TBD		
E) MicroChemLab (Liquid)	depending on analyte: 10-100 ppb for chemicals; sub-toxic (picomoles) for biotoxins	very high	hours	< 5 min	handheld	5 Watts	LCD display or laptop	< \$10K		

### Summary and recommendations

This report has identified regulatory standards, policies, and needs associated with monitoring environmental contaminants for drinking water, storm water, pretreatment, and ambient air quality. Table 14 presents a summary and relative comparison of the general requirements for different environmental monitoring applications. The required concentration limits, sampling frequency, sampling method, and sampling phase are listed in relative terms to provide metrics for evaluation of the sensor technologies.

**Table 14.** Summary and comparison of relative requirements for different environmental monitoring applications.

Requirements	Drinking Water	Storm Water	Pre-Treatment	Ambient Air
<b>Concentration</b>	Lowest concentrations (ppb to ppm in aqueous phase)	Higher concentrations than drinking water (e.g., arsenic is 160 ppb in storm water for wood preservers while drinking water is 10 ppb)	Concentration are higher than drinking water (e.g., TCE is 69 ppb (daily) compared to 5 ppb for drinking water); almost all biological except for a few industries that manufacture chemicals; INDUSTRY SPECIFIC	Air concentrations are typically in the ppm range
<b>Sampling Frequency</b>	Most frequent sampling of the three water applications (would like real time, continuous monitoring)	Only need to sample occasionally (during rain storms)	More frequent monitoring than for storm water but less than for drinking water	Continuous (current methods average over a period of time using continuous flow)
<b>Sampling Method</b>	On-line, continuous with remote telemetry	Can be hand-held for occasional sampling	On-line or hand-held	Continuous air monitoring with remote telemetry
<b>Sample Phase</b>	Aqueous	Aqueous	Aqueous	Gas

Sensor technologies have been identified that may be compatible with the needs of the various environmental monitoring applications. Based on these surveys, Table 15 lists some of the viable sensor technologies that appear to have the highest potential in addressing the needs of these environmental monitoring applications.

**Table 15.** Summary of potential sensor technologies that can address environmental monitoring needs.

Sensor Technology	Application	Analyte	Comments
LIBS	Drinking Water, Storm Water, Pretreatment	Trace Metals	The cost of the laser and spectrometer are high. Additional development needs to bring the price down and package it for use in water applications. Could potentially be used to simultaneously identify 9 RCRA metals plus arsenic. Sampling interval ranges from 1 s to ~1 minute (for signal averaging). Can be run continuously.
Nanoelectrode Array	Drinking Water, Storm Water, Pretreatment	Trace Metals	Less selective than LIBS. Commercial company in Washington. Sampling interval on the order of seconds. Still under development to discern among multiple target analytes present.
Miniature Chemical Flow Probe Sensor	Drinking Water, Storm Water, Pretreatment	VOCs, Trace Metals	Expensive because of spectrometry (like LIBS). Reagents need to be supplied. Need to acquire sample to introduce reagent in a side-stream.
RadFET	Drinking Water	Radioisotopes	Need to use filters to allow speciation. Sensitivity in water for alpha and beta emitters is questionable given the attenuation through water.
Low-energy Pin Diodes Beta Spectrometer	Drinking Water	Radioisotopes	Commercially available. May not need any additional development. Sensitivity in water for alpha and beta emitters is questionable given the attenuation through water.
Cadmium Zinc Telluride Detectors	Drinking Water	Radioisotopes	Commercially available. Sensitivity in water for alpha and beta emitters is questionable given the attenuation through water.
SAWS	Drinking Water, Storm Water, Pretreatment, Air	VOCs	Sensitivity can get down to ~ppm, but fluctuations in environmental parameters (e.g., humidity, temperature) can reduce the sensitivity and accuracy. Sensor signal drifts over time. Cannot analyze more than three contaminants at once.
Chemiresistors	Drinking Water, Storm Water, Pretreatment, Air	VOCs	Sensitivity is limited (hundreds of ppm). Needs preconcentration. These can also be used to monitor in-situ remediation activities (patent pending: SD-7097 Automated Monitoring and Remediation System for Volatile Subsurface Contaminants).
MicroHound/Ion Mobility Spectrometer (IMS)	Drinking Water, Storm Water, Pretreatment, Air	Semi-Volatile Organic Compounds	Gas-phase detection; need to develop a sampling system to introduce water samples to IMS. Should be able to detect semi-volatile chlorinated hydrocarbons (e.g., polychlorinated biphenyls (PCBs)). Can detect pesticides, organic nitrates.
MicroChemLab (gas)	Drinking Water, Storm Water, Pretreatment, Air	VOCs	MCL is manufacturing these for ~\$10K per unit. Additional development work is needed to adapt these systems for VOCs.
MicroChemLab (liquid)	Drinking Water	Biological	Cost is high.
FAME	Drinking Water	Biological	Sampling is currently done manually.

The list of sensors presented in Table 15 is culled even further to identify the most promising technologies for each analyte considered (i.e., trace metals, radioisotopes, VOCs, semi-volatiles, and biological pathogens). Table 16 provides a summary of the future development required for these technologies to be adapted for use in environmental monitoring applications.

**Table 16.** Summary of the most promising technologies for each analyte class that could benefit from further development.

Sensor	Analyte	Future Development Required
LIBS	Trace Metals	LIBS systems employ diffraction gratings that must be scanned to cover the spectral range of metal contaminants with sufficient resolution for positive identification and quantification. Speed could be increased through the use of Sandia's programmable diffraction grating. Simultaneous determination could be made through the computer-aided design of holographic diffraction gratings.
CZT	Radioisotopes	These detectors are inexpensive and sensitive to regulated radiation levels. Commercial spectrometer systems are available. A low level effort could adapt the spectrometer for water monitoring. Alpha emitting contaminants in water can not be detected by radiation events as alpha radiation is nonpenetrating.
MicroChemLab, gas phase	VOCs	Due to the wide variety of organic contaminants that can be present in air or water, separation is essential for analysis. The MicroChemLab can be adapted to collect and analyze in both air and water. Leveraging funding could direct development towards specific targets.
MicroHound/Ion Mobility Spectrometry	Semi-Volatiles	The ion mobility spectrometer behind this instrument can be used in positive mode for common semi-volatiles or negative mode for highly selective detection of pesticides and halogenated semivolatiles. The diffusion-based separation could benefit from a pre-separation using a chromatography column.
Bio-SAW Sensor	Biological Pathogens	Sensors with bioreceptors are highly selective, providing detection amplification over background contaminants. Still, biofouling can occur. Further development is needed to array significant numbers of sensors into a small area for multi-pathogen monitoring.

The advancement of the LIBS technology would be focused on developing a continuous LIBS sensor for water-monitoring applications. Ideally, the sensor would be able to simultaneously detect the nine RCRA metals plus arsenic at low ppb levels. The development of holographic diffraction gratings would increase the speed and efficiency of the LIBS ability to simultaneously detect these trace metals.

For the CZT sensors, a low-level effort is needed to adapt these sensors for water applications. A significant challenge will be to detect alpha-emitting contaminants since the radiation is attenuated rapidly. A continuous CZT sensor with spectrometry would need to be adapted for aqueous environments.

The MicroChemLab device requires additional development to detect VOCs in aqueous environments. Sampling, analysis, and parameter optimization (e.g., polymer selection) for target VOCs need to be pursued. With preconcentration, the sensitivity of these devices can be in the ppb range, but repeatability and drift are significant issues with MicroChemLab.

The ion mobility spectrometer implemented in the MicroHound shows promise for detecting semi-volatile compounds such as pesticides and halogenated contaminants at low concentrations. Sampling methods would need to be developed to introduce aqueous samples to the IMS. Separation is based on the different “drift” times of the different ions through the IMS tube, but additional separation could be obtained by adding a chromatography column at the inlet. A great deal of research invested in the MicroHound project can be leveraged for applications in water monitoring and ambient-air monitoring (e.g., new materials and designs for the IMS drift tube).

The Bio-Saw sensor, and other continuous, real-time biological sensors, still require significant research and development before they can be applied to environmental monitoring applications. Bio-assay test kits are available that can provide detection of biological agents, but these require manual operation and interfacing.

Of the sensors identified in Table 16, we believe that LIBS (for trace metals) and ion-mobility spectrometry (for semi-volatiles) show the most promise in terms of capabilities, adaptability, and potential impact. Both have the capability to detect concentrations at or below regulatory levels, and the ability to detect trace metals and semi-volatiles is needed in a number of environmental applications ranging from drinking-water to ambient-air monitoring.

A primary consideration that still remains to be addressed is the performance of these sensors in each of the field applications. Features such as sensitivity, stability, selectivity, speed, size, and cost need to be tested and evaluated under actual operating conditions. Harsh and fluctuating environmental conditions can degrade the performance of many of these sensors. Nevertheless, a market analysis presented in the beginning of this report indicates that a wide-ranging (and commercially viable) need can be filled by the successful development and application of these sensors to environmental monitoring applications. The sensor technologies identified in Table 15 and Table 16 appear to be the strongest candidates that can be further developed and adapted to address these needs.

## Acknowledgments

The authors thank Sue Collins, Steve Martin, Graham Yelton, and Jennifer Ellison for their insightful discussions and assistance with this report. Sandia is a multiprogram laboratory operated by Sandia Corporation, a Lockheed Martin Company for the United States Department of Energy's National Nuclear Security Administration under contract DE-AC04-94AL85000.

## References

1. Looney, B.B; Falta, R.W., (Eds.) *Vadose zone Science and Technology Solutions*. Battelle Press, Columbus, OH, **2000**, pp. 1540.
2. Wilson, L.G.; Everett, L.G.; Cullen, S.J., (Eds.) *Handbook of Vadose Zone Characterization & Monitoring*, CRC Press, Boca Raton, FL, **1995**.
3. U.S. DOE. *Assessment of the 2000 and 2001 Environmental Management Industry Times They Are A-Changin'*, Prepared for the U.S. Department of Energy Office of Environmental Management, Office of Science and Technology (EM-50). Prepared by YAHS GS Llc., Richland, Wa, August **2002**.
4. Stetter, J. *TES Workshop on Technology Needs as Part of a Conference on Analytical Chemistry and Applied Spectroscopy*, Pittsburg, Pa, **2001**.
5. U.S. Department of Energy. *From Cleanup to Stewardship, a Companion Report to Accelerating Cleanup: Paths to closure and Background Information to Support the Scoping Process Required for the 1998 PEIS Settlement Study*. U.S. Department of Energy, Office of Environmental Management, October **1999**.
6. U.S. Department of Energy (DOE). *Market Study to Determine Needs and Present Usage of Chemical Sensor Systems for Environmental Analytical Applications*. Final Report. Submitted to: Characterization, Monitoring and Sensing Technology Crosscutting Program, Department of Energy, Ames Laboratory, Iowa State University, Ames, IA 50011-3020 Prepared by: The Unimar Group, Ltd. 325 Market St. , Alton, Il. 62002, May **1996**.
7. Inspector General (IG) Report. *Departmental Position on the Office of Inspector General Report IG-0461, "Groundwater Monitoring Activities at Department of Energy Facilities."* To: Phillip L. Holbrook, Deputy Inspector General for Audit Services.
8. 65 Federal Register 64746. *Final Reissuance of National Pollutant Discharge Elimination System (NPDES) Storm Water Multi-Sector General Permit for Industrial Activities; Notice*, October 30, **2000**.
9. 40 CFR Part 403. *General Pretreatment Regulations for Existing and New Sources of Pollution*. EPA, Washington, DC, **2000**.
10. 40 Code of Federal Regulations (CFR). Part 414, Section 111, *Organic Chemicals, Plastics, and Synthetic Fibers*. EPA, Washington, DC, **2003**.

11. American Conference of Governmental Industrial Hygienists (ACGIH). Threshold Limit Values for Chemical Substances and Physical Agents and Biological Exposure Indices, ACGIH, Cincinnati, **2000**.
12. Horton, R.J. "Sensor development: Micro-analytical solutions for water monitoring applications" SAND2003-2575P, Sandia National Laboratories, Albuquerque, NM, **2003**.
13. Ashby, C.I.H.; Kelly, M.J.; Yelton, W.G.; Pfeifer, K.B.; Muron, D.J.; Einfeld, W.; Siegal, M.P. Functionalized nanoelectrode arrays for in situ identification and quantification of regulated chemicals in water. *LDRD Annual Report*, **2002**, 364.
14. Hahn, D.W.; Hencken, K.R.; Johnsen, H.A. Performance testing of a laser-induced breakdown spectroscopy (LIBS) based continuous metal emissions monitor at a pyrolytic waste treatment facility. SAND97-8270, Sandia National Laboratories, Albuquerque, NM, **1997**.
15. Matalucci, R.V.; Esparza-Baca, C.; Jimenez, R.D. Characterization, monitoring, and sensor technology catalogue. SAND95-3062, Sandia National Laboratories, Albuquerque, NM, **1995**.
16. Blevins, L.G.; Shaddix, C.R.; Sickafoose, S.M.; Walsh, P. M. Laser-induced breakdown spectroscopy at high temperatures in industrial boilers and furnaces. SAND2003-8151J, Sandia National Laboratories, Albuquerque, NM, **2003**.
17. Moreno, D.J.; Hughes, R.C.; Jenkins, M.W.; Drumm, C.R. A simple ionizing radiation spectrometer/dosimeter based on radiation sensing field effect transistors (RadFETs). SAND97-0255C, Sandia National Laboratories, Albuquerque, NM, **1997**.
18. Murray, W.S.; Butterfield, K.B.; Baird, W. Automated radioisotope identification using fuzzy logic and portable CZT detectors. LA-UR-00-4791 (LANL), **2000**.
19. Doyle, B.L.; Vizkelethy, G.; Walsh, D. Ion beam induced charge collection (IBICC) studies of cadmium zinc telluride (CZT) radiation detectors. SAND99-0917C, Sandia National Laboratories, Albuquerque, NM, **1999**.
20. Wampler, W.R.; Doyle, B.L. Low-energy beta spectroscopy using pin diodes to monitor tritium surface contamination. *Nuclear Instruments and Methods in Physics Research A*, **1994**, 349, 473.
21. Schwank, J.R.; et. al. "Common-source TLD and RADFET characterization of Co-60, Cs-137, and x-ray irradiation sources" SAND97-1440J, Sandia National Laboratories, Albuquerque, NM, **1997**.
22. Carlson, G.A.; Lorence Jr., L.J.; Vehar, D.W. Particle size effect in CaF<sub>2</sub>: Mn-teflon TLD response at photon energies from 5 to 1250 KeV. SAND89-1788J, Sandia National Laboratories, Albuquerque, NM, **1989**.
23. Garcia, N. Site hears latest news on four key R&D projects. *Sandia Lab News*, Sandia National Laboratories, Albuquerque, NM, March 5, **2004**, 56, 5, 3.

24. Blair, D.S. Evaluation of an evanescent fiber optic chemical sensor for monitoring aqueous volatile organic compounds. SAND97-0782, Sandia National Laboratories, Albuquerque, NM, **1997**.
25. Zaidi, S.; McNeil, J.R.; Kelly, M.J.; Sweatt, W.C.; Kemme, S.A.; Blair, D.S.; Brodsky, A.M., Smith, S.A. Grating light reflection spectroelectrochemistry for detection of trace amounts of aromatic hydrocarbons in water. SAND2000-1018, Sandia National Laboratories, Albuquerque, NM, **2000**.
26. Ricco, A.; Xu, C.; Allred, R.; Crooks, R. SAW chemical sensor arrays using new thin-film materials. SAND94-0241C, Sandia National Laboratories, Albuquerque, NM, **1994**.
27. Cernosek, R.W.; Frye, G.C.; Martin, S.J. Method and apparatus for phase and amplitude detection. U.S. Patent # 5763283, **1994**.
28. Sandia National Laboratories, "µChemLab" [online], December 9, <http://www-irm.sandia.gov/organization/mstc/organization/micro-analytical/chemlab.html>, **2002**.
29. Linker, K.L.; Brusseau, C.A.; Mitchell, M.A.; Adkins, D.R.; Pfeifer, K.B.; Rumpf, A.N.; Rohde, S.B. "Portable explosives detection system: MicroHound. SAND2003-2254C, Sandia National Laboratories, Albuquerque, NM, **2003**.
30. Koehler, F.W.; Haaland, D.M. Quantitative determination of 2D hyperspectral image data. SAND99-2133A, Sandia National Laboratories, Albuquerque, NM, **1999**.
31. Timlin, J.A.; Haaland, D.M.; Sinclair, M.B. Hyperspectral imaging and multivariate data analysis for biological and biomedical applications. SAND2003-3955A, Sandia National Laboratories, Albuquerque, NM, **2003**.
32. Ho, C.K.; McGrath, L.K.; Davis, C.E.; Thomas, M.L.; Wright, J.L.; Kooser, A.S.; Hughes, R.C. Chemiresistor microsensors for in-situ monitoring of volatile organic compounds: final LDRD report. SAND2003-3410, Sandia National Laboratories, Albuquerque, NM, **2003**.
33. Hughes, R.C.; Casalnuovo, S.A.; Wessendorf, K.O.; Savignon, D.J.; Hietala, S; Patel, S.V.; Heller, E.J. Integrated chemiresistor array for small sensor platforms, *SPIE Proceedings Paper 4038-62*, AeroSense 2000, Orlando, Florida, **2000**, 519.
34. Ho, C.K.; Hughes R.C. *In-Situ* Chemiresistor sensor package for real-time detection of volatile organic compounds in soil and groundwater, *Sensors*, **2002**, 2, 23.
35. Mowry, C.; Morgan, C.; Kottenstette, R.; Dulleck Jr., G.; Manginell, R.; Wally, K.; Baca, Q.; Theisen, L.; Chambers, W.; Trudell, D. LDRD annual report, Sandia National Laboratories, Albuquerque, NM, **2002**, 65.
36. Simmons, B.A.; Cauley, T.H.; Charest, J.L. High-throughput insulative dielectrophoresis (iDEP) in bulk manufactured polypropylene. SAND2003-8512P, Sandia National Laboratories, Albuquerque, NM, **2003**.

37. Brozik, S.M.; Branch, D.W.; Osbourn, G.C.; Morgan, C.H.; Sasaki, D.Y. LDRD annual report. Sandia National Laboratories, Albuquerque, NM, **2002**, 168.
38. Napolitano, L.M.; Potter, K.S.; Hasselbrink, E.; Brinker, C.J.; Wheeler, D.R.; Brozik, S.M.; Sasaki, D.Y.; Shepodd, T.J.; Singh, A.K.; Burns, A.R.; Casalnuovo, S.A.; Kemme, S.A.; Loy, D.A.; Bunker, B.C.; Thompson, A.P.; Potter, B.G.; Schoeniger, J.S. LDRD annual report. Sandia National Laboratories, Albuquerque, NM, **2002**, 438.
39. Nolan, P. Sandia National Laboratories annual report 2003-2004. Sandia National Laboratories, Albuquerque, NM, **2004**, 47.

© 2005 by MDPI (<http://www.mdpi.org>). Reproduction is permitted for non-commercial purposes.

## **Automated Ground-Water Sampling and Analysis of Hexavalent Chromium using a “Universal” Sampling/Analytical System**

**Scott R. Burge<sup>1,\*</sup>, Dave A. Hoffman<sup>1</sup>, Mary J. Hartman<sup>2</sup> and Richard J. Venedam<sup>3</sup>**

<sup>1</sup> Burge Environmental, 6100 Burge Environmental South Maple, Suite 141, Tempe, AZ 85283

<sup>2</sup> Pacific Northwest Laboratory, 3110 Port of Benton Blvd., Richland, WA 99354

<sup>3</sup> Bechtel Nevada, P.O. 98521, MS NTS 188, Las Vegas, NV 89193

\* Author to whom correspondence should be addressed. Email: [burgenv@globalcrossing.net](mailto:burgenv@globalcrossing.net)

*Received: 28 September 2004 / Accepted: 02 December 2004 / Published: 28 February 2005*

---

**Abstract:** The capabilities of a “universal platform” for the deployment of analytical sensors in the field for long-term monitoring of environmental contaminants were expanded in this investigation. The platform was previously used to monitor trichloroethene in monitoring wells and at groundwater treatment systems (1,2). The platform was interfaced with chromium (VI) and conductivity analytical systems to monitor shallow wells installed adjacent to the Columbia River at the 100-D Area of the Hanford Site, Washington. A groundwater plume of hexavalent chromium is discharging into the Columbia River through the gravels beds used by spawning salmon. The sampling/analytical platform was deployed for the purpose of collecting data on subsurface hexavalent chromium concentrations at more frequent intervals than was possible with the previous sampling and analysis methods employed at the Site.

**Keywords:** field monitoring, hexavalent chromium, colorimetric, automated analysis.

---

## Introduction

The development of platforms to deploy analytical systems in the field has not kept pace with development of the analytical sensors. Researchers that develop new sensors eventually encounter the problem of supporting, communicating, calibrating and cleaning sensors deployed in the field. This lack of presenting a complete solution to the users slows, inhibits, and is often the “valley of death” for the use of sensor technologies. The development of a “universal platform” has greatly decreased the time and cost required to deploy analytical sensors for analyzing trace environmental contaminants in the field. The platform was designed in a “plug and play” configuration for several types of analytical systems including trichloroethene (TCE), carbon tetrachloride, volatile aromatics, hexavalent chromium and lead. The platform has previously been used to monitor for trichloroethene TCE, 1 to 200 ppb concentration range, using a TCE-specific optrode. The trichloroethene monitoring system has been used successfully in monitoring TCE treatment systems in Arizona and California [1-2], and in monitoring wells at an Air Force Base in California [3].

The platform was modified to monitor hexavalent chromium and conductivity from shallow groundwater wells (aquifer tubes) adjacent to the Columbia River at the 100-D Area of the Hanford Site, Washington [4]. Sodium dichromate, the source of the hexavalent chromium, was formerly used at the 100-D Area to control corrosion in the piping of a nuclear reactor. Releases from the piping and other discharges resulted in soil and ground water contamination. A groundwater plume of hexavalent chromium is discharging through the riverbed and into the Columbia River (Figure 1). Hexavalent chromium can be toxic to aquatic organisms; of special concern are the juvenile stages of salmon using the riverbed as spawning habitat.

To evaluate exposure risk for aquatic receptors, hexavalent chromium concentration data are needed (a) from a variety of river environment locations, and (b) at a frequency greater than that associated with traditional monitoring methods. The best location for monitoring concentrations is near the point of discharge to the river. Previous work has demonstrated successful methods for establishing access to shallow ground water using sampling ports and tubing that extends to onshore locations. The weakness of current monitoring capabilities is the impracticality of obtaining frequent hexavalent chromium measurements sufficient to characterize the temporal changes that occur in shallow ground water. These changes occur as a consequence of daily, weekly, and seasonal cycles in river discharge, which is controlled by upstream dams. A field-deployable, automated hexavalent chromium measurement system offered a means to fully characterize the conditions in this sensitive aquatic habitat. Key specifications for the system include: (a) practical quantitation limit of at least 5 ppb -- the relevant regulatory standard is 10 ppb; (b) ability to make at least hourly measurements; (c) field independence for at least two weeks; (d) provision for automated, internal calibration using standards; and (e) reasonable cost of operation when compared to the current costs of manual collection of field samples for laboratory analysis.

The Burge platform offered a simple solution to deploy a colorimetric system for the analysis of hexavalent chromium using 1,2-diphenylcarbazide. The diphenylcarbazide reagent is used in EPA methods for the analysis of hexavalent chromium. It was assumed that the more an analysis conforms to EPA protocols, the greater the probability of regulatory acceptance. Therefore, the colorimetric analysis was automated and interfaced to the sampling/calibration platform. This paper presents the design and preliminary performance data for an automated “universal” system. The automated system

is capable of performing automated sampling, analysis and calibration without the requirement of a resident operator.

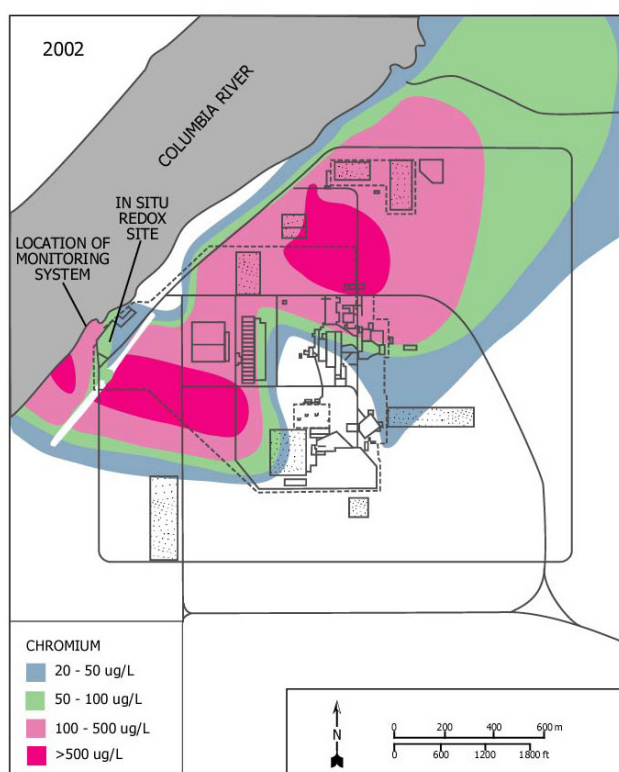


**Figure 1.** Site 100 D – Hanford site, Washington, hexavalent chromium groundwater plume.

### “Universal” sampling/ analytical system

The system was developed and programmed to perform the following operations:

#### Sampling

- Wells, surface water and treatment systems
- Up to four ports: monitoring wells, surface water, etc.
- Wells 2 inches and larger
- Up to four depths in a single well (Multi-Level Sampling)
- Low-flow sampling
- Low energy requirements (solar cells)

#### Calibration and quality control

- Creating blank water (for cleaning and calibration)
- Three-point calibration curve
- Standard additions
- Mid-calibration checks
- Spikes and splits

#### Analytical

- Accommodating many types of sensors (TCE, Cr(VI), aromatics)
- Operates of two sensor systems simultaneously with temperature and conductivity

A diagram of the complete universal platform deployed in the field is illustrated on Figure 2. The monitoring system is composed of several modules for sample collection, calibration, analysis, data acquisition/control, communication and waste treatment. The entire monitoring system was deployed in a field deployment box. The field deployment box is used to mount the solar cell panels and house the batteries, air system, and communication module. A 20.25-cm (8-in.) outside diameter (OD) casing passed through the bottom of the field deployment box and housed the analytical and calibration modules. The bottom of the casing extended approximately 90 cm (3 ft) into the soil. The analytical and calibration modules were mounted inside the well casing for temperature control.

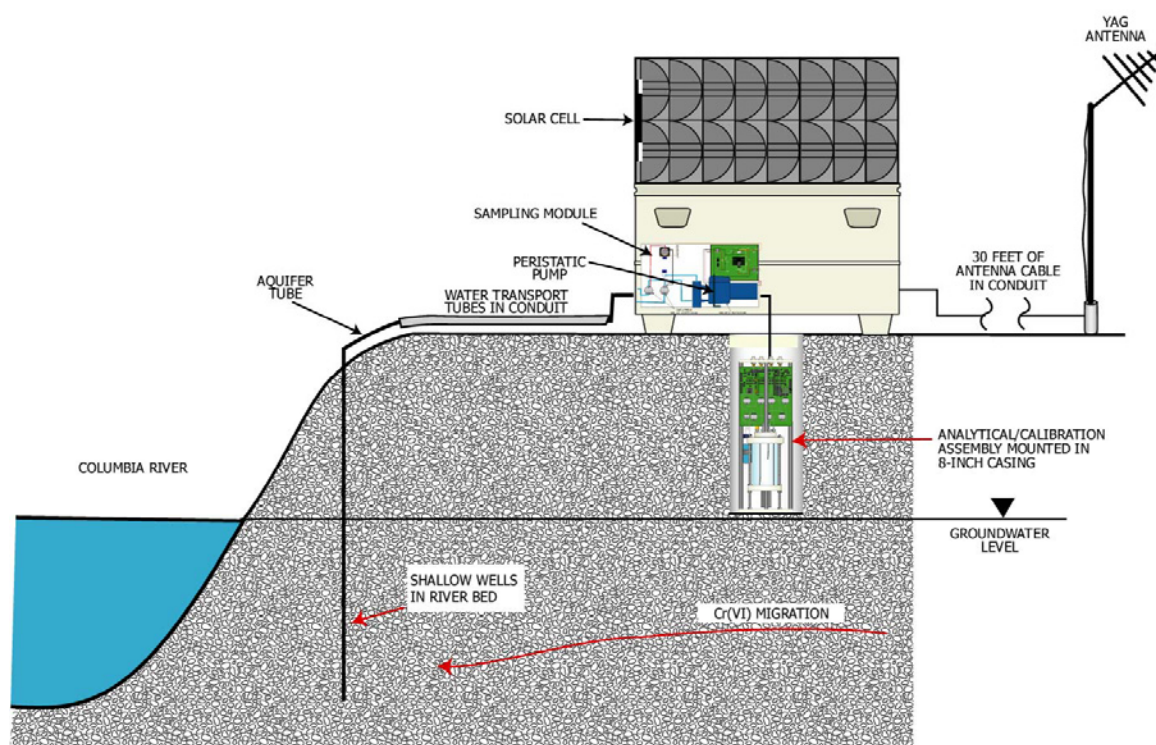


**Figure 2.** Field implementation schematic.

Two 75-watt photovoltaic cells and a solar controller charged two 90 amp-hour sealed deep charge batteries. Compressed air operated many of the functions of the calibration and analytical modules. A 12-volt, 1/10-hp air compressor with an automatic pressure switch 8 to 10.9 kPa (55 to 75 psi) supplied air to a 19 cubic liter (5 cubic ft) tank. Two air regulators provided two levels of air pressure, 0.22 to 1.45 kPa (1.5 and 10 psi), to the calibration and analytical systems.

### *Sampling module*

The water samples were collected from aquifer tubes placed into the banks of the Columbia River (Figure 1). Two aquifer tubes (DD-39-1 and DD-39-3) were selected for the investigation. The entrance ports of the aquifer tubes (DD-39-1 and DD-39-3) were located 1.7 and 4.5 m below the surface of the riverbed. The aquifer tubes were 0.47 cm inner diameter (ID) polymer tubes with 15.2 cm stainless screens located at the terminal end of the tubes to prevent particles from entering the aquifer tubes. The tubes were installed in the cobble beach sediment of the river by advancing a temporary casing into the riverbed and inserting the aquifer tubes. The temporary casing was slowly withdrawn allowing the gravels to collapse around the aquifer tubes.

The distance between the field deployment box and the location of the aquifer tubes entered the subsurface was approximately 13 m. Fluorocarbon tubing (0.16 cm ID) was passed through the 0.47 cm ID aquifer tube from the stainless steel screen located in the subsurface to the field deployment box for transporting the sample to the sampling module. The sampling module was composed of four three-way sample selection valves and a peristaltic pump and was capable of monitoring up to five shallow wells. A monitoring program allowed the user to select the aquifer tube to be sampled by activating the corresponding sample selection valve, and the peristaltic pump that then drew in sample water into the analytical/calibration unit. Upon completion of a sampling episode, the three-way sample selection valve was deactivated, which opened a vent to the atmosphere and cleared the sample from the sample tube. This eliminated the contamination of the walls of the sample tube caused by prolonged storage of sample water in the tube.

#### *Analytical / calibration assembly*

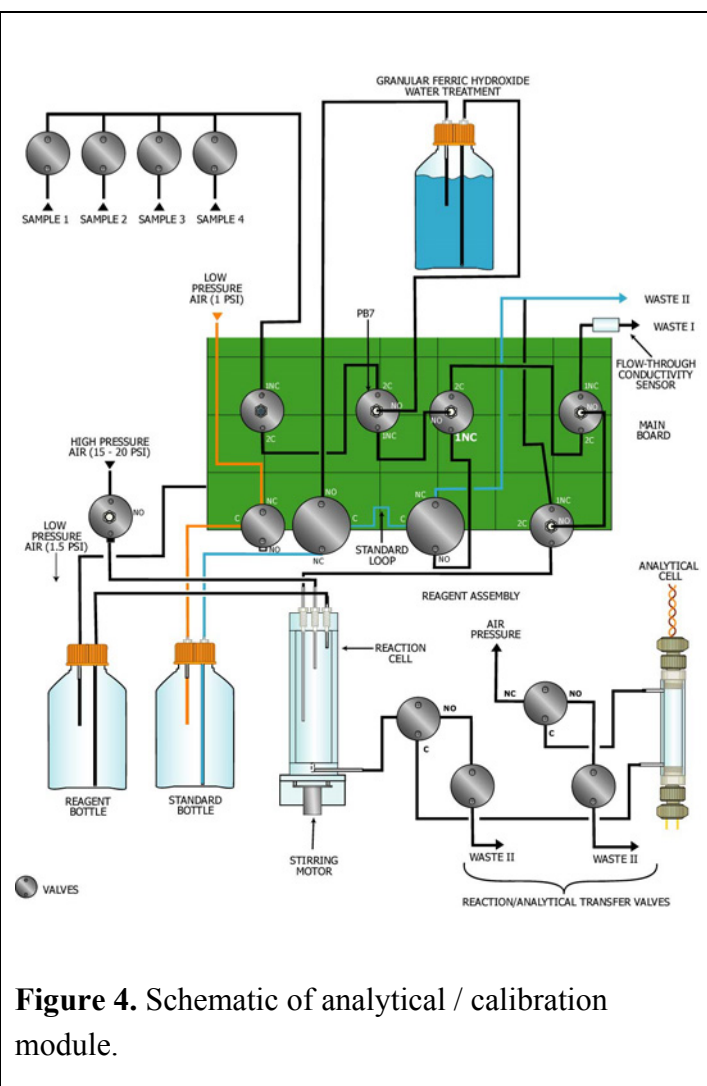
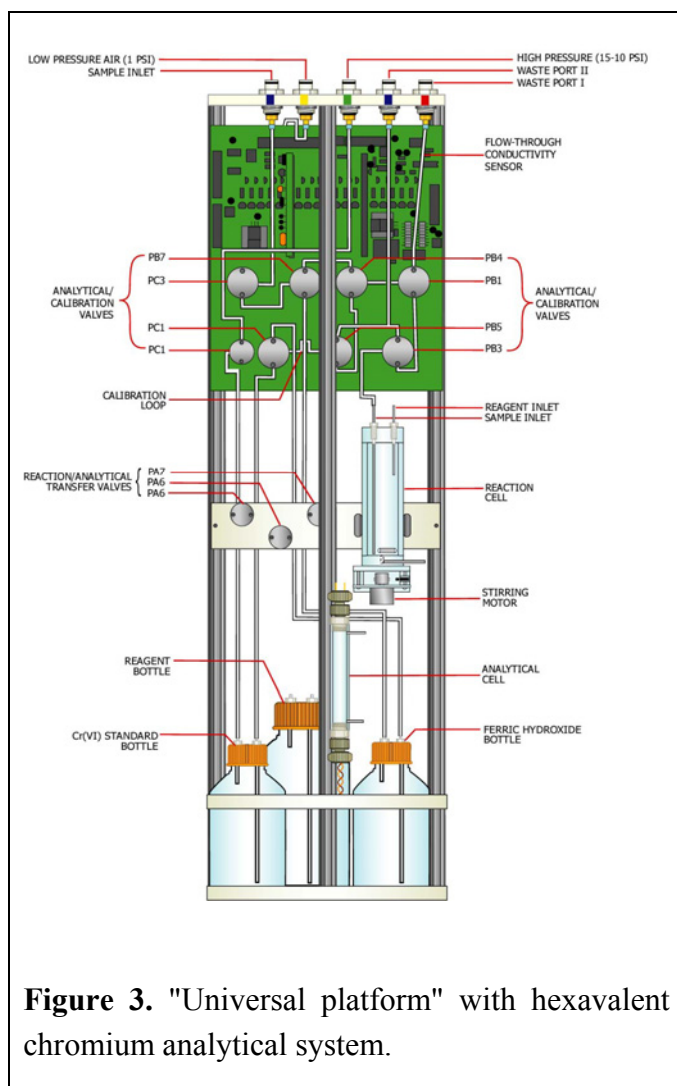
The analytical and calibration modules were combined in a cylindrical instrument 19.6 cm (7 3/4 in.) in diameter and 50.6 cm (20 inch.) high (Figure 3). The instrument was cylindrical in shape to allow for installation into the 20.25 cm OD casing located under the field deployment box (Figure 2). The analytical module was composed of the analytical cell, reaction cell, and the reagent delivery system. The calibration module was composed of several valves, and a hexavalent chromium removal (granular ferric hydroxide) and standard bottles. Schematic illustrations of the analytical and calibration modules are presented as Figures 3 and 4.

#### *Analytical module*

The analytical module had two cells: reaction and analytical cells (Figures 3 and 4). The sample reaction cell was used to mix the sample water with the colorimetric reagent forming a red solution. The resulting colored solution was transferred to the analytical cell for colorimetric measurement of the attenuation of a pulsed green light through the red solution. The analytical methodology is automated method of standard methods used in analysis of wastewater [5].

#### *Analytical cell*

Analytical cells were fabricated from a polycarbonate tube (1.26 cm, 0.5 in. ID) in lengths that varied from 1 to 15 cm (Figure 5). The length of the cell was selected based on the hexavalent chromium concentration in the water to be monitored. A limit of detection of 0.5 ppb was attained for a 15-cm tube. A 4-cm tube with an effective path length of 3 cm was used in this investigation (30 to 120 ppb concentration range).



The analytical cell had 5/16-24 threads at the terminal ends of the tube and two ports with 10-32 threads located near the end of the tube. The 10-32 ports were used to introduce and drain the sample from the analytical tube. In addition, the 10-32 fittings served as electrodes for a conductivity detector for determining when the analytical cell was filled with sample.

The source and detector of the analytical cells were fabricated from commercially available polymer chromatography fittings that connected to the 5/16-24 threads at the ends of the analytical tube. The PEEK chromatography fittings (Upchurch Scientific, Oak Harbor, WA) were modified to allow a green light emitting diode (source) and a photodetector (detector) to be mounted in the body of the fittings. The light emitting diode had a  $\lambda_{\text{max}}$  at 550 nm. A length of 400/400 silica fiber optic (Polymicro Technologies, Phoenix, AZ) was passed through the commercially available sleeves and ferrules to create watertight seals between the source and detector mounted in the fittings, and the sample contained in the analytical cell. Electrical cables connected the LED and photodetector to an electronic board for pulsing (30 Hz) the source and a lock-in amplifier to amplify and process the signal.

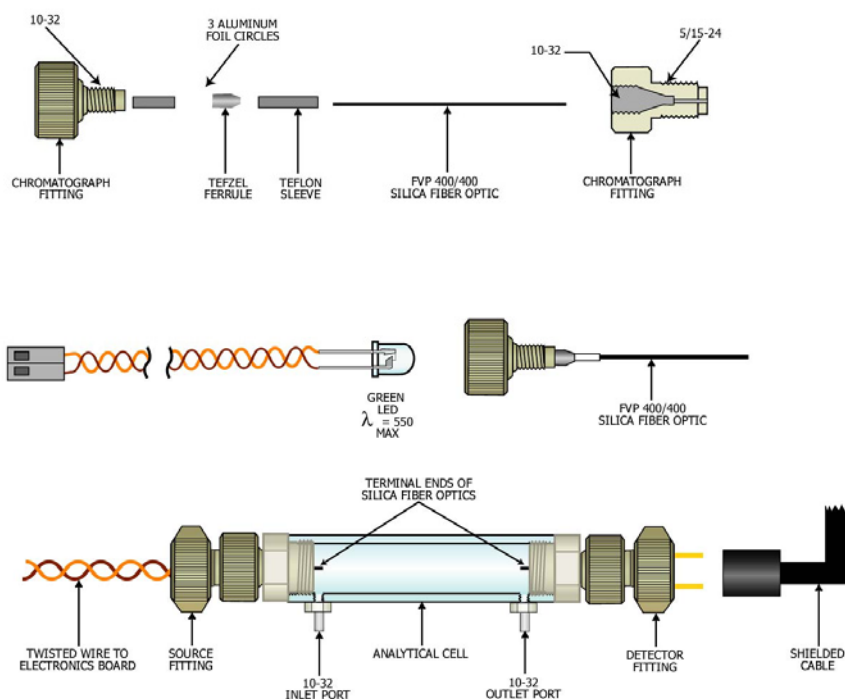


**Figure 5.** Analytical cell.

### *Reaction cell*

The reaction cell was used to mix the reagent and sample (or standard). The reagent was 250 mg of the phenylcarbazide in 500 mL of 0.1 N HCl. The reaction cell was fabricated from 3/4-inch ID polycarbonate tube and three conductivity sensors to regulate the addition of the sample water and reagent. This investigation used 10 mL of sample water and 2.5 mL of reagent for each analysis. The reagent was stored in a 500-mL bottle for dispensing into the reagent chamber. The bottle had sufficient reagent to perform over 200 analyses.

The water sample was delivered to the reaction cell by the peristaltic pump and the reagent was delivered by pressurizing (1.5 PSI) the reagent bottle. The sample/reagent solution contained in the reaction cell was mixed with a small magnetic stirrer. After the reaction was complete, the reaction cell was pressurized (1.5 PSI), transferring solution to the analytical cell for colorimetric analysis. The reactivity of the reagent was variable and the hexavalent chromium signal attenuated over time because of the reagent stability. Reagent stability was compensated by the ability of the system to recalibrate at any time the reagent lost reactivity.

### *Calibration module*

The calibration module performed two functions: creation of the blank water and creation of a three-step calibration curve. The calibration module had a three-way valve (Valve PB7 on Fig. 3 and Fig. 4) to divert sample water directly to the analytical chamber or through the calibration module. Sample water diverted directly to the reaction chamber was used for analysis of the sample water. Sample water diverted to the calibration module was passed through a filter of granular ferric hydroxide to remove the hexavalent chromium from the water (the “blank water”). Blank water was used to clean the system and create the three-step calibration curve. The three-step calibration curve

was created by injecting a stock chromium standard (2 mg/mL), using a calibration loop (0.3 mL), into the reaction cell. The program diluted the injected standard in the reaction cell with blank water to a total volume of 10 mL. The three-step calibration curve was constructed by analyzing blank, mid-value and high concentration standards. The mid-value standard was created by one injection of a loop volume into the reaction cell, and the high standard was created by two injections of a loop volume into the reaction cell. For this investigation, a hexavalent standard of 2 µg/mL was used to create a three-step calibration curve of 0, 60 and 120 ppb. The hexavalent chromium bottle contained 500 mL of stock standard capable of performing over 100 calibration curves. The hexavalent standard has been used for over 8 months in the laboratory without any significant decreases in the chromium signal.

### *Conductivity detector*

After the first deployment, it was recognized that conductivity was an important parameter to be monitored in conjunction with hexavalent chromium. The design of the monitoring system was reviewed and it was recognized that a conductivity sensor used in the operation of the monitoring system could be adapted as a flow-through conductivity cell to provide conductivity data concerning the water being sampled. The design of the conductivity detector is not similar to commercially available detectors and was not optimized for highly accurate conductivity measurements. The conductivity detector incorporated into the system allowed users to determine whether the water being sampled through the aquifer tubes was from ground water or from the Columbia River. The water conductivity of the Columbia River is significantly lower than the conductivity of ground water. The operating program of the monitoring system was modified to allow the use of the conductivity cell. The location of the flow-through conductivity cell with the analytical/calibration assembly is illustrated on Figures 3 and 4. The conductivity data were collected beginning with the second deployment on August 10, 2004.

### *Waste system*

The waste system consisted of two water treatment canisters and a 210 liter (55-gallon) plastic drum to store the treated water. Two types of wastewater were produced during the operation of the monitoring system. Wastewater I was produced during purging of sample tubes from the entrance of the aquifer tubes located in the gravel bed of the river through the analytical/calibration system. Wastewater I contained low concentrations (30 to 200 ppb) of hexavalent chromium from the ground water. Wastewater I was passed through a canister of granular ferric hydroxide to remove the hexavalent chromium from the wastewater before discharge into the 55-gallon drum. Wastewater II was produced during analysis of water samples. Wastewater II contained hydrochloric acid with reacted and unreacted reagent. Wastewater II was passed through a canister containing marble chips and activated carbon to react with the acid and remove the reagent from the wastewater prior to discharge into the 55-gallon drum. Each sampling and analysis of a sample produced approximately 50 mL of water. Assuming the monitoring system can perform 200 analyses before the colorimetric reagent must be replenished, approximately 10 liters of wastewater is produced. However the actual amount of wastewater contained in the drum, over a field deployment of several months, was significantly less than the calculated wastewater produced because of evaporation.

### *Communication system*

Communication between the remote user and the monitoring system was established with a spread spectrum frequency hopping radio modem (SRM6000, Data-Linc, Bellevue, Washington). A serial cable connected the modem located in the field deployment box to a small PLC (ADR-1000, Ontrack Control Systems, Sudbury, Ontario) located on the analytical/calibration unit. The monitoring system was controlled by a PC located at a remote location, a trailer was approximately ½ mile from the monitoring location. The program on the PC sent commands and received data via the modem from the PLC located on the analytical/calibration unit. The modem was capable of operating at distances of 12 miles. The PC located in the trailer was remotely controlled by users in Tempe, Arizona, using PC Anywhere™.

### *Analysis and quality control*

The monitoring system was designed to perform many of the analytical techniques used in fixed laboratories. The calibration system created and delivered blank (water), mid-value, and high concentration standards to the analytical chamber for analysis. The program allowed spiking of samples with the mid-value standard, and collecting duplicate samples. A typical analysis was the analysis of a calibration curve, initial blank, samples from the aquifer tube, and a final mid standard to ensure the calibration curve was valid during the analysis of the samples. The preparation and analysis of the calibration standards, midcals, samples, spikes and duplicates were automated and performed each time the user-requested sampling/analytical episode. The ability to calibrate multiple sensors with standards in the field eliminated variability between sensors in a multi-system monitoring program.

## **Results**

### *First Deployment, July 19 to July 27, 2004*

The system was first deployed adjacent to the Columbia River on July 19, 2004. The system was operated for several days until a problem developed with the analytical cell (leakage). The calibration curves and the results of the first deployment are presented on Table 1. The standards used to construct the calibrations curves for the first deployment were blank, 600 and 1200 ppb. Two calibration curves were used during the first deployment. The first curve was constructed prior to the field deployment and was used to generate the sample analysis data of July 19, 2004. The second calibration curve was constructed on July 26, 2004 and was used to generate the sample analysis data of July 26, 2004. Water samples were collected from two aquifer tubes on July 19, 2004 for laboratory analysis. The laboratory result for the sample collected from DD-39-3 was 102 ppb and the sample collected from DD-39-1 was 32 ppb. The monitoring system recorded concentrations of 104, 104, 103 and 104 ppb for DD-39-3 and 47 and 40 ppb for DD-39-1 on July 21 and July 26, 2004. The large concentration range (0, 600, 1200) of the calibration curve was not optimal for the hexavalent chromium concentrations (30 to 100 ppb) being monitored in this deployment.

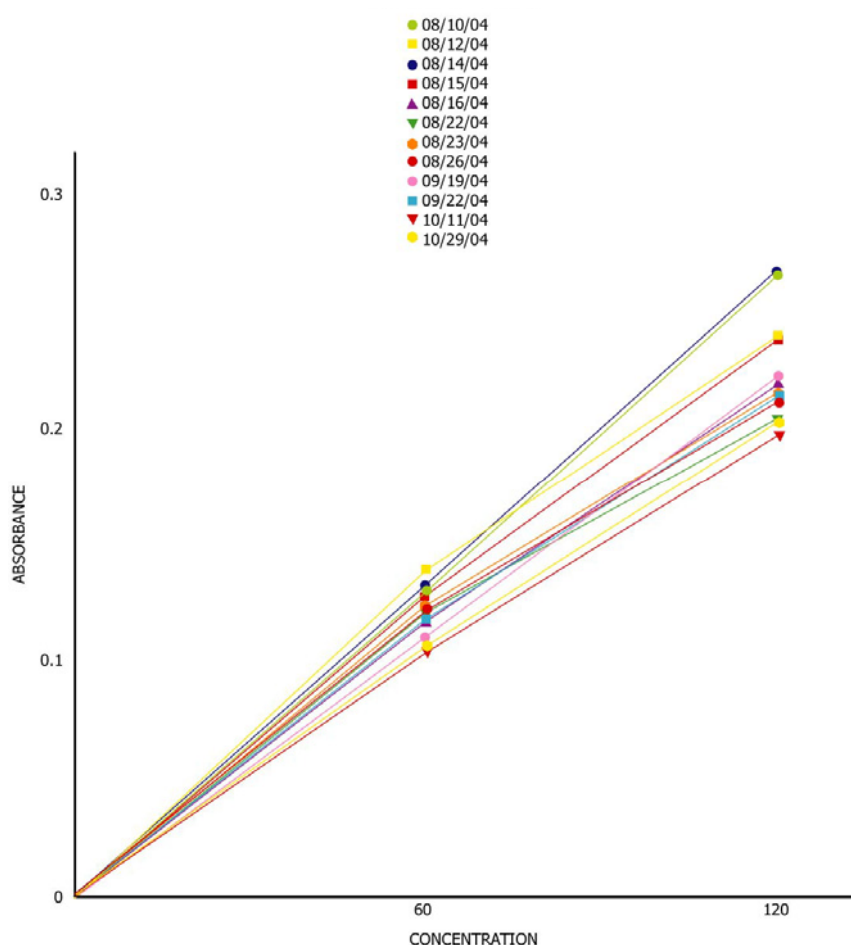
**Table 1.** Sample results for first hanford deployment July 19-July 26, 2004.

Date	Sample Name	Time	Cr(VI) Conc. ppb
7/21/04	DD-39-3		104
	DD-39-3	12:31	104
	DD-39-1	12:30	47
	Midcal	13:09	537
7/26/04	DD-39-3	15:05	103
	DD-39-1		40
	DD-39-3		104

### *Second Deployment, August 10 to October 29, 2004*

The system was redeployed to the field on August 10, 2004. The monitoring system was modified to allow for the collection of conductivity data. The system was operated continuously from August 10 until the date of the preparation of the paper on October 29, 2004. The operations were suspended from August 25 to September 22 because the reagent required replenishment.

A total of nine calibration curves were generated during this time period (Figure 6). The analytical results for the two-aquifer tubes (DD-39-1 and DD-39-3) during this time period are presented on Figures 7 and 8.

**Figure 6.** Cr(VI) calibration curves (0, 60, 120 ppb) 2<sup>nd</sup> deployment.

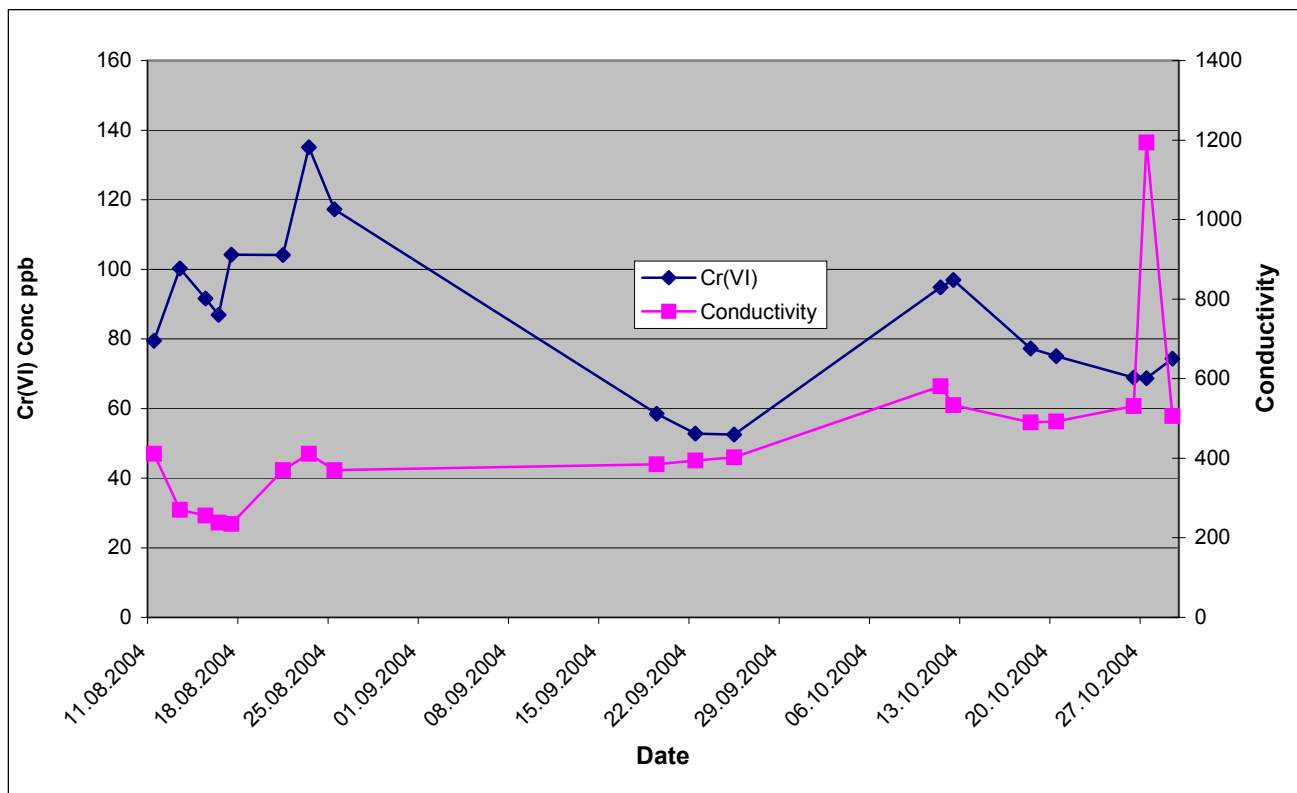


**Figure 7.** Hexavalent chromium & conductivity for aquifer tube DD-39-1 August 11-October 29, 2004.

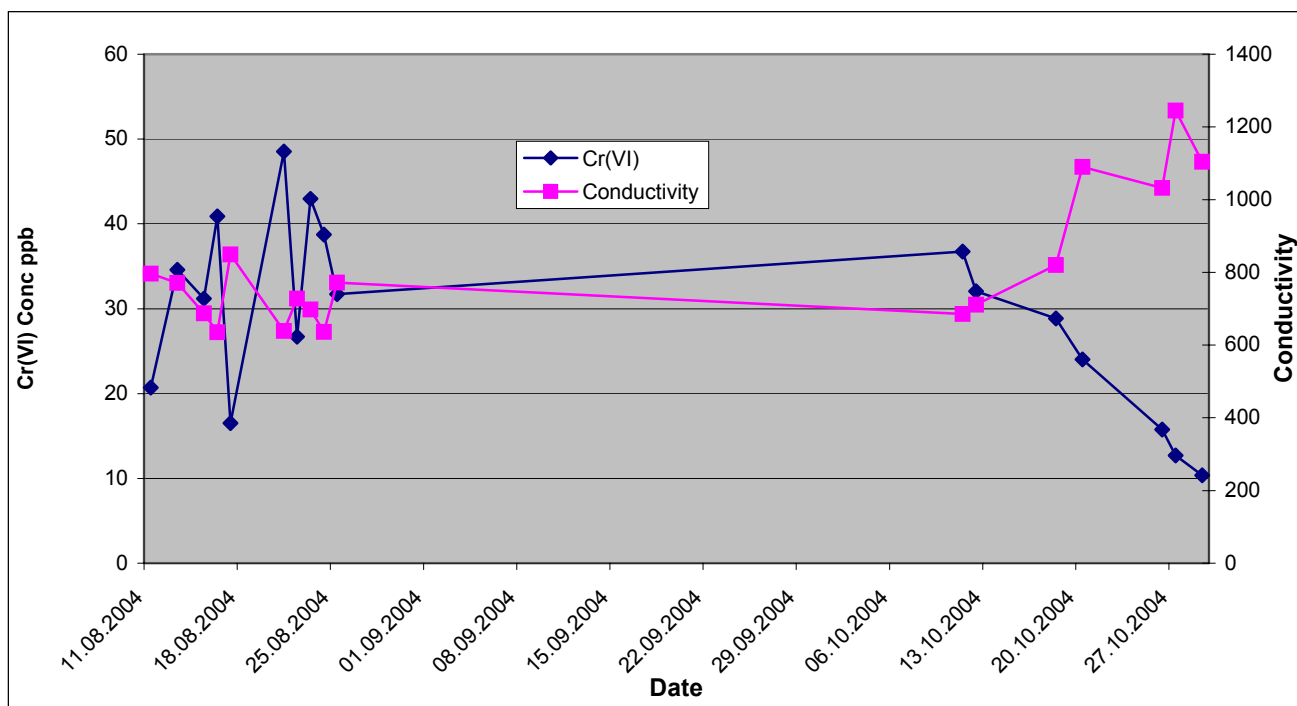


**Figure 8.** Hexavalent chromium & conductivity for aquifer tube DD-39-3 August 11-October 29, 2004.

There is a very significant difference in the hexavalent chromium concentrations for the monitoring of DD-39-3 between the analyses performed prior to August 25, 2004, and analyses collected after September 20, 2004. The water level in the Columbia River dropped (2 to 3 feet) during this timeframe.

One of the conductivity sensors of the monitoring system was modified to allow collection of conductivity data. The conductivity cell was a flow-through cell. The conductivity data for aquifer tube DD-39-1 was more stable than for the data produced by aquifer tube DD-39-3. The flow-through conductivity cell is very sensitive to the presence of air bubbles. If the water tubes were not completely flushed of air bubbles, the conductivity data is not representative of the water being sampled. It is believed that air bubbles were being generated during the sampling of DD-39-3. The source of the air bubbles was probably in the sample selection valve and associated tubing in the sample module, or incomplete purging of the line before conductivity measurements.

### Quality control data

The monitoring system was capable of analyzing a system blank and final mid-value calibration standard as a continuing check on the validity of data being produced by the system. The concentrations of the mid value calibration standards analyzed are illustrated on Figure 9.

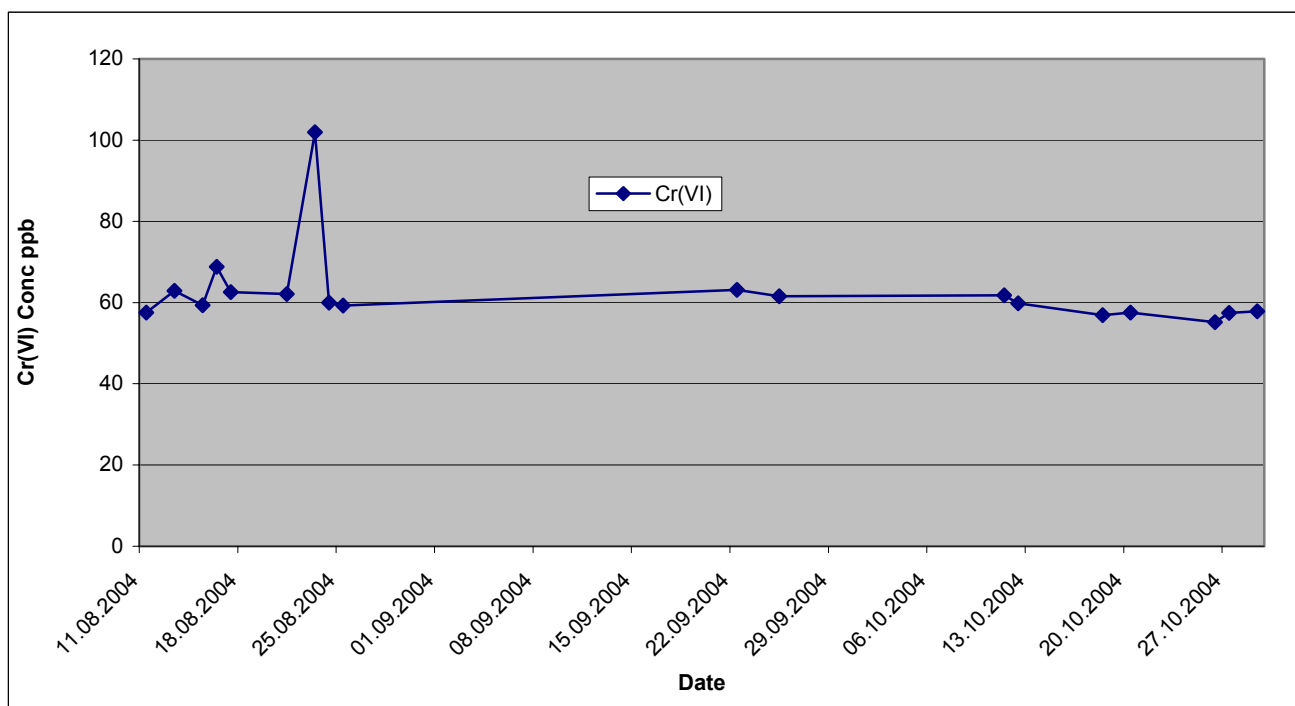


**Figure 9.** Results of mid-calibration standards August 11-October 29, 2004.

### Conclusions

The hexavalent chromium monitoring system has been shown to be a reliable system for collecting and analyzing of aquifer tube samples over the course of over two months. The system was capable of monitoring in the concentration range of 30 to 120 ppb with internal calibration. The system

demonstrated the ability to exceed the key specifications present in the introduction. After the beginning of the second deployment (August 10, 2004), the operation and maintenance of the system was restricted to one replenishment of reagent. The system is capable of performing 100 analyses before replenishing the colorimetric reagent. The system can be used to collect and analyze samples every fifteen minutes. Compared to current monitoring methods, the system is capable of determining with greater resolution and frequency the hexavalent chromium concentrations in the gravels beneath the river.

This investigation demonstrated:

- A robust application of an automated ‘universal’ monitoring system
- Accurate calibration can be performed automatically in the field
- Low cost sampling and analysis
- Agreement with current sampling and analytical laboratory results
- Ability to adopt standard methods for automated field use
- Ability to incorporate transition ready technologies into field application

## Acknowledgements

This work was funded by the US Department of Energy, Advanced Monitoring System Initiative (AMSI), John Jones, Manager, with support from Bechtel Nevada and the Nevada Test Site. Special thanks to Dr. Scott Peterson and Jerry Isaacs of Flour Hanford, Dr. John Hartman, Dr. Robert Peterson, and Wayne Martin of PNNL for continued on-site field support. Shira Garza, Michael Clay, and Evan Arntzen of PNNL provided field support. The Pacific Northwest Laboratory (PNNL) is a multi-program national laboratory operated by U.S. Department of Energy by Battelle Memorial Institute.

## References

1. Burge, S.R.; Hoffman, D.A. Automated monitoring of chloroform and trichloroethene using a halocarbon-specific optrode. *American Laboratory*, **2003**, *35*, 24.
2. Burge, S.R. Automated analysis of trichloroethene and chloroform. *Proceedings of the 9<sup>th</sup> International Conference of Environmental Remediation and Radioactive Waste Management*, September 25, **2004**, Oxford, England.
3. Burge, S.R.; May, J. Automated ground water sampling and analysis of trichloroethene using a “universal” sampling/analytical system. *Ground Water Monitoring & Remediation*, In press.
4. Hartman, M.J.; Morasch, L.F.; Webber, W.D., (Eds.) Summary of Hanford site groundwater monitoring for fiscal year 2003. Pacific Northwest Laboratory, PNNL 14548-SUM, **2004**, pp. 14.
5. Clesceri, L.S.; Greenburg, A.E.; Trussel, R.R.,(Eds.) Standard methods for the examination of water and wastewater. American Public Health Association, **1989**, pp. 3.

## **Cerenkov Counter for In-Situ Groundwater Monitoring of $^{90}\text{Sr}$**

**Robert C. Runkle\***, Ronald L. Brodzinski, David V. Jordan, John S. Hartman, Walter K. Hensley, Melody A. Maynard, William A. Sliger, John E. Smart and Lindsay C. Todd

Pacific Northwest National Laboratory, 902 Battelle Boulevard, P.O. Box 999, Richland, WA, 99352

\* Author to whom correspondence should be addressed. E-mail: [robert.runkle@pnl.gov](mailto:robert.runkle@pnl.gov)

*Received: 07 September 2004 / Accepted: 03 December 2004 / Published: 28 February 2005*

---

**Abstract:** Groundwater contamination from  $^{90}\text{Sr}$  is an environmental challenge posed to present and former nuclear weapons related sites. Traditional methods of extracting groundwater samples and performing laboratory analyses are expensive, time-consuming and induce significant disposal challenges. The authors present here a prototype counter capable of measuring  $^{90}\text{Sr}$  groundwater concentrations in-situ at or below the drinking water limit of 8 pCi/liter. The  $^{90}\text{Y}$  daughter of  $^{90}\text{Sr}$  produces high-energy electrons, which can create Cerenkov light. Photomultiplier tubes convert the Cerenkov light into an electronic pulse, which then undergoes signal processing with standard electronics. Strontium-90 concentrations near the drinking water limit can be measured in a matter of hours if it is in secular equilibrium with the  $^{90}\text{Y}$  daughter. The prototype counter is compact, can be deployed in an American Standard 6-inch, well while operated by a single person, and transmits the results to a central monitoring location.

**Keywords:** strontium-90, groundwater monitoring, Cerenkov light.

---

## Introduction

The radionuclide  $^{90}\text{Sr}$  is a common fission product with a half-life of 28.78 years. Large quantities of  $^{90}\text{Sr}$  exist in effluent produced by fuel reprocessing and reactor operation. Because it concentrates in the skeletal system of humans, it presents an environmental challenge to the Department of Energy (DOE) at nuclear weapons related sites such as: Savannah River, South Carolina; Oak Ridge, Tennessee; Los Alamos, New Mexico; and Hanford, Washington. This issue is especially pertinent to the Hanford site where plumes of  $^{90}\text{Sr}$  effluent present in ground water enter the Columbia River.

Groundwater concentrations are presently monitored in areas where known  $^{90}\text{Sr}$  plumes reside. The goal is to ensure that the concentrations entering the Columbia River remain well below the free-release limit of 8 pCi/liter and to assess the performance of remediation efforts. Current monitoring practices are time-consuming and expensive. They require extracting down well samples, performing laboratory analysis, and waste disposal.

The authors present here a significantly more efficient method for monitoring  $^{90}\text{Sr}$  groundwater concentrations, which can be performed in-situ and on a daily basis. This method also provides immediate results and creates no disposal problems. The prototype counter described below is an improvement over previous designs [1] that measure  $^{90}\text{Sr}$  concentrations via the Cerenkov light produced from beta-decays.

## Detector concept

Strontium-90 decays via beta-decay and emits an electron with a maximum energy of 546 keV. The daughter nucleus,  $^{90}\text{Y}$ , has a half-life of only 64.10 hours and also undergoes beta-decay with a maximum electron energy of 2282 keV. The decay of  $^{90}\text{Y}$  produces the stable isotope  $^{90}\text{Zr}$ . Figure 1 shows the relative intensity of the emitted electrons as a function of energy. Note that the majority of  $^{90}\text{Y}$  decays have electron energies above the  $^{90}\text{Sr}$  endpoint.

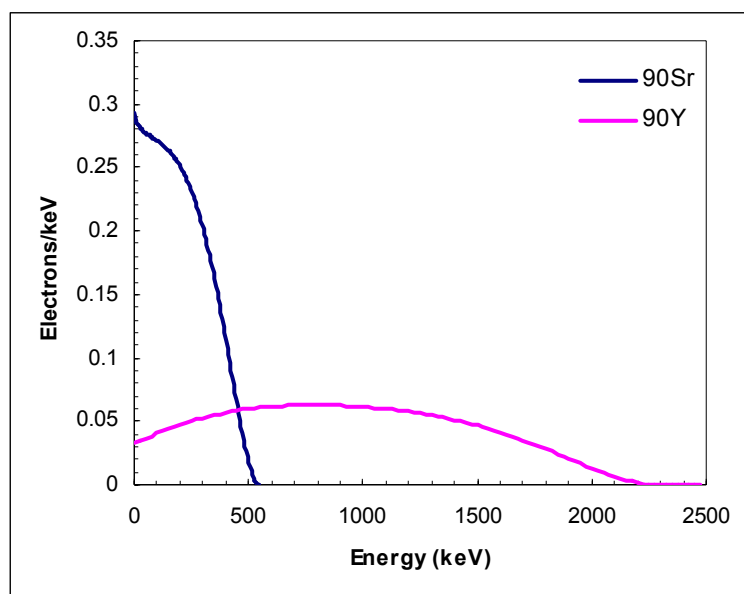


**Figure 1.** Graph of relative intensity for electrons emitted by  $^{90}\text{Sr}$  and  $^{90}\text{Y}$ .

High energy charged particles (electrons above  $\sim 250$  keV in water) traveling through optically transparent materials with an index of refraction greater than unity produce Cerenkov light. The particle's momentum restricts this light emission to a cone centered along the direction of the particle's path. The Cerenkov light that reaches the photocathode of a photomultiplier tube (PMT) can be converted into an electronic signal. The pulse height of this signal is proportional to the energy of the charged particle.

Since water is transparent to Cerenkov light and can easily be confined to a known volume, measurement of Cerenkov light provides a simple technique for measuring high-energy beta decays occurring in a groundwater sample. The majority of  $^{90}\text{Sr}$  decays will not produce Cerenkov light since their energy will be below the  $\sim 250$ -keV threshold. In contrast,  $^{90}\text{Y}$  is a prolific producer of Cerenkov light, due to its higher mean beta-decay energy. An unambiguous measurement of decays from  $^{90}\text{Y}$  results from only counting events recorded above the  $^{90}\text{Sr}$  endpoint. A sample's  $^{90}\text{Y}$  activity is a function of the initial  $^{90}\text{Sr}$  and  $^{90}\text{Y}$  activities,  $A_{^{90}\text{Sr}}^o$  and  $A_{^{90}\text{Y}}^o$ , and the decay constants,  $\lambda$ , for each nuclei:

$$A_{^{90}\text{Y}} = A_{^{90}\text{Y}}^o \cdot e^{-\lambda_{^{90}\text{Y}}t} + \frac{\lambda_{^{90}\text{Y}}A_{^{90}\text{Sr}}^o}{\lambda_{^{90}\text{Y}} - \lambda_{^{90}\text{Sr}}} \cdot \left( e^{-\lambda_{^{90}\text{Sr}}t} - e^{-\lambda_{^{90}\text{Y}}t} \right) \quad (1)$$

The  $^{90}\text{Sr}$  concentration of samples in secular equilibrium can be deduced from a single measurement of the  $^{90}\text{Y}$  activity, since secular equilibrium implies a  $^{90}\text{Sr}$  to  $^{90}\text{Y}$  initial activity ratio ( $A_{^{90}\text{Sr}}^o : A_{^{90}\text{Y}}^o$ ) of unity, which is temporally constant. But there is no assurance that samples collected in the field exist in secular equilibrium, since the chemical interactions in soil and other permeable barriers may affect the movement/retention of strontium and yttrium differently. Samples not in secular equilibrium may have an initial activity ratio of Sr/Y greater or less than one. Those with a ratio greater than unity correspond to environments where  $^{90}\text{Sr}$  more freely enters the groundwater, or, alternatively, where the  $^{90}\text{Y}$  would be preferentially removed from the groundwater by the soil. However, because soil generally has a larger affinity for  $^{90}\text{Sr}$ , an initial activity ratio less than unity is more common. In this case, the  $^{90}\text{Y}$  activity will decrease with time and asymptotically approach the point of secular equilibrium, where the two activities are equal.

Figure 2 shows the behavior of the  $^{90}\text{Y}$  activity for various initial activity ratios where the  $^{90}\text{Y}$  activity exceeds the  $^{90}\text{Sr}$  activity and has an initial value of unity (in arbitrary units). By securing the sample in the chemically stable environment of the counter, one ensures that  $^{90}\text{Sr}$  and  $^{90}\text{Y}$  are lost only via beta-decays. After measuring the  $^{90}\text{Y}$  activity at two or more points in time, the data can be fit to the decay curves of Figure 2; the  $^{90}\text{Sr}$  concentration can then be deduced.

Beta decay is not the only process that produces Cerenkov light; cosmic rays and terrestrial  $\gamma$ -rays may also contribute. Background from cosmic rays primarily results from high-energy (GeV) muons created in the upper atmosphere. These muons interact in the same way high-energy electrons do. Similarly, terrestrial  $\gamma$ -rays above approximately 410 keV can Compton scatter in water producing electrons of varying energies, which themselves then can create Cerenkov light. The principle sources of terrestrial radioactivity stem from nuclei in the  $^{232}\text{Th}$  and  $^{238}\text{U}$  decay chains along with  $^{40}\text{K}$ , all of which are present in soil.

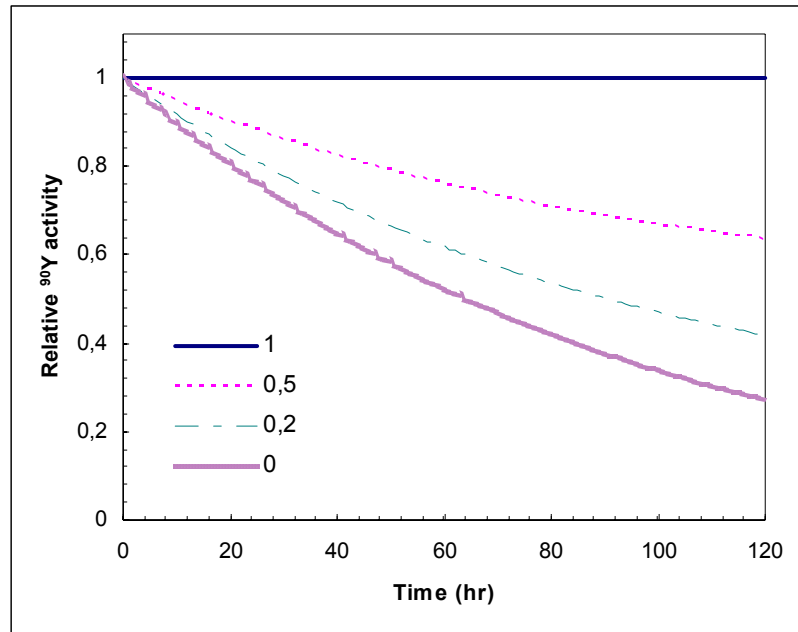


**Figure 2.** Graph of the relative  $^{90}\text{Y}$  activity as a function of the initial activity ratio ( $A_{^{90}\text{Sr}}^o : A_{^{90}\text{Y}}^o$ ). The four ratios plotted above are 1, 0.5, 0.2, and 0. The top line, corresponding to an initial activity ratio of unity, results from a sample initially existing in secular equilibrium. The remaining curves asymptotically approach secular equilibrium. The bottom curve, representing the case where no  $^{90}\text{Sr}$  is present, asymptotically approaches zero and is simply the  $^{90}\text{Y}$  decay curve with a 64.1 hour half-life. Not shown here are curves that would increase if the initial  $^{90}\text{Sr}$  concentration exceeded that of  $^{90}\text{Y}$ .

The contributions from these sources of background vary depending on the field environment. Bowyer, et al., [1] reported cosmic rays as the dominant source of background. However, for down-well applications, where the counter is surrounded by soil containing terrestrial radioactivity,  $\gamma$ -rays present the largest background.

### Physical modeling and conceptual design

The chief constraints on the detector design presented here derive from two factors. First, it has to fit down-well, which in our specific application implies a diameter of less than 15 cm and a maximum total length of 1.8 m. Second, the counter must accurately measure concentrations down to 8 pCi/liter, the drinking water limit, in a reasonable amount of time, i.e. hours. This requires maximizing the counter's detection efficiency. With these general parameters in mind, the authors investigated various geometries using the simulation code GEANT4 [2] which modeled all aspects of the detector from the energy distribution of electrons produced during beta-decay to the photomultiplier tube response.

Figure 3 displays a typical simulation geometry in which the counter is immersed in a volume of soil. Model calculations varied the inner diameter and length of the water cavity within the limits mentioned above. The top and bottom end of the cavity were fit with quartz windows while the inside surface was lined with Teflon (95% reflectivity). Calculations included light attenuation and internal reflections. All beta-decays were produced at points randomly distributed throughout the water volume. Although the simulation results were only used in constraining the design parameters

discussed below, prior to counter construction their accuracy was partially validated by reproducing the detection efficiency of the Bowyer counter [1].

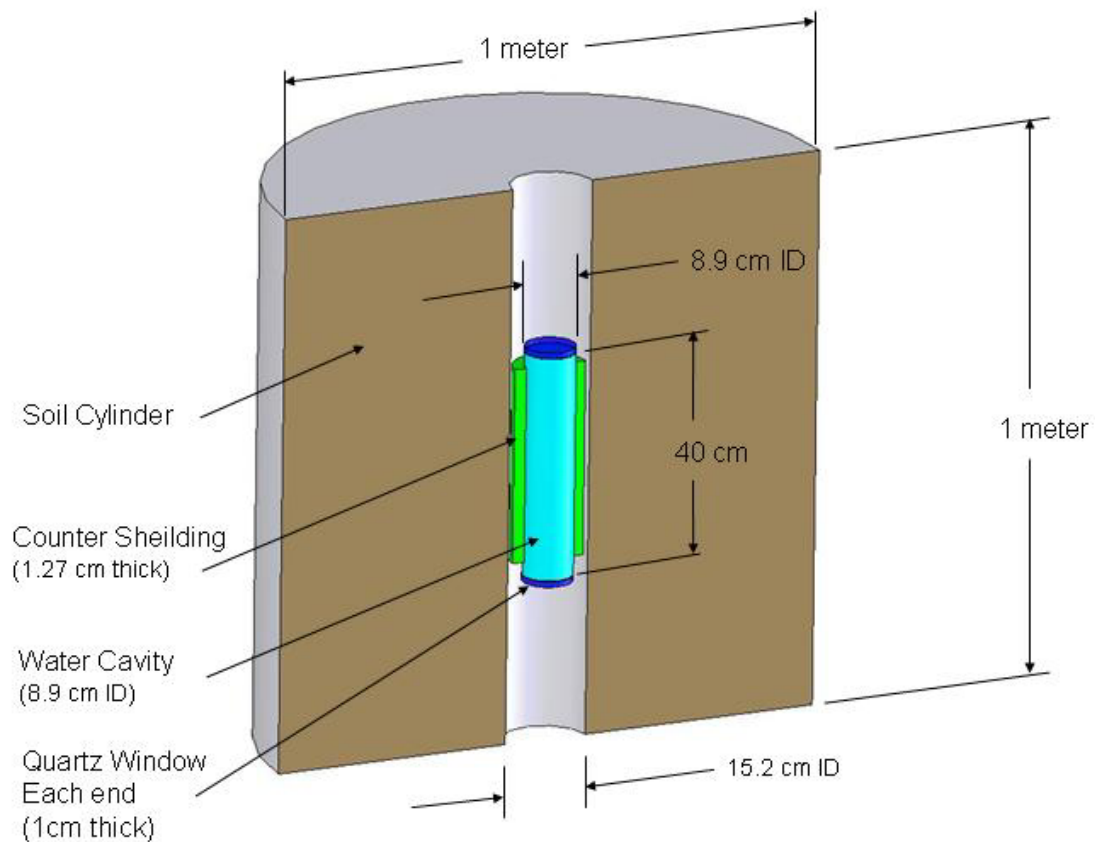


**Figure 3.** The simulation geometry includes a water cavity, shielding (active or passive), and surrounding soil. Essentially all of the gamma-ray flux entering the counter is accounted for with the 1-m right circular cylinder of soil shown here. Not shown in the figure is a disk above the counter from which trajectories of cosmic rays were calculated.

The most important design parameter influencing the detection efficiency, i.e. count rate, is the water cavity volume. For a fixed diameter, the count rate increases with the counter length due to the presence of more beta-decays. The relationship is asymptotic due to the attenuation of light traveling through large distances of water. A further complexity is the existence of dark current in PMTs. PMT dark currents create electronic noise and false signals. One technique for dramatically reducing this effect is to require a coincidence between two PMTs. Since the propagation of Cerenkov light is restricted to a cone in the direction of the electron's momentum, requiring a coincidence between multiple PMTs installed on one of the counter's ends is one option for reducing noise, i.e. single-ended coincidence. A second option is to employ one PMT on each end surrounded by a Teflon reflecting ring.

As shown in Figure 4, light that is emitted towards one end of the tube will reflect and, if not attenuated, create a coincidence at the opposite end, i.e. two-end coincidence.

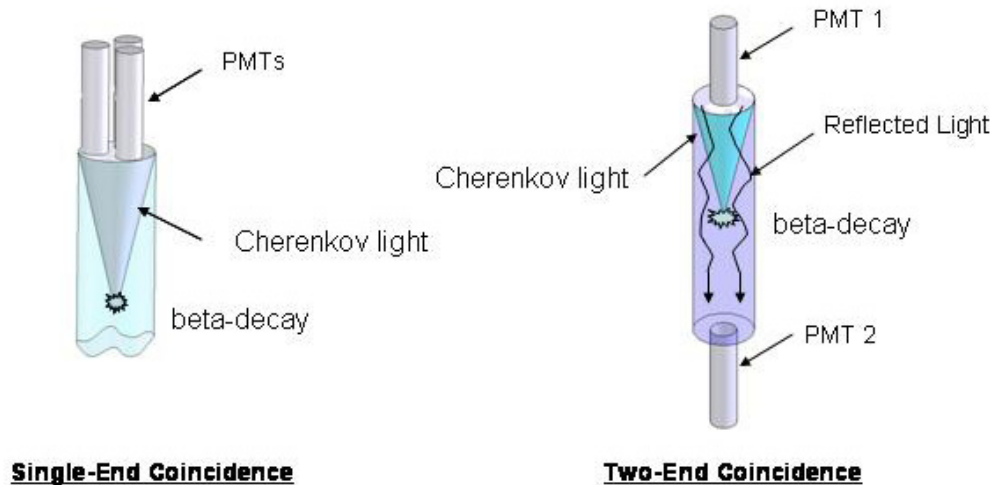


**Figure 4.** Two possible coincidence techniques that serve to reject PMT dark current events.

Figure 5 compares the signal rate for various PMT configurations as a function of water cavity length and coincidence requirements. Single-ended coincidence schemes have an asymptotic behavior while configurations with an opposite-end coincidence requirement have an optimal length. This peaked behavior results from a balance of having more signal events in a longer counter with the attenuation of the reflected light over the length of the counter.

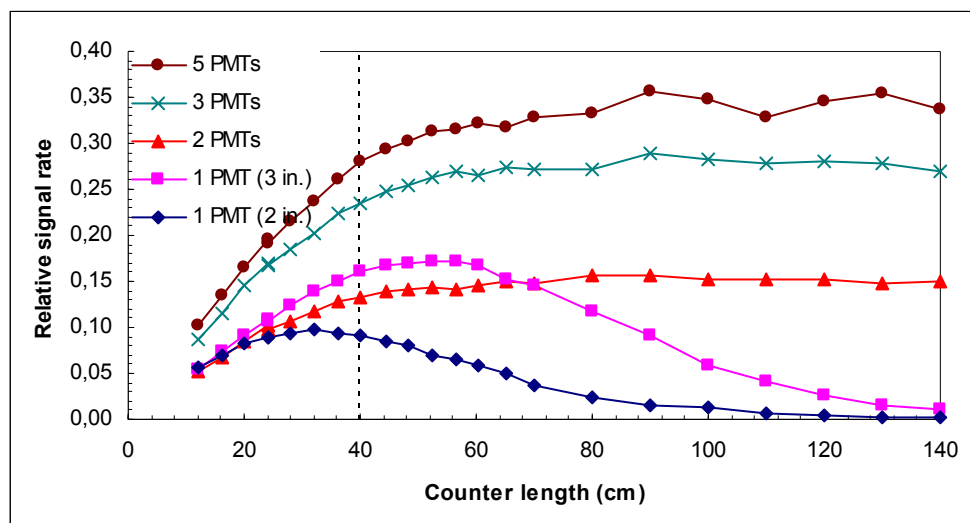


**Figure 5.** Graph of the relative event rate in the water cavity as a function of counter length and number of PMTs on each end. Configurations with more than one PMT per end have single-end coincidence requirements while those with only one PMT have a two-end requirement.

The second crucial design parameter is the background shielding configuration. Both terrestrial gamma rays and cosmic rays were included in the background simulation. The soil served as a generator of the  $\gamma$ -ray background, and the model assumed soil activity concentrations of 0.7 pCi/g for  $^{232}\text{Th}$ , 0.4 pCi/g for  $^{238}\text{U}$ , and 10 pCi/g for  $^{40}\text{K}$  [3]. The cosmic-ray generator consisted of muons with initial positions uniformly distributed on a disk-shaped surface above the counter with a momentum distribution given by Kremer, et al., [4] and an angular distribution of  $\cos^2(\theta)$ , where  $\theta$  is the angle

normal to the soil. The resulting event rates in an 8.9-cm diameter by 40-cm long cylinder with no shielding were 1800 Hz for gamma rays and 5 Hz for cosmic rays. This result focused the design on eliminating the terrestrial  $\gamma$ -ray background.

To this end, the authors considered both active and passive configurations for background reduction. The goal of active shielding is to detect the penetrating radiations so that coincident signals in the Cerenkov counter can be vetoed and not misidentified as beta-decay events; passive configurations attempt to absorb penetrating radiations before they enter the counter. The active method modeled here was a veto shield surrounding the sample cylinder composed of BGO, NaI(Tl) or CsI(Na). Both gamma rays and cosmic rays have a high probability of depositing some energy in these materials, especially BGO. The authors also considered passive shields of lead and tungsten, which absorb gamma rays from the surrounding soil but have little impact on cosmic rays because of their enormous energy. Another background reduction strategy is to reject cosmic-ray events depositing large energies. An upper-level pulse height cut applied to the PMT signal above the maximum  $^{90}\text{Y}$  energy greatly assists in reducing the cosmic-ray background rate. The count rates for a 1.27 cm thick annulus surrounding the water cavity from each approach are displayed in Figure 6. The active veto shields are significantly more effective in rejecting background radiation.

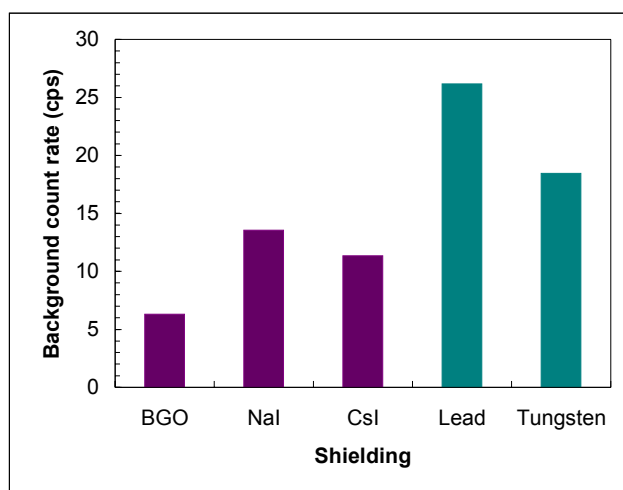


**Figure 6.** Background count rates for a cylindrical water cavity 40 cm long and 8.9 cm in diameter with 4 PMTs at each end operated in a single-ended coincidence mode. In each case, the shield is an annulus 1.27 cm in diameter. The three active shields considered were the scintillators BGO, NaI(Tl) and CsI(Na); lead and tungsten are passive shields.

### Counter design

Based on the simulation results discussed above and costs associated with design, materials, and electronics, the decision to build a prototype counter with a single PMT on each end and passive tungsten shielding was made. The prototype counter design consists of a cylindrical water cavity, 8.9 cm in diameter and 40 cm long, defined by a tungsten annulus of thickness 2.1 cm, as shown in Figure 7. Two quartz windows provide a water tight and transparent seal for 5.08-cm diameter PMTs on each end. The 40-cm cavity length is optimal for this PMT configuration. The inside of the tungsten

cavity is coated with a Teflon reflector including the annular area adjacent to the PMTs. A stainless-steel housing encloses the tungsten annulus, PMTs, and space for a water pump, vent line, and electronics.

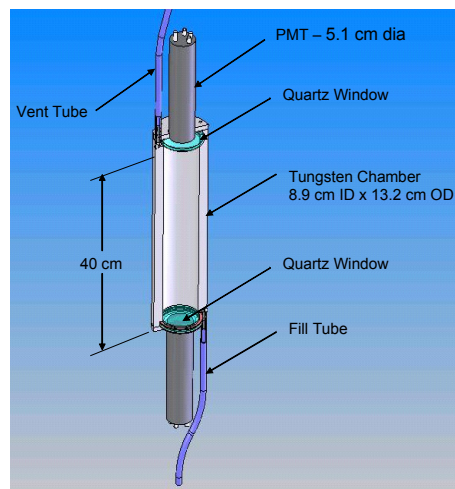


**Figure 7.** Schematic of the  $^{90}\text{Sr}$  final design which includes a passive tungsten shield and two 5.1-cm diameter PMTs.

In the prototype design reported here, all signal processing occurs at the surface of the well is using standard NIM electronics. High voltage enters, and signals exit, the counter through water-tight connections on its top. The signal processing electronics shown in Figure 8 have two principal features: 1) a lower level discriminator on each PMT and a coincidence requirement between both PMTs to prevent triggering on electronic noise; and 2) an upper level discriminator on the sum of both PMT signals to reject cosmic-ray events above the maximum  $^{90}\text{Y}$  electron energy. Signals remaining after applying these criteria are counted as potential  $^{90}\text{Y}$  decays and sent to a laptop computer.

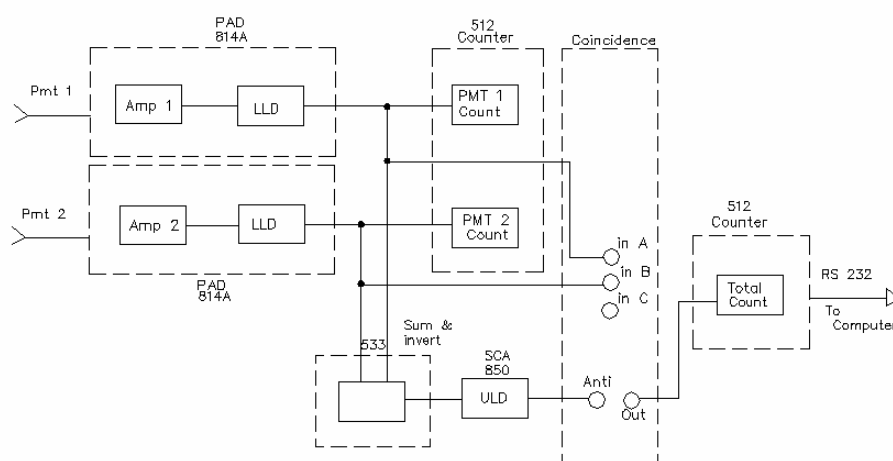


**Figure 8.** The signal processing electronics, presently located above ground, incorporate the Canberra modules noted above. The two essential criteria are the coincidence requirement between each phototube and an anti-coincidence veto if the signal exceeds an upper level discriminator.

The authors tested this counter with samples from a Hanford site well whose  $^{90}\text{Sr}$  concentrations were  $\sim 1000$  pCi/liter, and which are in secular equilibrium. The authors counted the samples in an above ground laboratory environment where background from soil was reduced relative to down well operation. Figure 9 displays a pulse height spectrum for this sample. The region to the right of the vertical dashed line corresponds to the region above the lower level discriminator of Figure 8 while the right end of the graph marks the upper level cosmic-ray discriminator.

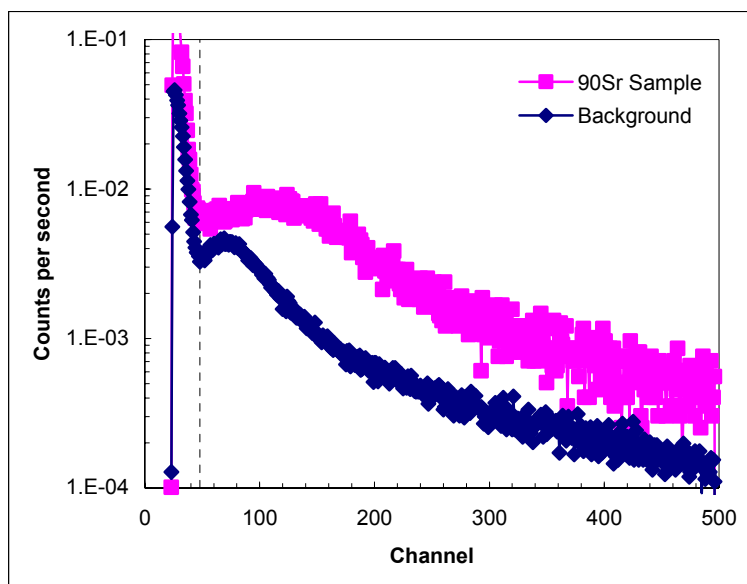


**Figure 9.** Pulse height spectrum for PMTs in two-end coincidence mode. The pulse height represents the sum of both PMTs.

### Field operation

The ultimate use of this counter is for unmanned field measurements. The prototype presented here can be deployed from the back of a pickup truck and lowered into a well. (Future incarnations will contain all signal processing inside the stainless steel shell located down-well.) In either case, a power supply and transmitter located above ground feed the results via cellular communications to a central monitoring station. Water samples will be pumped into and out of the counter through an in-counter pump and particulate filter.

### Conclusions

The authors constructed and calibrated a prototype counter for monitoring  $^{90}\text{Sr}$  contamination in ground water. It consists of a cylindrical water cavity, 8.9 cm in diameter and 40 cm long. Groundwater samples with  $^{90}\text{Sr}$  concentrations down to the drinking water limit of 8 pCi/liter can be analyzed on a daily basis. The detector is a field-deployable device and is equipped with wireless communications for remote monitoring.

## Acknowledgements

This work is funded by the US DOE Office of Environmental Management's Advanced Monitoring System Initiative (AMSI), which is managed the DOE Nevada Operations Office with assistance from Bechtel Nevada and the Nevada Test Site. The Pacific Northwest National Laboratory is a multiprogram national laboratory operated for the U.S. Department of Energy by Battelle Memorial Institute. The authors wish to thank Fluor Hanford for providing groundwater samples. This report is PNNL-SA-42973.

## References

1. Bowyer, T.W.; Geelhood, B.D.; Hossbach, T.W.; Hansen, R.; Wilcox, W.A. In situ, high sensitivity, measurement of  $^{90}\text{Sr}$  in ground water using Cerenkov light. *Nuclear Instruments and Methods in Physics Research A.*, **2000**, 441, 577.
2. Agostinelli, S.; Allison, J.; Amako, K.; Apostolakis, J.; Araujo, H.; Arce, P.; Asai, M.; Axen, D.; Banerjee, S.; Barrand, G.; et. al. GEANT4 -- a simulation toolkit. *Nuclear Instruments and Methods in Physics Research A.*, **2003**, 506, 250.
3. Lide, D.R., (Eds.) Handbook of Chemistry and Physics. CRC Press, **1978-1979**; 59<sup>th</sup> edition, pp. F-199.
4. Kremer, J. Measurements of ground-level muons at two geomagnetic locations. *Physics Review Letters*, **1999**, 83, 4241.

## **In-situ LIF Analysis of Biological and Petroleum-based Hydraulic Oils on Soil**

**Matthias Lemke, Rebeca Fernández-Trujillo and Hans-Gerd Löhmannsröben\***

University of Potsdam, Institute of Chemistry, Karl-Liebkecht-Str. 24-25, D-14476 Potsdam-Golm

\* Author to whom correspondence should be addressed. Email: [pcs@chem.uni-potsdam.de](mailto:pcs@chem.uni-potsdam.de)

*Received: 02 September 2004 / Accepted: 20 December 2004 / Published: 28 February 2005*

---

**Abstract:** Absorption and fluorescence properties of 4 hydraulic oils (3 biological and 1 petroleum-based) were investigated. *In-situ* LIF (laser-induced fluorescence) analysis of the oils on a brown sandy loam soil was performed. With calibration, quantitative detection was achieved. Estimated limits of detection were below ca. 500 mg/kg for the petroleum-based oil and ca. 2000 mg/kg for one biological oil. A semi-quantitative classification scheme is proposed for monitoring of the biological oils. This approach was applied to investigate the migration of a biological oil in soil-containing compartments, namely a soil column and a soil bed.

**Keywords:** *in-situ* optical oil sensor, lubricants, hydraulic oils, soil, laser induced fluorescence.

---

## Introduction

Due to the limitation of petroleum resources and to potential environmental risks arising from the usage of petroleum products there is a strong interest to substitute petroleum-based lubricants, oils and fuels by renewable and better biodegradable products. Properties, environmental benefits and risk assessment of so-called green lubricants, often also referred to as oleochemical or vegetable-based lubricants, have been discussed [1-3]. For Germany, the following numbers may be illustrating [1]: In the year 1998, about 1 million tons of lubricants were sold, ca. 150,000 tons among these were hydraulic oils (ca. 100,000 tons for stationary, 50,000 tons for mobile devices, [4]). It is believed that about 50%, i.e. ca. 500,000 tons of lubricants, entered the environment as pollutants [5]. As an estimate, only 2.5% of the lubricants are considered to be of biological origin [1]. In the last years much effort has been undertaken to replace petroleum products as constituents of hydraulic oils. The German federal environmental agency (Umweltbundesamt UBA, Berlin) has awarded readily biodegradable hydraulic oil products. Nevertheless, most hydraulic oil products still contain petroleum product constituents. Today, biological hydraulic oils are composed of the following types of basic liquids: Unsaturated (native) esters (rape seed oil, sunflower oil, etc.), unsaturated, synthetic ethers (trimethylolpropane-, TMP-oleates, etc.), saturated synthetic esters (dicarbonic acid esters, etc.), polyglycoles, and other basic fluids (petroleum product-based, polyalpha-olefines (PAO), etc.).

Over the last decades, laser-induced fluorescence (LIF) spectroscopy has been employed and continuously been improved as powerful analytical tool for the analysis of petroleum products in the environment [6-8]. A particular advantage of LIF spectroscopy is the potential for *on-site*, *in-situ* and sub-surface characterization of contaminated waters and soils. Oil fluorescence properties such as spectral signature, intensity and decay time, can be used to identify and to quantify oils in the environment. In the following, we will demonstrate the application of LIF spectroscopy to characterize biological and petroleum-based oils, and to monitor the migration of a biological oil in soil-containing compartments, namely a soil column and a soil bed. This work is thus part of our attempt to employ laser-based techniques for environmental analysis and to make progress from laboratory to field applications ([9-11, 15] and literature cited therein).

## Experimental

The following oils were investigated: Oil 1 (Plantohyd 40N, Fuchs, Mannheim, Germany, yellow liquid) and oil 2 (Bio Hy Gard, John Deere, Bruchsal, Germany, reddish orange liquid) contain natural esters from vegetable oils, oil 3 (ECONA E46, DEA, Hamburg, Germany, yellow liquid) contains ethers synthesized from vegetable oil precursors, whereas oil 4 (J 20 C, John Deere, Bruchsal, Germany, brownish yellow liquid) is a conventional petroleum product.

A mobile LIF spectrometer was obtained from Optimare GmbH (Wilhelmshaven, Germany). This device, called OPTIMOS (oil pollution transportable independent monitoring system), has been described in detail [15]. Briefly, it includes a flash lamp-pumped Nd:YAG-laser (pulse duration ca. 10 ns) as excitation source and an intensified CCD camera (1024×128 pixels, minimum gate width less than 5 ns) in combination with a spectrograph as detection system (typical spectral resolution ca. 3 – 5 nm). For the measurements, the OPTIMOS was operated at  $\lambda_{exc}=266$  nm (typical pulse energy

500  $\mu\text{J}$ ) or 355 nm (5 mJ) using cut-off filters (WG 295 or GG 385 Schott/ITOS, Mainz, Germany), respectively, to reduce backscattered excitation light. Background correction (CCD noise) was achieved by subtracting the signal of a dark measurement. LIF measurements from soil surfaces were performed using a simple sensor head with bifurcated fiber bundles (quartz fibers with ca. 100  $\mu\text{m}$  diameter for excitation and detection) connected to a plain circular metal plate. This resulted in an anti-parallel orientation of excitation and emission optical paths ( $180^\circ$ -geometry). Towards the soil surfaces, the fiber was protected by a quartz glass window of 3 mm thickness. For earlier investigations a demo-setup using a  $\text{N}_2$ -laser as the excitation light source ( $\lambda_{\text{exc}} = 337 \text{ nm}$ ) was used [15].

As model soil, an air-dry brown sandy loam from the site of the Federal Agricultural Research Center (FAL) in Braunschweig, Germany, was used. Soil columns were packed by FAL staff in plexiglass tubes, typically with 100 mm inner diameter, 3 mm wall thickness. As soil bed, turfs of natural soil with grassy vegetation were sampled at the FAL site and placed upon sandy loam in a frame (size 180 x 180 cm size), in which the grass was grown. To monitor oil migration, for each investigation 1 l of oil 2 was added with a funnel at the top of the soil column and at different positions of the soil bed. For the latter, three angles of inclination were chosen ( $3^\circ$ ,  $10^\circ$ ,  $15^\circ$ , with respect to the earth surface). For each measurement approximately 100 locations were scanned using LIF spectroscopy.

Absorption and fluorescence spectra of neat and diluted oils were recorded on a Lambda 2 photometer and LS 50 luminescence spectrometer (both Perkin-Elmer, Überlingen, Germany), respectively (typical spectral resolutions ca. 1 – 3 nm). All solvents used in the study were of analytical reagent grade. For the preparation of oil-spiked soil samples, a solution of the oils in n-pentane was added to the soil. After mixing using a spade, the samples were placed on a shaking tablett and n-pentane was evaporated in the fume cabin by skaking for three hours. The samples were analyzed immediately upon preparation. Limits of detection (LOD) were calculated by division of the threefold standard deviation of five measurements of the uncontaminated sandy loam by the slope of the calibration line.

## Results and discussion

The absorption spectra of the oils are characterized by a continuous increase from the red to strong absorbances in the UV spectral region. Absorption onsets of diluted oils were concentration dependent and were found, for example, in the 350 to 400 nm region for a dilution of 5 g/L oil in cyclohexane (Figure 1). In the semi-logarithmic representation, the oils showed long-wavelength absorption tails with almost linear behavior. In Figure 1, this is most pronounced for oil 2. Such a behavior, which has also been found for crude oils, asphaltenes, humic substances, etc., has been interpreted in terms of the so-called Urbach phenomenology [12-15].

Under laser irradiation the neat (i.e., undiluted) oils under investigation showed distinct native fluorescence. As examples, LIF spectra (fluorescence intensity  $I_F$  vs. wavelength  $\lambda$ ) obtained with 355 and 266 nm excitation are shown in Figures 2 and 3.

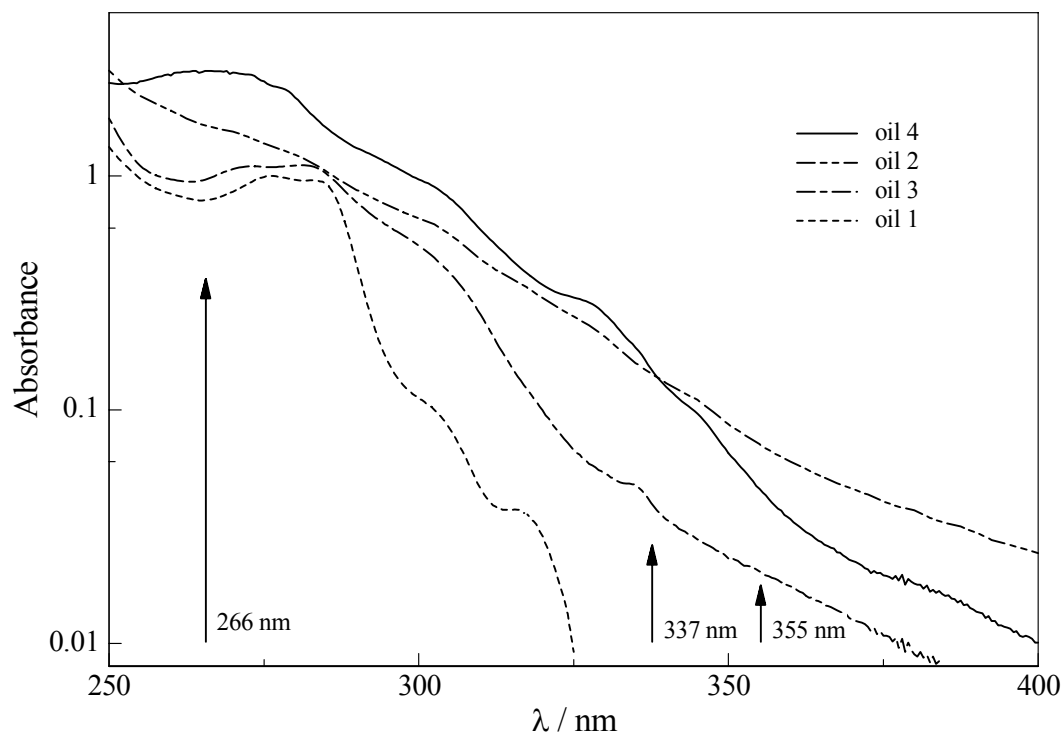


**Figure 1.** Absorption spectra (semi-logarithmic representation) of the hydraulic oils in cyclohexane solution (5 g/L, 1 cm optical path length). Arrows denote the laser excitation wavelengths employed.

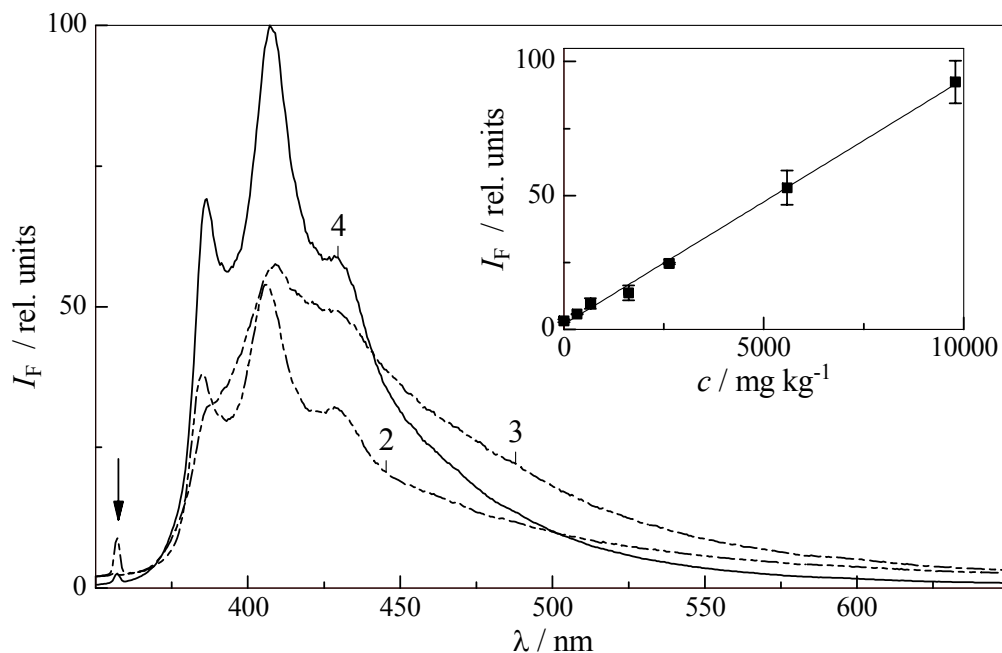


**Figure 2.** Fluorescence spectra of the neat hydraulic oils ( $\lambda_{\text{exc}}=355$  nm). The arrow marks a spectral feature originating from laser stray light. For oil 2 maxima can be assigned at 386, 407 and 429 nm. The location of the fluorescence onset at ca. 375 nm and of the first peak at 386 nm might be influenced by the cut-off filter. The inset shows calibration data for oil 2 on the brown soil ( $\lambda_{\text{exc}}=266$  nm).

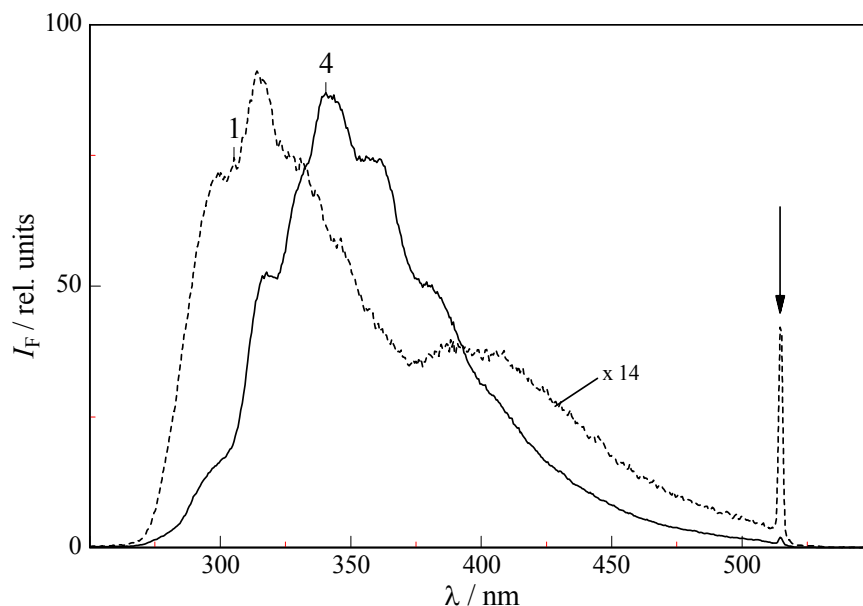


**Figure 3.** LIF spectra of neat oil product 1 and 4 ( $\lambda_{\text{exc}}=266$  nm, arrow marks stray light). The location of the fluorescence onsets might be influenced by the cut-off filters.

Usually, LIF spectra of oil products are featureless with single broad maxima in the 350 to 500 nm spectral region. It is therefore noteworthy that the oils 1 – 4 exhibited more structured emissions, displaying between 300 and 430 nm partly resolved minima and maxima and some clearly discernible shoulders. Since we do not precisely know origin, processing and composition of the commercial oil products, the fluorescence spectra obtained cannot be related to fluorophoric oil components. Rather, the overall signals are taken as spectral signatures characteristic for the neat oils. Closer inspection of the spectra in Figure 2 allows the following observations: (i) The fluorescence appearance of the biological oils 2 and 3 clearly resembles that of the petroleum-based oil 4. This may be due to identical or at least similar additives present in the oils. (ii) The fluorescence spectra strongly depend on excitation wavelength. Oil 1, which showed no fluorescence under 337 and 355 nm excitation due to the negligible absorption, can conveniently be excited at 266 nm (cf. Figure 3). Also the fluorescence onsets correlate with excitation wavelengths, as illustrated by comparison of oil 4 fluorescence signals in Figure 2 ( $\lambda_{\text{exc}}=355$  nm, onset at ca. 375 nm) and Figure 3 ( $\lambda_{\text{exc}}=266$  nm, onset ca. 275 nm). (iii) Quantitatively, the fluorescence efficiencies, as measured by the integrated LIF spectra, of the oils vary considerably. E.g., for excitation at 266 nm, where the oil absorbances are expected to be similar (cf. Figure 1), the overall fluorescence of oil 1 is more than one order of magnitude below that of oil 4 (Figure 3). This is in accordance with our earlier finding that, for a given excitation wavelength, fluorescence efficiencies of neat (petroleum-based) oils can be strongly different [15]. Also, there is a clear indication that biological oils are less fluorescent than petroleum-based oils.

Natural soils are strongly light scattering and usually also strongly light absorbing media of very heterogeneous nature. In comparison to solution phase investigations, LIF analysis of oils directly from soil surfaces is therefore much more difficult. Shown in Figure 4 are LIF spectra of oil 4 in a concentration range of  $c = 300 - 6.000$  mg/kg on the brown soil (sandy loam) and the background signal from the undoped soil (blank).

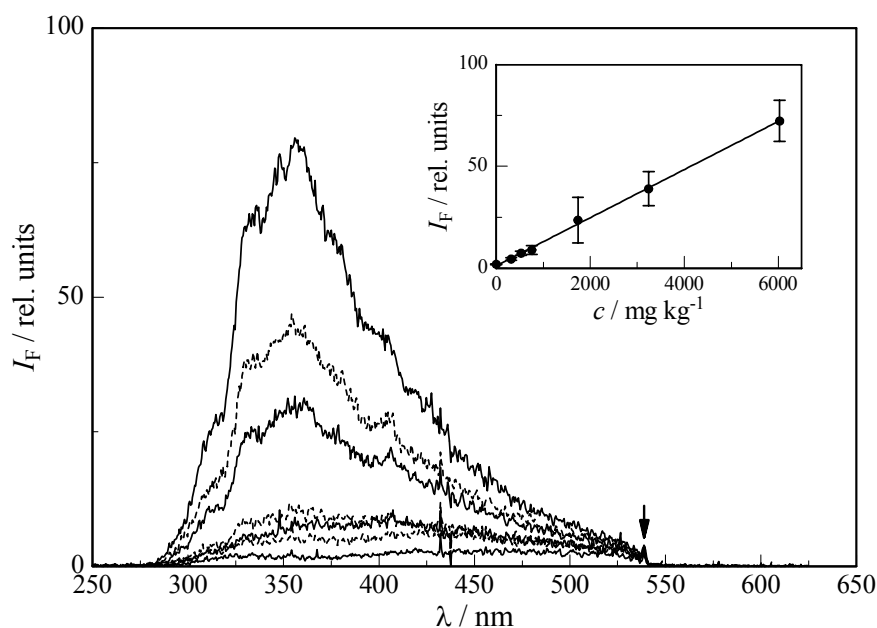


**Figure 4.** LIF spectra of hydraulic oil 4 on the brown soil ( $\lambda_{\text{exc}} = 266$  nm, arrow marks stray light). The inset shows calibration data for two independently spiked soil series ( $\lambda_{\text{exc}} = 266$  nm,  $I_F$  values obtained from integrated spectra).

The reduced quality of the fluorescence signals obtained is the price paid for *in-situ* soil investigation, i.e. an analysis without prior separation of analyte (oil) and matrix (soil). Despite somewhat reduced signal-to-noise ratio, the LIF signal intensities were clearly suitable for quantification of the oil content. This is illustrated by the calibration plot showing a linear relationship between  $I_F$  and  $c$  (inset of Figure 4). The limit of detection for oil 4 on the typical German soil are estimated to be below 500 mg/kg, which meets the requirements of typical regulatory values for petroleum-based oils as given for instance by the so-called Dutch list [16]. This list gives two values for petroleum product contaminations of soils: A reference concentration (R value) of 1,000 mg/kg above which additional investigations of the soils are recommended, and an intervention concentration (I value) of 5,000 mg/kg above which soil remediation is proposed. Thus, with appropriate calibration, *in-situ* LIF analysis of soils contaminated with petroleum-based oils can be performed quantitatively (even, as first approximation, without consideration of soil optical properties [15]). Given their significantly lower fluorescence efficiencies it was found that such a procedure is not very useful for biological oils. For example, the detection limit for oil 2 on the sandy loam is estimated to be around 2000 mg/kg (inset of Figure 2). More precise limits of detection are therefore not given for oils 1 – 3. In the following we will instead propose an alternative approach.

For environmental monitoring and screening purposes it is often sufficient to infer the presence of an analyte with a classification scheme. Better than the most simple detect/non-detect scheme is e.g., a three-level classification with the following regimes: Below threshold (non-detect, level 3), intermediate concentrations (level 2), and excess concentration (level 1), e.g. in neat or saturated oil zones. We have taken this approach to study and visualize the migration of oils in soil-containing compartments, namely a soil column and a grass-covered soil bed. As example, Figure 5 shows LIF spectra of oil 2 which has migrated down the soil column.

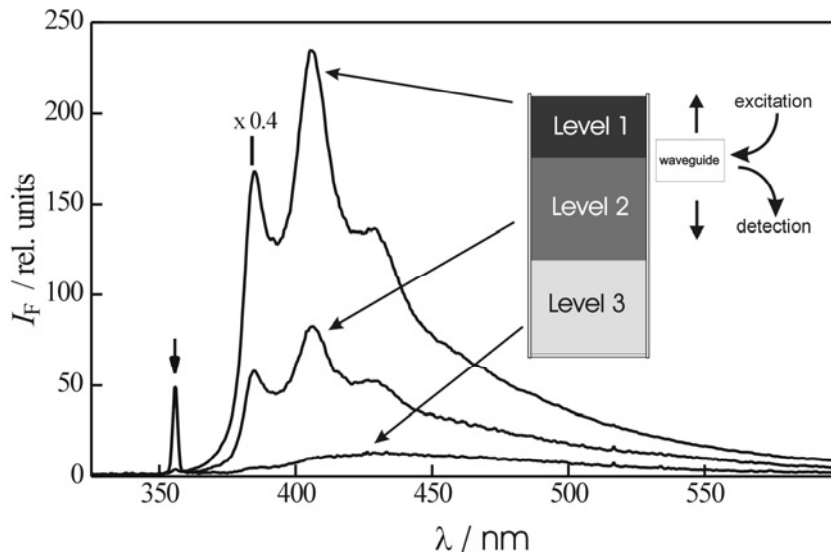


**Figure 5.** LIF spectra of hydraulic oil 2 on a column packed with a sandy loam.

In this example of a semi-quantitative application, various concentration levels are assigned to LIF spectra on the basis of spectral features and fluorescence intensities. Level 1 corresponds to the LIF signal of the pure oil phase, exemplified in Figure 5 by the upper trace with a maximum relative  $I_F$  signal of ca. 600. Level 2 is characterized by significantly lower LIF signals, albeit with clearly discernible spectral signature of oil fluorescence. This is exemplified by the middle trace with a maximum relative  $I_F$  signal of ca. 80 and corresponds to the soil zone which is less than oil-saturated. At level 3 below that (compare lowest trace in Figure 5 with a maximum relative  $I_F$  signal of ca. 12), signals were recorded which did not display these spectral signatures. This can be signals from the soil background or slightly above. Figure 6 gives an example of an imaging application of LIF spectroscopy for oil 2 migrating down the grass-covered soil bed for different angles of inclination ( $3^\circ$ ,  $10^\circ$ ,  $15^\circ$ ).

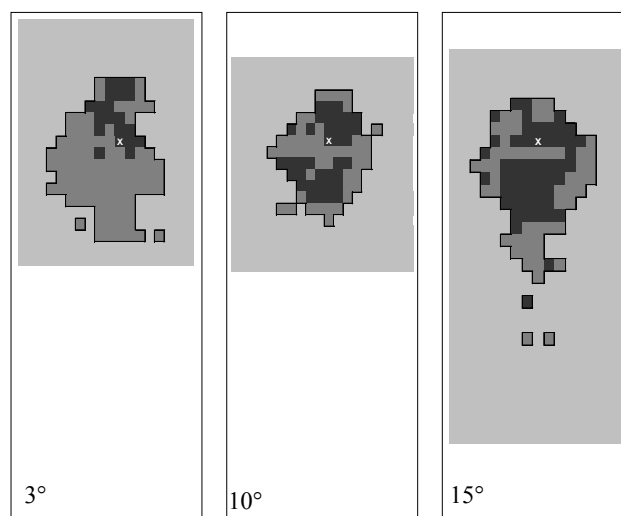


**Figure 6.** LIF spectroscopy for *in situ* profiling of spreading hydraulic oil 2 on a grass covered soil surface. The “X” denotes the point where the oil was added.

As described above,  $I_F$  signal intensities and oil levels have been assigned by a triple grey code: Dark areas represent oil-saturated zones (level 1), middle grey regions are below oil saturation, and the light grey regions reflect background signals. From Figure 6, it is clearly visible that the higher angle of inclination leads to increased oil mobility on the grassy surface.

## Conclusions

In comparison to the petroleum-based oil, the biological oils under investigation exhibited significantly reduced fluorescence efficiencies. Instead of a calibration-based quantitative analysis, as suitable for petroleum-based oils, a three-level classification scheme is proposed for the semi-quantitative *in-situ* analysis of biological oils in soil containing compartments. As example, oil migration in soil-column and soil bed was addressed. Future work is necessary to improve the *in-situ* detection of biological oils and to elucidate their transport behavior more comprehensively.

## Acknowledgements

This work was performed in co-operation with the Bundesforschungsanstalt für Landwirtschaft (Braunschweig, Germany). It is a pleasure to thank Wolfgang Paul and Christine Schütt for the fruitful collaboration and the Fachagentur Nachwachsende Rohstoffe (Gülzow, Germany) for financial support.

## References

1. Willing, A. Lubricants based on renewable resources - an environmentally compatible alternative to mineral oil products *Chemosphere*, **2001**, *43*, 89.
2. Boyde, S. Green lubricants. Environmental benefits and impacts of lubrication. *Green Chemistry*, **2002**, *4*, 293.
3. Maleque, M.A.; Masjuki, H.H.; Sapuan, S.M. Vegetable-based biodegradable lubricating oil additives. *Industr. Lubr. Tribol.*, **2003**, *55*, 137.
4. Heine, C., In *Bioschmierstoffe in der kommunalen Praxis*, Gülzower Fachgespräche, Hamm 26. Mai. 1999, Fachtagung lokale Agenda 21, Fachagentur nachwachsende Rohstoffe e.V. **1999**, 78.
5. [www.Pflanzenoelinitiative.de/English/inhalt.htm](http://www.Pflanzenoelinitiative.de/English/inhalt.htm) (access Sept. 17, **2003**).
6. Balshaw-Biddle, K.; Oubre, C.L.; Ward, C.H. (eds.) *Subsurface monitoring using laser fluorescence*, Lewis Publishers, Boca Raton, FL, **2000**.
7. Lieberman, S.H.; Knowles, D.S. Cone penetrometer deployable in situ video microscope for characterizing sub-surface soil properties. *Field Anal. Chem. Technol.*, **1998**, *2*, 127.
8. Quinn, M.F.; Alemeddine, O.; Al-Awadi, E.; Mukhopadhyay, A.; Qabazard, A.M.; Al-Rasheedi, M.; Ismail A.J. The application of laser-induced fluorescence techniques for the measurement of hydrocarbons in the groundwater of Kuwait. *Instr. Science Technol.*, **2002**, *30*, 79.

9. Löhmannsröben, H.-G.; Roch, Th.; Schultze, R.H. Laser-induced fluorescence (LIF) spectroscopy for in situ analysis of petroleum products and biological oils in soils. *Polycyclic Aromatic Compounds*, **1999**, *3*, 165.
10. Löhmannsröben, H.-G.; Roch, Th. In situ laser-induced fluorescence (LIF) analysis of petroleum product-contaminated soil samples. *J. Environ. Monit.*, **2000**, *2*, 17.
11. Fernandez-Trujillo, R.; Hengstermann, T.; Lemke, M.; Löhmannsröben, H.-G.; Schober, L.; Schultze, R.H. *In Field screening Europe 2001*, Breh, W. et al. (Eds.), Kluwer Academic Publishers, Dordrecht, Boston, **2002**, pp. 145.
12. Mullins, O.C.; Zhu, Y. First observation of the Urbach tail in a multicomponent organic system. *Appl. Spec.* **1992**, *46*, 354.
13. Mullins, O.C.; Mitra-Kirtley, S.; Zhu, Y. The electronic absorption edge of petroleum. *Appl. Spec.* **1992**, *46*, 1401.
14. Illenseer, C.; Löhmannsröben, H.-G.; Schultze, R.H. Application of laser-based ion-mobility (IM) spectrometry for the analysis of polycyclic aromatic compounds (PAC) and petroleum products in soils. *J. Environ. Monit.* **2003**, *5*, 780.
15. Schultze, R.H.; Lemke, M.; Löhmannsröben, H.-G., In *Laser in environmental and life sciences*, P. Hering; Lay, J.P.; Stry, S., (Eds.), Springer, Berlin, **2004**, 79.
16. Rosenkranz, D.; Einsele, G.; Harreß, H.-M. *Bodenschutz*. E. Schmidt, Berlin, chapter 8935, vol. 2, p. 1-27 and chapter 8936, vol. 2, 1, **1995**.

## Phytochelatin Modified Electrode Surface as a Sensitive Heavy-Metal Ion Biosensor

Vojtech Adam<sup>1,4</sup>, Josef Zehnalek<sup>1</sup>, Jitka Petrlova<sup>1</sup>, David Potesil<sup>1,4</sup>, Bernd Sures<sup>2</sup>, Libuse Trnkova<sup>3</sup>, Frantisek Jelen<sup>5</sup>, Jan Vitecek<sup>6</sup> and Rene Kizek<sup>1\*</sup>

<sup>1</sup> Department of Chemistry and Biochemistry and <sup>6</sup> Botany and Plant Physiology, Mendel University of Agriculture and Forestry, Zemedelska 1, 611 37 Brno, Czech Republic

<sup>2</sup> Univ. Karlsruhe, Zool. Inst. Okol Parasitol 1, Karlsruhe, D-76128 Germany

<sup>3</sup> Department of Theoretical and Physical Chemistry and <sup>4</sup> Department of Analytical Chemistry, Masaryk University Faculty of Science, Kotlarska 2, 611 37 Brno

<sup>5</sup> Laboratory of Biophysical Chemistry and Molecular Oncology, Institute of Biophysics, Academy of Sciences of the Czech Republic, Kralovopolska 135, Brno 612 65, Czech Republic

\* Author to whom correspondence should be addressed. Email: [kizek@sci.muni.cz](mailto:kizek@sci.muni.cz)

Received: 06 September 2004 / Accepted: 18 November 2004 / Published: 28 February 2005

---

**Abstract:** Electrochemical biosensors have superior properties over other existing measurement systems because they can provide rapid, simple and low-cost on-field determination of many biological active species and a number of dangerous pollutants. In our work, we suggested a new heavy metal biosensor based on interaction of heavy metal ions ( $\text{Cd}^{2+}$  and  $\text{Zn}^{2+}$ ) with phytochelatin, which was adsorbed on the surface of the hanging mercury drop electrode, using adsorptive transfer stripping differential pulse voltammetry. In addition, we applied the suggested technique for the determination of heavy metals in a biological sample – human urine and platinum in a pharmaceutical drug. The detection limits (3 S/N) of Cd(II), Zn(II) and *cis*-platin were about 1.0, 13.3 and 1.9 pmole in 5  $\mu\text{l}$ , respectively. On the basis of the obtained results, we propose that the suggested technique offers simple, rapid, and low-cost detection of heavy metals in environmental, biological and medical samples.

**Keywords:** phytochelatin, adsorptive transfer stripping, differential pulse voltammetry, mercury, cadmium, zinc, heavy metal sensor, human urine, *cis*-platin.

---

## Introduction

Industries produce a number of undesirable species such as pesticides, toxic organic compounds, heavy metals and so on [1-5]. An increasing concentration of heavy metals in the environment is a serious problem for human and animal health protection and production of foodstuffs in many countries around the world [6-8]. That is why easy and quick detection of heavy metals at very low concentrations levels in environmental and biological samples is necessary for assurance against acute intoxications and, first of all, against long-time exposure that may lead to many diseases and death [9-10]. Several analytical methods such as atomic absorption spectrometry [11-13], inductively coupled plasma with mass spectrometry [14-16] as well as electrochemistry [17-21], have been developed for these purposes. Electrochemical biosensors have superior properties over the other existing measurement systems because they can provide rapid, simple and low-cost on-field determination of many biological active species and number of dangerous pollutants [22-29]. In addition, biosensor technology is a powerful alternative to conventional analytical techniques, combining the specificity and sensitivity of biological systems in small devices. A number of recently published papers describe the determination of heavy metals using electrochemical biosensors based on their interactions with DNA [26,29-33], enzymes (first of all urease) [34-38], bacteria [39-41] and proteins [42-43].

Besides high molecular species – proteins such as metallothionein – it is possible to use low molecular heavy metal binding compounds such as phytochelatins (PCs) for construction of biosensors. PCs, cysteine-rich small peptides, consist of 4-23 amino acids abounding in plants as a response on heavy metal stress [44-47], participate in the detoxification of heavy metals, because they have an ability to transport heavy metal ions to vacuole [45,48], where an immediate toxicity do not menace yet. Phytochelatins have a basic formula  $(\gamma\text{-Glu-Cys})_n\text{-Gly}$  ( $n = 2$  to 11) and with the presented heavy metals (M) form M-PC complexes, in which the metal is bind via SH group of cysteine unit [48-49]; see Figure 1A. PCs are synthesized from glutathione, which is catalysed by PC synthase ( $\gamma$ -glutamylcysteine dipeptidyltranspeptidase, EC 2.3.2.15) activated by an increased concentration of the heavy metal (Cd, Cu, Hg, As or Pb) in a plant cytoplasm [47]. Reduced glutathione (GSH) itself plays the important role in cell protection against heavy metals, and reactive oxygen species (ROS) that are able to oxidize GSH to GSSG (oxidized glutathione; disulfide glutathione) [50]. The GSH:GSSG ratio was found as an indicator of cell damage and some diseases [50,51].

The aim of this paper was to suggest a new heavy metal biosensor based on interaction of heavy metal (cadmium and zinc) with phytochelatin using adsorptive transfer stripping (AdTS) differential pulse voltammetry (DPV). The basic scheme of the proposed heavy metals biosensor is shown in Figure 1B.

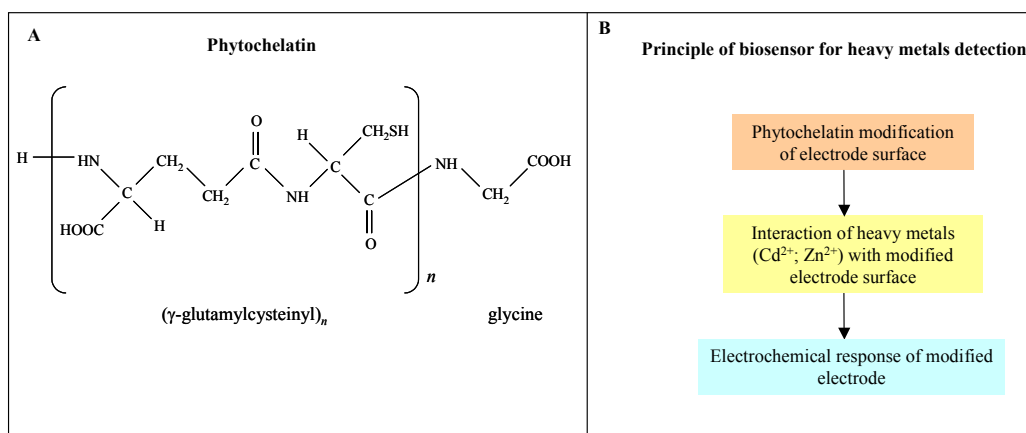


**Figure 1.** Chemical structure of phytochelatin (A). Scheme of basic principle of biosensor for heavy metals detection (B).

## Materials and methods

### Chemicals

Phytochelatin ( $\gamma\text{-Glu-Cys}$ )<sub>2</sub>-Gly (PC<sub>2</sub>) was synthesized in Clonestar Biotech; purity over 90% (Brno, Czech Republic). Tris(2-carboxyethyl)phosphine is produced by Molecular Probes (Eugen, Oregon, USA). Sodium chloride, cadmium nitrate, zinc nitrate and other used chemicals were purchased from Sigma Aldrich. The stock standard solutions of PC<sub>2</sub> at 10  $\mu\text{g}\cdot\text{ml}^{-1}$  were prepared by ACS water (Sigma-Aldrich, USA) and stored in the dark at -20 °C. Working standard solutions were prepared daily by dilution of the stock solutions. The pH value was measured using WTW inoLab Level 3 with terminal Level 3 (Weilheim, Germany), controlled by personal computer program (MultiLab Pilot; Weilheim, Germany). The pH electrode (SenTix- H, pH 0–14/3M KCl) was regularly calibrated by set of WTW buffers (Weilheim, Germany).

### Electrochemical measurements

Electrochemical measurements were performed with AUTOLAB Analyser (EcoChemie, Netherlands) connected to VA-Stand 663 (Metrohm, Switzerland), using a standard cell with three electrodes. The working electrode was a hanging mercury drop electrode (HMDE) with a drop area of 0.4 mm<sup>2</sup>. The reference electrode was an Ag/AgCl/3M KCl electrode and the auxiliary electrode was a graphite electrode. The supporting electrolyte was prepared by mixing buffer components. The analyzed samples were deoxygenated prior to measurements by purging with argon (99.999%) saturated with water for 240 s.

### -Adsorptive transfer stripping (AdTS) differential pulse voltammetry (DPV) of phytochelatin

The amount of PC<sub>2</sub> was measured using AdTS DPV. The samples of the PC<sub>2</sub> were reduced before each measurement by 1 mM tris(2-carboxyethyl)phosphine addition according to [52]. The supporting electrolyte (sodium chloride: 0.5 M NaCl, pH 6.4) from Sigma Aldrich in ACS purity was purchased. DPV parameters were as follows: an initial potential of -1.2 V, an end potential -0.3 V, a modulation

time 0.057 s, a time interval 0.2 s, a step potential of 1.05 mV/s, a modulation amplitude of 250 mV. All experiments were carried out at room temperature. For smoothing and baseline correction the software GPES 4.4 supplied by EcoChemie was employed.

### *Real samples*

#### -Preparation of human urine

Human urine (obtained from healthy laboratory staff) was filtered through a Teflon disc filter (0.45  $\mu\text{m}$  and 13 mm diameter, Alltech Associates, Deerfield, IL, USA) and 10 times diluted with 0.5 M sodium chloride (pH 6.4) before measurements. Moreover, we added to 10 times diluted solution of human urine Cd(II) and/or Zn(II) at 25, 50, 100, 225, 400, 600 and/or 50, 100, 200, 400, 600, 800  $\mu\text{M}$  concentrations, respectively.

#### -Preparation of cis-platin – pharmaceutical drug

*cis*-Platin was synthesized and provided by Pliva-Lachema (Brno, Czech Republic) [53]. The stock standard solutions of *cis*-platin at 10  $\mu\text{g}\cdot\text{ml}^{-1}$  were prepared by sodium chloride solution (0.5 M, pH 6.4) and stored in the dark at  $-20\text{ }^{\circ}\text{C}$ . Working standard solutions were prepared daily by dilution of the stock solutions.

### *Statistical analysis*

STATGRAPHICS® (Statistical Graphics Corp®, USA) was used for statistical analyses. Results are expressed as mean  $\pm$  S.D. unless noted otherwise. A value of  $p < 0.05$  was considered significant.

## **Results and discussion**

Papers concerning the construction of heavy metals biosensors, where fungi, bacteria, proteins or peptides served as biological part of these sensors, were recently published [3,30,33-34,38,40-43,54-62]. Due to increasing interest in heavy metals biosensor development, we engaged with electrochemical determination of heavy metals by means of their interaction with a phytochelatin (PC<sub>2</sub>)-modified mercury electrode. Basic electrochemical behaviour of heavy metal binding thiols (e.g., glutathione, phytochelatin, metallothionein) has already been studied by many techniques such as chronopotentiometric stripping analysis [23,24,63-64], cyclic voltammetry [18,25,65-66] and differential pulse voltammetry [67-70]. Primarily, it was necessary to observe in detail the electrochemical behaviour of PC<sub>2</sub> on the surface of hanging mercury electrode (HMDE) by differential pulse voltammetry in combination with adsorptive transfer stripping technique (AdTS DPV) with the view to use them for construction of a heavy metal biosensor because the AdTS DPV technique has not been used for these purposes yet.

### *Adsorptive transfer stripping technique as a base of electrochemical biosensor*

Adsorptive transfer stripping technique (AdTS) was developed as a suitable tool for electrochemical detection of biomolecules such as proteins, peptides and/or DNA [29,71-79]. Principle of the technique

is in an adsorbing of studied analyte on surface of the working electrode – in our case of HMDE at open electrode system; see Figure 2A<sub>2</sub>.

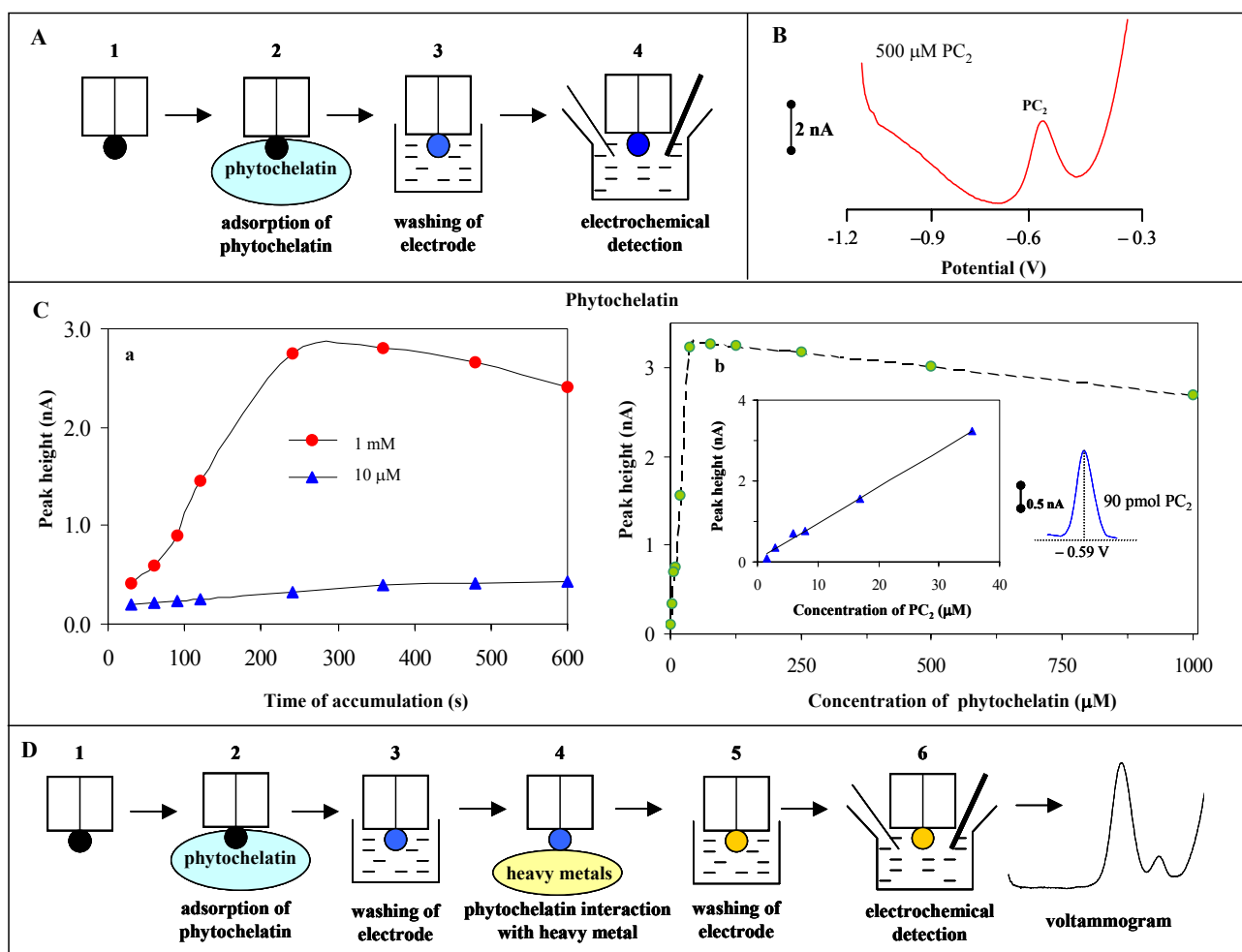


**Figure 2.** Scheme of adsorptive transfer stripping technique used for the detection of peptide – phytochelatin; (1) renewing of hanging mercury drop electrode (HMDE) surface; (2) adsorbing of PC<sub>2</sub> in a drop solution onto HMDE surface; (3) washing electrode in sodium chloride (0.5 M, pH 6.4); (4) measurement of PC<sub>2</sub> by differential pulse voltammetry (DPV) in 0.5 M sodium chloride, pH 6.4 (A). Typical DPV voltammograms of 500 μM PC<sub>2</sub> (B) obtained by AdTS DPV technique. DPV parameters were as follows: an initial potential of –1.2 V, an end potential –0.3 V, a modulation time 0.057 s, a time interval 0.2 s, a step potential of 1.05 mV/s, a modulation amplitude of 250 mV, an accumulation time of 120 s. Dependence of PC<sub>2</sub> peak height on accumulation time at its two different concentrations – 1 mM and 10 μM (Ca). Influence of phytochelatin concentrations on PC<sub>2</sub> peak height (Cb and inset in Cb). Inset in Figure Cb: peak of PC<sub>2</sub> (17 μM – 90 pmol of PC<sub>2</sub> in 5 μl drop) after baseline correction. Scheme of adsorptive transfer stripping technique used for the detection of heavy metals; (1) renewing of hanging mercury drop electrode (HMDE) surface; (2) adsorbing of PC<sub>2</sub> in a drop solution onto HMDE surface; (3) washing electrode in sodium chloride (0.5 M, pH 6.4); (4) interaction of heavy metal (cadmium and/or zinc) in a drop solution with peptide modified HMDE surface; (5) washing electrode in sodium chloride (0.5 M, pH 6.4); (6) measurement of PC<sub>2</sub> by DPV in 0.5 M sodium chloride, pH 6.4 (D).

After the absorbing, the electrode is removed from the solution and redundancy of analyte is washed from the surface of the working electrode in buffer (Figure 2A<sub>3</sub>). The adsorbed analyte is finally detected in the presence of an indifferent electrolyte (Figure 2A<sub>4</sub>). It was proved that during the described process running on the surface of HMDE, only one assembled layer of the adsorbed analyte, which can be bio-macromolecules species and/or compounds capable of adsorbing on the electrode surface, could form [80]. On the base of the above-mentioned description of the transfer technique, we were concerned with the possibility of using of a peptide (PC<sub>2</sub>) modified HMDE surface for heavy metals determination. Primarily, we focused on the optimisation of the modification of the electrode surface by phytochelatin.

#### *Using the adsorptive transfer stripping technique for determination of phytochelatin*

An electrochemical behaviour of the phytochelatin 2 (key plant peptide binding heavy metals; PC<sub>2</sub>) was studied on the surface of the HMDE by differential pulse voltammetry (DPV) in combination with adsorptive transfer stripping technique (AdTS). The voltammogram of 500 µM PC<sub>2</sub> accumulated on the HMDE surface during the time of 120 s and analysed in 0.5 M NaCl (pH 6.4) is shown in Figure 2B. On the obtained record, we observed the signal at potential -0.57 V, which probably correspond to adduct of the PC<sub>2</sub> with mercury on the surface of the HMDE (HS-peptide + Hg = HgS-peptide) [81-82].

It was necessary to know the way of probable interaction of peptide with the working electrode surface with the view to use the modified HMDE as a suitable toll for detection of heavy metals. On the most important index of status of electrode, the double-layer is dependent on the current response on the accumulation time [80,83]. An influence of the accumulation time of PC<sub>2</sub> at 1 mM and 10 µM concentrations on the electrochemical response (current height of PC<sub>2</sub> signal) was studied. The observed dependence at 1 mM PC<sub>2</sub> concentration steeply increased up to 240 s and resembled to the Langmuir isotherm (Figure 2Ca). From the obtained results it follows that the signal of PC<sub>2</sub> increased up to 240 s of the peptide accumulation time, which is probably connected with sequent filling up of the electrode surface. The maximum of the presented curve at 240 s probably relates with needed time for filling up of the HMDE electrode surface by one layer of PC<sub>2</sub> – surface assembled monolayer (SAM) [84]. After 240 s, the signal of adsorbed peptide did not increase, contrariwise decreased, which probably relates with formation of the poly-layer of the PC<sub>2</sub> on the HMDE surface – decreasing the possibility of the detection of adsorbed molecules. In the case of lower tested PC<sub>2</sub> concentration (10 µM), we observed the increase of PC<sub>2</sub> peak height with increasing accumulation time at all tested values (Figure 2C(a)). In addition, we indeed observed very low increase of the peak height (about 4 %) from the accumulation time of 360 s. Due to using of PC<sub>2</sub> at 1 mM concentration for the determination of heavy metals, we used the accumulation time of 240 s, because up this time the surface assembled monolayer is formed.

The next important index of behaviour of phytochelatin on the HMDE surface was the change of PC<sub>2</sub> current response according to its different concentrations. At the accumulation time of 240 s, concentrations of PC<sub>2</sub> varying from 2.5 to 1000 µM were tested (Figure 2C(b)). The obtained dependence set from the obtained PC<sub>2</sub> current responses according to its different concentrations was linear in the concentration range 0 – 40 µM ( $y = 0.0894 + 0.0621x$ ;  $R^2 = 0.9969$ , inset in Figure 2C(b)).

In addition, we observed a decrease of the current responses from the PC<sub>2</sub> concentration of 100 µM. This phenomenon probably relates with a forming of poly-layer on the electrode surface [80,83,85].

#### *Modification of the HMDE surface by phytochelatin*

For our purposes, we used the HMDE as the physical-chemical part and phytochelatin 2, which is able to bind heavy metals [68,70,86-93], as the biological part of the suggested heavy metals biosensor. That is why we could suggest following experiments: i) on the HMDE surface adsorb PC<sub>2</sub>; ii) remove redundant PC<sub>2</sub>; iii) expose the adsorbed PC<sub>2</sub> to interaction with heavy metal; iv) detect changes in the signals of PC<sub>2</sub> (Figure 2D). We selected for our purposes two heavy metals – cadmium and zinc.

That is why we were interested if free ions of selected heavy metal are able to adsorption and transfer on the HMDE surface. If we accumulated (120 s) only free ions of Cd(II) and/or Zn(II) without MT on the surface of the mercury working electrode, we did not observe any signal corresponding to heavy metal species (not shown). The described effect prove that free ions of heavy metals are not able to transfer and consequently to detect.

#### *Electrochemical behaviour of phytochelatin-modified HMDE in presence of Cd(II) and Zn(II)*

Phytochelatin 2 (1 mM) was adsorbed on the HMDE surface for the duration of 240 s. Then, the modified electrode was washed in the basic electrolyte solution and consequently, interacted with 500 µM of Cd(II) and/or Zn(II) for the duration of 300 s that was established as the most effective. The obtained voltammograms are shown in Figure 3A (Cd) and 4B (Zn). In the presence of Cd(II) we recorded except original signal PC<sub>2</sub> also another two signals that we named CdPC<sub>2</sub> (−0.76 V) and PC<sub>2</sub>(Cd) (−0.45 V). In addition, we observed a linear decrease of PC<sub>2</sub> signal and increase of CdPC<sub>2</sub> and PC<sub>2</sub>(Cd) signals according to the rise of Cd(II) added concentration. The equations of the mentioned rising linear curves were in case of CdPC<sub>2</sub>:  $y = 0.0128x + 0.2085$ ;  $R^2 = 0.9918$ ; and PC<sub>2</sub>(Cd):  $y = 0.0999x - 4.8325$ ;  $R^2 = 0.9997$ . The detection limit (3 S/N) of Cd(II) calculated from increase of PC<sub>2</sub>(Cd) peak was about 1.055 pmole in 5 µl (0.211 µM); see Figure 3C.

In the case of Zn(II) determination by PC<sub>2</sub> modified HMDE, we observed only one additive signal, which was named ZnPC<sub>2</sub>: −1.09 V, in comparison with control detection of PC<sub>2</sub> without interaction with Zn(II). The signal of PC<sub>2</sub> linear decreased and ZnPC<sub>2</sub> signal linearly increased ( $y = 0.8496x - 18.598$ ,  $R^2 = 0.9961$ ) according to rising Zn(II) concentration. The detection limit (3 S/N) of Zn(II) calculated from increase of ZnPC<sub>2</sub> peak was about 13.30 pmole in 5 µl (2.66 µM); see Figure 3D.

#### *Determination of Cd(II) and Zn(II) by PC<sub>2</sub> modified HMDE in biological matrix*

We decided to test our peptide-modified heavy metal biosensor by means of detection of Cd(II) and/or Zn(II) in the presence of the biological matrix (human urine). In the concrete, PC<sub>2</sub> (1 mM) was adsorbed (240 s) on the HMDE surface, washed (0.5 NaCl) and then the modified electrode interacted with Cd(II) and/or Zn(II) in the presence of human urine (10× diluted) for the duration of 300 s. Subsequently, the electrode was washed (0.5 NaCl) and placed to an electrochemical cell-containing supporting electrolyte (0.5 M NaCl; pH = 6.4). Human urine contained additions of Cd(II) and/or

Zn(II) at concentrations (25, 50, 100, 225, 400, 600 and/or 50, 100, 200, 400, 600, 800  $\mu\text{M}$ , respectively). All studied signals embodied very similar electrochemical behaviour in the course of their analysis both in buffered solution and biological matrix (not shown). The only two differences between analysis in buffered and non-buffered medium, which we found out, are peak heights and their relationship. In the presence of human urine, heights of all studied signals were lower than in the buffered medium – sodium chloride (differences from 10 to 15%). This effect is probably caused by impurities included with real sample that may complex with heavy metal ions.

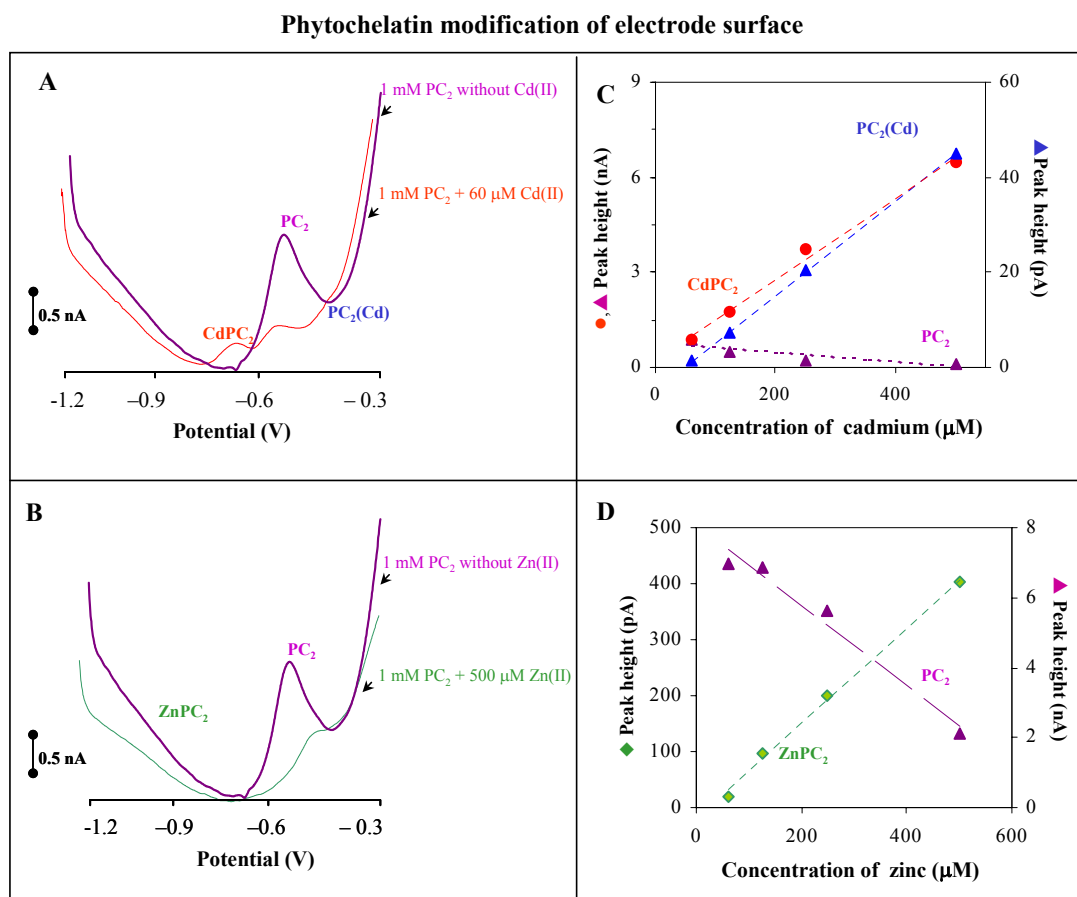


**Figure 3.** Phytochelatin. Typical DPV voltammograms of 1 mM PC<sub>2</sub> without addition of Cd(II) and 1 mM PC<sub>2</sub> + 60  $\mu\text{M}$  cadmium ions (A), and 1 mM PC<sub>2</sub> without addition of Zn(II) and 1 mM PC<sub>2</sub> + 500  $\mu\text{M}$  zinc ions (B). DPV parameters: time of accumulation 240 s, time of interaction 300 s. Dependence of CdPC<sub>2</sub>, PC<sub>2</sub>(Cd) and PC<sub>2</sub> peak heights on interaction time (C). Dependence of ZnPC<sub>2</sub> and PC<sub>2</sub> peak heights on interaction time (D). PC<sub>2</sub> concentration: 1 mM. For other details, see Figure 2.

#### Using of peptide-modified HMDE to study of anticancer drug – cis-platin

We attempted to use our suggested peptide modified heavy metal biosensor for the determination of the anticancer drug – cis-platin  $[\text{Pt}^{\text{II}}(\text{NH}_3)_2\text{Cl}_2]^0$ ; MW 303. A prepared solution of Pt complex interacted with PC<sub>2</sub> modified HMDE for the duration of 300 s. A resulting voltammogram is shown in Figure 4A. A phytochelatin-modified HMDE surface formed with presented Pt complex that we detected at potential  $-0.96\text{ V}$  and named as PtPC<sub>2</sub>. In addition, we studied the influence of different

durations of interaction between the PC<sub>2</sub>-modified electrode surface and Pt on height of the presented PtPC<sub>2</sub> signal. We selected a duration of 300 s as most suitable for the Pt complex interaction with the PC<sub>2</sub>-modified electrode surface (not shown). The dependence of heights of the PC<sub>2</sub> and PtPC<sub>2</sub> signals on *cis*-platin concentration is shown in Figure 4B. The PC<sub>2</sub> signal decreased and PtPC<sub>2</sub> linearly increased ( $y = 0.0532x - 5.7079$ ;  $R^2 = 0.9946$ ) in the studied concentration of *cis*-platin varying from 100 to 750  $\mu\text{M}$ . The detection limit (3 S/N) of *cis*-platin ( $[\text{Pt}^{\text{II}}(\text{NH}_3)_2\text{Cl}_2]^0$ ) calculated from increase of PtPC<sub>2</sub> peak was about 1.958 pmole in 5  $\mu\text{l}$  (0.392  $\mu\text{M}$ ) at the interaction time of 300 s.

### *Cis*-platin – $[\text{Pt}^{\text{II}}(\text{NH}_3)_2\text{Cl}_2]^0$ ; anticancer drug

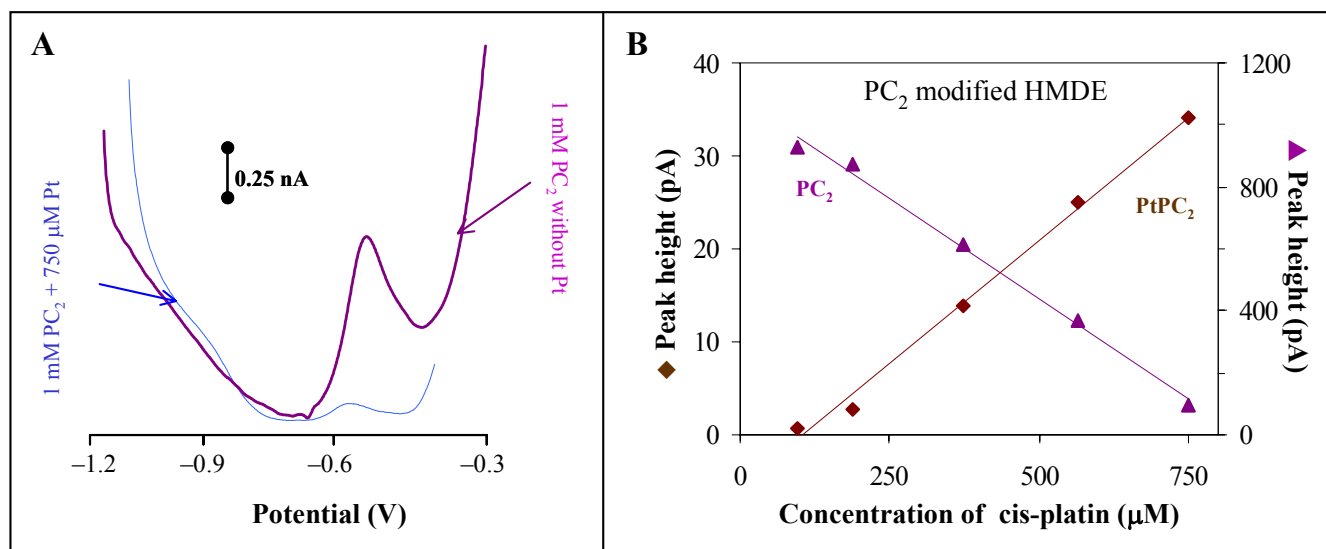


**Figure 4.** *Cis*-platin –  $[\text{Pt}^{\text{II}}(\text{NH}_3)_2\text{Cl}_2]^0$ ; anticancer drug. Typical DPV voltammograms of 1 mM PC<sub>2</sub> without addition of *cis*-platin and 1 mM PC<sub>2</sub> + 750  $\mu\text{M}$  of *cis*-platin (A). DPV parameters: time of accumulation 240 s, time of interaction 300 s. Dependences of PtPC<sub>2</sub> and PC<sub>2</sub> peak heights on different concentration of *cis*-platin (B). PC<sub>2</sub> concentration: 1 mM. DPV parameters: time of accumulation 240 s, time of interaction 300 s. For other details, see Figure 2.

## Conclusions

A development of easy and rapid renewable sensors for the detection of different species is one of the most important tasks of analytical chemistry and biochemistry. We suggested a simple sensor for the determination of Cd(II) and Zn(II) using a modification of the hanging mercury drop electrode surface by phytochelatin. The main advantage of using HMDE in comparison with other solid electrodes (carbon, gold and so on) is sensitivity. On the basis of the obtained results we propose that the suggested technique offers simple, rapid, and low-cost detection of heavy metals in environmental, biological, and medical samples.

## Acknowledgements

This work was supported by grants: GA CR No. 525/04/P132 and FRVS 2348/2005.

## References

1. Zehnalek, J.; Adam, V.; Kizek, R. Influence of heavy metals on production of protecting compounds in agriculture plants. *Listy Cukrov*, **2004**, *120*, 222.
2. Zehnalek, J.; Vacek, J.; Kizek, R. Application of higher plants in phytoremediation of heavy metals. *Listy Cukrov*, **2004**, *120*, 220.
3. Kizek, R.; Vacek, J.; Trnkova, L.; Klejdus, B.; Kuban, V. Electrochemical biosensors in agricultural and environmental analysis. *Chem. Listy*, **2003**, *97*, 1003.
4. Sures, B.; Knopf, K. Parasites as a threat to freshwater eels? *Science*, **2004**, *304*, 208.
5. Speir, T.W.; van Schaik, A.P.; Lloyd-Jones, A.R.; Kettles, H.A. Temporal response of soil biochemical properties in a pastoral soil after cultivation following high application rates of undigested sewage sludge. *Biol. Fertil. Soil*, **2003**, *38*, 377.
6. Zimmermann, S.; Sures, B. Significance of platinum group metals emitted from automobile exhaust gas converters for the biosphere. *Environ. Sci. Pollut. Res.* **2004**, *11*, 194.
7. Sures, B.; Siddall, R.; Taraschewski, H. Parasites as accumulation indicators of heavy metal pollution. *Parasitology Today*, **1999**, *15*, 16.
8. Sures, B. Environmental parasitology: Relevancy of parasites in monitoring environmental pollution. *Trends Parasitol.* **2004**, *20*, 170.
9. Wu, A.H.B.; McKay, C.; Broussard, L.A.; Hoffman, R.S.; Kwong, T.C.; Moyer, T.P.; Otten, E.M.; Welch, S.L.; Wax, P. National academy of clinical biochemistry laboratory medicine practice guidelines: Recommendations for the use of laboratory tests to support poisoned patients who present to the emergency department. *Clin. Chem.*, **2003**, *49*, 357.
10. Nordberg, G.; Jin, T.; Leffler, P.; Svensson, M.; Zhou, T.; Nordberg, M. Metallothioneins and diseases with special reference to cadmium poisoning. *Analisis*, **2000**, *28*, 396.
11. Dong, L.M.; Yan, X.P.; Li, Y.; Jiang, Y.; Wang, S.W.; Jiang, D.Q. On-line coupling of flow injection displacement sorption preconcentration to high-performance liquid chromatography for speciation analysis of mercury in seafood. *J. Chrom. A.*, **2004**, *1036*, 119.
12. Soylak, M.; Narin, I.; Divrikli, U.; Saracoglu, S.; Elci, L.; Dogan, M. Preconcentration-separation of heavy metal ions in environmental samples by membrane filtration-atomic absorption spectrometry combination. *Anal. Letters*, **2004**, *37*, 767.
13. Apostoli, P. Elements in environmental and occupational medicine. *J. Chrom. B*, **2002**, *778*, 63.
14. Lewen, N.; Mathew, S.; Schenkenberger, M.; Raglione, T. A rapid ICP-MS screen for heavy metals in pharmaceutical compounds. *J. Pharm. Biomed. Anal.*, **2004**, *35*, 739.
15. Karami, H.; Mousavi, M.F.; Yamini, Y.; Shamsipur, M. On-line preconcentration and simultaneous determination of heavy metal ions by inductively coupled plasma-atomic emission spectrometry. *Anal. Chim. Acta*, **2004**, *509*, 89.

16. Zhang, B.; Li, F.M.; Houk, R.S.; Armstrong, D.W. Pore exclusion chromatography-inductively coupled plasma-mass spectrometry for monitoring elements in bacteria: A study on microbial removal of uranium from aqueous solution. *Anal. Chem.*, **2003**, *75*, 6901.
17. Szlyk, E.; Szydłowska-Czerniak, A. Determination of cadmium, lead, and copper in margarines and butters by galvanostatic stripping chronopotentiometry. *J. Agr. Food Chem.*, **2004**, *52*, 4064.
18. Vacek, J.; Petrek, J.; Kizek, R.; Havel, L.; Klejdus, B.; Trnkova, L.; Jelen, F. Electrochemical determination of lead and glutathione in a plant cell culture. *Bioelectrochemistry*, **2004**, *63*, 347.
19. Mikkelsen, O.; Schroder, K.H. Amalgam electrodes for electroanalysis. *Electroanalysis*, **2003**, *15*, 679.
20. Baldo, M.A.; Daniele, S.; Ciani, I.; Bragato, C.; Wang, J. Remote stripping analysis of lead and copper by a mercury-coated platinum microelectrode. *Electroanalysis*, **2004**, *16*, 360.
21. Pei, J.H.; Tercier-Waeber, M.L.; Buffle, J. Simultaneous determination and speciation of zinc, cadmium, lead, and copper in natural water with minimum handling and artifacts, by voltammetry on a gel-integrated microelectrode array. *Anal. Chem.*, **2000**, *72*, 161.
22. Kizek, R.; Vacek, J.; Trnková, L.; Klejdus, B.; Havel, L. Application of catalytic reactions on a mercury electrode for metallothionein electrochemical detection. *Chem. Listy*, **2004**, *98*, 160.
23. Strouhal, M.; Kizek, R.; Vacek, J.; Trnková, L.; Němec, M. Electrochemical study of heavy metals and metallothionein in yeast *Yarrowia lipolytica*. *Bioelectrochemistry*, **2003**, *60*, 29.
24. Trnkova, L.; Kizek, R.; Vacek, J. Catalytic signal of rabbit liver metallothionein on a mercury electrode: A combination of derivative chronopotentiometry with adsorptive transfer stripping. *Bioelectrochemistry*, **2002**, *56*, 57.
25. Šestáková, I.; Vodičková, H.; Mader, P. Voltammetric methods for speciation of plant metallothioneins. *Electroanalysis*, **1998**, *10*, 764.
26. Fojta, M. Electrochemical sensors for DNA interactions and damage. *Electroanalysis*, **2002**, *14*, 1449.
27. Cukrowska, E.; Trnkova, L.; Kizek, R.; Havel, J. Use of artificial neural networks for the evaluation of electrochemical signals of adenine and cytosine in mixtures interfered with hydrogen evolution. *J. Electroanal. Chem.*, **2001**, *503*, 117.
28. Kizek, R.; Trnkova, L.; Sevcikova, S.; Smarda, J.; Jelen, F. Silver electrode as a sensor for determination of zinc in cell cultivation medium. *Anal. Biochem.*, **2002**, *301*, 8.
29. Fojta, M.; Havran, L.; Kizek, R.; Billova, S.; Palecek, E. Multiply osmium-labeled reporter probes for electrochemical DNA hybridization assays: Detection of trinucleotide repeats. *Biosen. Bioelectron.*, **2004**, *20*, 985.
30. Babkina, S.S.; Ulakhovich, N.A. Amperometric biosensor based on denatured DNA for the study of heavy metals complexing with DNA and their determination in biological, water and food samples. *Bioelectrochemistry*, **2004**, *63*, 261.

31. Rodriguez-Mozaz, S.; Marco, M.P.; de Alda, M.J.L.; Barcelo, D. Biosensors for environmental applications: Future development trends. *Pure Appl. Chem.*, **2004**, *76*, 723.
32. Berggren, C.; Bjarnason, B.; Johansson, G. Capacitive biosensors. *Electroanalysis*, **2001**, *13*, 173.
33. Lu, Y.; Liu, J.W.; Li, J.; Bruesehoff, P.J.; Pavot, C.M.B.; Brown, A.K. New highly sensitive and selective catalytic DNA biosensors for metal ions. *Biosen. Bioelectron.*, **2003**, *18*, 529.
34. Aiken, A.M.; Peyton, B.M.; Apel, W.A.; Petersen, J.N. Heavy metal-induced inhibition of *Aspergillus niger* nitrate reductase: Applications for rapid contaminant detection in aqueous samples. *Anal. Chim. Acta*, **2003**, *480*, 131.
35. Dzyadevych, S.V.; Soldatkin, A.P.; Korpan, Y.I.; Arkhypova, V.N.; El'skaya, A.V.; Chovelon, J.M.; Martelet, C.; Jaffrezic-Renault, N. Biosensors based on enzyme field-effect transistors for determination of some substrates and inhibitors. *Anal. Bioanal. Chem.*, **2003**, *377*, 496.
36. Han, S.B.; Zhu, M.; Yuan, Z.B.; Li, X. A methylene blue-mediated enzyme electrode for the determination of trace mercury(II), mercury(I), methylmercury, and mercury-glutathione complex. *Biosen. Bioelectron.*, **2001**, *16*, 9.
37. Krajewska, B.; Zaborska, W.; Chudy, M. Multi-step analysis of Hg<sup>2+</sup> ion inhibition of jack bean urease. *J. Inorg. Biochem.*, **2004**, *98*, 1160.
38. Kuswandi, B. Simple optical fibre biosensor based on immobilised enzyme for monitoring of trace heavy metal ions. *Anal. Bioanal. Chem.*, **2003**, *376*, 1104.
39. Horswell, J.; Speir, T.W.; van Schaik, A.P. Bio-indicators to assess impacts of heavy metals in land-applied sewage sludge. *Soil Biol. Biochem.*, **2003**, *35*, 1501.
40. Qian, Z.R.; Tan, T.C. BOD measurement in the presence of heavy metal ions using a thermally-killed-Bacillus subtilis biosensor. *Water Res.*, **1999**, *33*, 2923.
41. Bontidean, I.; Lloyd, J.R.; Hobman, J.L.; Wilson, J.R.; Csoregi, E.; Mattiasson, B.; Brown, N.L. Bacterial metal-resistance proteins and their use in biosensors for the detection of bioavailable heavy metals. *J. Inorg. Biochem.*, **2000**, *79*, 225.
42. Wu, C.-M.; Lin, L.-Y. Immobilization of metallothionein as a sensitive biosensor chip for the detection of metal ions by surface plasmon resonance. *Biosen. Bioelectron.*, **2004**, *4*, 864.
43. Bontidean, I.; Ahlqvist, J.; Mulchandani, A.; Chen, W.; Bae, W.; Mehra, R.K.; Mortari, A.; Csoregi, E. Novel synthetic phytochelatin-based capacitive biosensor for heavy metal ion detection. *Biosen. Bioelectron.*, **2003**, *18*, 547.
44. Bae, W.; Chen, W.; Mulchandani, A.; Mehra, R.K. Enhanced bioaccumulation of heavy metals by bacterial cells displaying synthetic phytochelatin. *Biotechnol. Bioeng.*, **2000**, *70*, 518.
45. Cobbett, C.S. Phytochelatin biosynthesis and function in heavy-metal detoxification. *Curr. Opin. Plant Biol.*, **2000**, *3*, 211.
46. di Toppi, S.L.; Gabbrielli, R. Response to cadmium in higher plants. *Environ. Exp. Bot.*, **1999**, *41*, 105.
47. Zenk, M.H. Heavy metal detoxification in higher plants – a review. *Gene*, **1996**, *179*, 21.

48. Cobbett, C.S.; Goldsbrough, P.B. Phytochelatins and metallothioneins: Roles in heavy metal detoxification and homeostasis. *Annu. Rev. Plant Biol.*, **2002**, *53*, 159.
49. Grill, E.; Winnacker, E.-L.; Zenk, M.H. Phytochelatins: The principal heavy-metal complexing peptides of higher plants. *Science*, **1985**, *320*, 674.
50. Townsend, D.M.; Tew, K.D.; Tapiero, H. The importance of glutathione in human disease. *Biomed. Pharmacother.*, **2003**, *57*, 145.
51. Sastre, J.; Pallardo, F.V.; Vina, J. Glutathione, oxidative stress and aging. *Age*, **1996**, *19*, 129.
52. Kizek, R.; Vacek, J.; Trnkova, L.; Jelen, F. Cyclic voltammetric study of the redox system of glutathione using the disulfide bond reductant tris(2-carboxyethyl)phosphine. *Bioelectrochemistry*, **2004**, *63*, 19.
53. Dolezel, P.; Kuban, V. Mass spectrometric study of platinum complexes based on cisplatin. *Chem. Pap-Chem. Zvesti.*, **2002**, *56*, 236.
54. Palchetti, I.; Marrazza, G.; Mascini, M. New procedures to obtain electrochemical sensors for heavy metal detection. *Anal. Lett.*, **2001**, *34*, 813.
55. Tsai, H.C.; Doong, R.A.; Chiang, H.C.; Chen, K.T. Sol-gel derived urease-based optical biosensor for the rapid determination of heavy metals. *Anal. Chim. Acta*, **2003**, *481*, 75.
56. May, L.M.; Russell, D.A. Novel determination of cadmium ions using an enzyme self-assembled monolayer with surface plasmon resonance. *Anal. Chim. Acta*, **2003**, *500*, 119.
57. Leth, S.; Maltoni, S.; Simkus, R.; Mattiasson, B.; Corbisier, P.; Klimant, I.; Wolfbeis, O.S.; Csoregi, E. Engineered bacteria based biosensors for monitoring bioavailable heavy metals. *Electroanalysis*, **2002**, *14*, 35.
58. Lehmann, M.; Riedel, K.; Adler, K.; Kunze, G. Amperometric measurement of copper ions with a deputy substrate using a novel *Saccharomyces cerevisiae* sensor. *Biosen. Bioelectron.*, **2000**, *15*, 211.
59. Kukla, A.L.; Kanjuk, N.I.; Starodub, N.F.; Shirshov, Y.M. Multienzyme electrochemical sensor array for determination of heavy metal ions. *Sens. Actuators B*, **1999**, *57*, 213.
60. Gooding, J.J.; Hibbert, D.B.; Yang, W. Electrochemical metal ion sensors. Exploiting amino acids and peptides as recognition elements. *Sensors*, **2001**, *1*, 75.
61. Corbisier, P.; van der Lelie, D.; Borremans, B.; Provoost, A.; de Lorenzo, V.; Brown, N.L.; Lloyd, J.R.; Hobman, J.L.; Csoregi, E.; Johansson, G.; Mattiasson, B. Whole cell- and protein-based biosensors for the detection of bioavailable heavy metals in environmental samples. *Anal. Chim. Acta*, **1999**, *387*, 235.
62. Brabec, V. DNA sensor for the determination of antitumor platinum compounds. *Electrochim. Acta*, **2000**, *45*, 2929.
63. Kizek, R.; Trnkova, L.; Palecek, E. Determination of metallothionein at the femtomole level by constant current stripping chronopotentiometry. *Anal. Chem.*, **2001**, *73*, 4801.

64. Tomschik, M.; Havran, L.; Palecek, E.; Heyrovský, M. The "presodium" catalysis of electroreduction of hydrogen ions on mercury electrodes by metallothionein. An investigation by constant current derivative stripping chronopotentiometry. *Electroanalysis*, **2000**, *12*, 274.
65. Sestaková, I.; Mader, P. Voltammetry on mercury and carbon electrodes as a tool for studies of metallothionein interactions with metal ions. *Cell. Mol. Biol.*, **2000**, *46*, 257.
66. Yosypchuk, B.; Novotny, L. Cathodic stripping voltammetry of cysteine using silver and copper solid amalgam electrodes. *Talanta*, **2002**, *56*, 971.
67. Erk, M.; Ivankovic, D.; Raspor, B.; Pavicic, J. Evaluation of different purification procedures for the electrochemical quantification of mussel metallothioneins. *Talanta*, **2002**, *57*, 1211.
68. Díaz-Cruz, M.S.; Mendieta, J.; Esteban, M. Combined use of differential pulse plarography and multivariate curve resolution: As applied to the study of metal mixed complexes of the metallothionein related hexapeptide Lys-Cys-Thr-Cys-Cys-Ala. *Electroanalysis*, **2002**, *14*, 50.
69. Yosypchuk, B.; Sestakova, I.; Novotny, L. Voltammetric determination of phytochelatin using copper solid amalgam electrode. *Talanta*, **2003**, *59*, 1253.
70. Díaz-Cruz, M.S.; Mendieta, J.; Tauler, R.; Esteban, M. Cadmium-binding properties of glutathione: A chemometrical analysis of voltammetric data. *J. Inorg. Biochem.*, **1997**, *66*, 29.
71. Palecek, E.; Postbieglová, I. Adsorptive stripping voltammetry of biomacromolecules with transfer of the adsorbed layer. *J. Electroanal. Chem.*, **1986**, *214*, 359.
72. Palecek, E. Adsorptive transfer stripping voltammetry: Effect of electrode potential on the structure of DNA adsorbed at the mercury surface. *Bioelectrochem. Bioenerg.*, **1992**, *28*, 71.
73. Palecek, E. New trends in electrochemical analysis of nucleic acids. *Bioelectrochem. Bioenerg.*, **1988**, *20*, 179.
74. Palecek, E. Adsorptive transfer stripping voltammetry - determination of nanogram quantities of DNA immobilized at the electrode surface. *Anal. Biochem.*, **1988**, *170*, 421.
75. Fojta, M.; Havran, L.; Billova, S.; Kostecka, P.; Masarik, M.; Kizek, R. Two-surface strategy in electrochemical DNA hybridization assays: Detection of osmium-labeled target DNA at carbon electrodes. *Electroanalysis*, **2003**, *15*, 431.
76. Ozkan, D.; Kara, P.; Kerman, K.; Meric, B.; Erdem, A.; Jelen, F.; Nielsen, P.E.; Ozsoz, M. DNA and PNA sensing on mercury and carbon electrodes by using methylene blue as an electrochemical label. *Bioelectrochemistry*, **2002**, *58*, 119.
77. Palecek, E.; Jelen, F.; Postbieglova, I. Adsorptive transfer stripping voltammetry offers new possibilities in DNA research. *Studia Biophysica*, **1989**, *130*, 51.
78. Jelen, F.; Tomschik, M.; Palecek, E. Adsorptive stripping square-wave voltammetry of DNA. *J. Electroanal. Chem.*, **1997**, *423*, 141.
79. Fojta, M.; Havran, L.; Fulneckova, J.; Kubicarova, T. Adsorptive transfer stripping AC voltammetry of DNA complexes with intercalators. *Electroanalysis*, **2000**, *12*, 926.

80. Kizek, R.; Havran, L.; Kubicarova, T.; Yosypchuk, B.; Heyrovsky, M. Voltammetry of two single-stranded isomeric end-labeled -SH deoxyoligonucleotides on mercury electrodes. *Talanta*, **2002**, *56*, 915.
81. Heyrovsky, M. Early polarographic studies on proteins. *Electroanalysis*, **2004**, *16*, 1067.
82. Heyrovsky, M.; Mader, P.; Vavřička, S.; Veselá, V.; Fedurco, M. The anodic reactions at mercury electrode due to cysteine. *J. Electroanal. Chem.*, **1997**, *430*, 103.
83. Kelley, S.O.; Jackson, N.M.; Hill, M.G.; Barton, J.K. Long-range electron transfer through DNA films. *Angewandte Chemie-International Edition*, **1999**, *38*, 941.
84. Tlili, A.; Abdelghani, A.; Hleli, S.; Maaref, M.A. Electrical characterization of a thiol SAM on gold as a first step for the fabrication of an immunosensors based on a quartz crystal microbalance. *Sensors*, **2004**, *4*, 105.
85. Fawcett, W.R.; Fedurco, M.; Kovacova, Z.; Borkowska, Z. Adsorption study of cysteine, N-acetylcystamine, cysteinesulphinic acid and cysteic acid on a polycrystalline gold electrode. *J. Electroanal. Chem.*, **1994**, *368*, 275.
86. Dabrio, M.; Rodriguez, A.R. Complexing properties of the beta metallothionein domain with cadmium and/or zinc, studied by differential pulse polarography. *Analysis*, **2000**, *28*, 370.
87. Dabrio, M.; Rodriguez, A.R. Electrochemical study of human foetal liver metallothionein: Influence of the additions of cadmium and zinc. *Anal. Chim. Acta*, **2000**, *406*, 171.
88. Dabrio, M.; Rodriguez, A.R. Study of complexing properties of the alpha-metallothionein domain with cadmium and/or zinc, using differential pulse polarography. *Anal. Chim. Acta*, **2000**, *424*, 77.
89. Dabrio, M.; Rodriguez, A.R.; Bordin, G.; Bebianno, M.J.; De Ley, M.; Sestakova, I.; Vašák, M.; Nordberg, M. Recent developments in quantification methods for metallothionein. *J. Inorg. Biochem.*, **2002**, *88*, 123.
90. Dabrio, M.; Van Vyncht, G.; Bordin, G.; Rodriguez, A.R. Study of complexing properties of the alpha and beta metallothionein domains with cadmium and/or zinc using electrospray ionisation mass spectrometry. *Anal. Chim. Acta*, **2001**, *435*, 319.
91. Diaz-Cruz, M.S.; Diaz-Cruz, J.M.; Mendieta, J.; Tauler, R.; Esteban, M. Soft- and hard-modeling approaches for the determination of stability constants of metal-peptide systems by voltammetry. *Anal. Biochem.*, **2000**, *279*, 189.
92. Diaz-Cruz, M.S.; Esteban, M.; Rodriguez, A.R. Square wave voltammetry data analysis by multivariate curve resolution: application to the mixed-metal system. *Anal. Chim. Acta*, **2001**, *428*, 285.
93. Diaz-Cruz, M.S.; Mendieta, J.; Monjonell, A.; Tauler, R.; Esteban, M. Study of the zinc-binding properties of glutathione by differential pulse polarography and multivariate curve resolution. *J. Inorg. Biochem.*, **1998**, *70*, 91.

## **Circuit and Noise Analysis of Odorant Gas Sensors in an E-Nose**

**Fengchun Tian**<sup>1</sup>, **Simon X. Yang**<sup>2,\*</sup> and **Kevin Dong**<sup>2</sup>

<sup>1</sup> College of Communication Engineering, Chongqing University, Chongqing, P.R. China 400044

<sup>2</sup> School of Engineering, University of Guelph, Guelph, ON, Canada, N1G 2W1

\* Author to whom correspondence should be addressed: [syang@uoguelph.ca](mailto:syang@uoguelph.ca)

*Received: 08 September 2004 / Accepted: 12 December 2004 / Published: 28 February 2005*

---

**Abstract:** In this paper, the relationship between typical circuit structures of gas sensor circuits and their output noise is analyzed. By using averaged segmenting periodical graph and improved histogram estimation methods, we estimated their noise power spectra and optimal probability distribution functions (*pdf*). The results were confirmed through experiment studies.

**Keywords:** gas sensor, circuit, noise, power spectrum, probability distribution function.

---

## Introduction

Electronic noses (e-noses) are more and more widely used in environmental monitoring, food production and medicine such as odour evaluation [1-4]. The response of all sensors in the e-nose together constitutes a unique profile that gives the “fingerprint” of odour. The noises from the sensor array comprised by several odorant gas sensors may result in inaccurate cluster analysis of the tested material [5]. In our experiments, it is observed that the noise of gas sensors cannot be ignored. In the worst case, the noise magnitude could become up to 20% of the signal magnitude of some sensors. The gas sensors of the e-nose have the following features:

- (1) The sensors in the array interfere with each other.
- (2) Different types of sensors are used, some of which have large heating current and power dissipation.
- (3) Some sensors require amplifiers with extremely high input impedance (e.g., higher than  $10^{11}$  Ohm) that makes them susceptible to interference.
- (4) Some sensors have large dynamic current that produces electromagnetic disturbances to the output of other sensors in the same array.

The drawback of the gas sensors lies in:

- (1) The sensors are very sensitive to temperature and humidity.
- (2) The baseline of sensors shifts with time.
- (3) Large noise exists in sensor output.

This paper is to study the noise features of several typical gas sensors used in the e-nose developed in our research laboratory (shown in Figure 1), including their probability distribution functions (*pdf*) and power spectrum estimation, which are essential in noise cancelling [6-8] and odour analyzing by noise power spectrum [9].

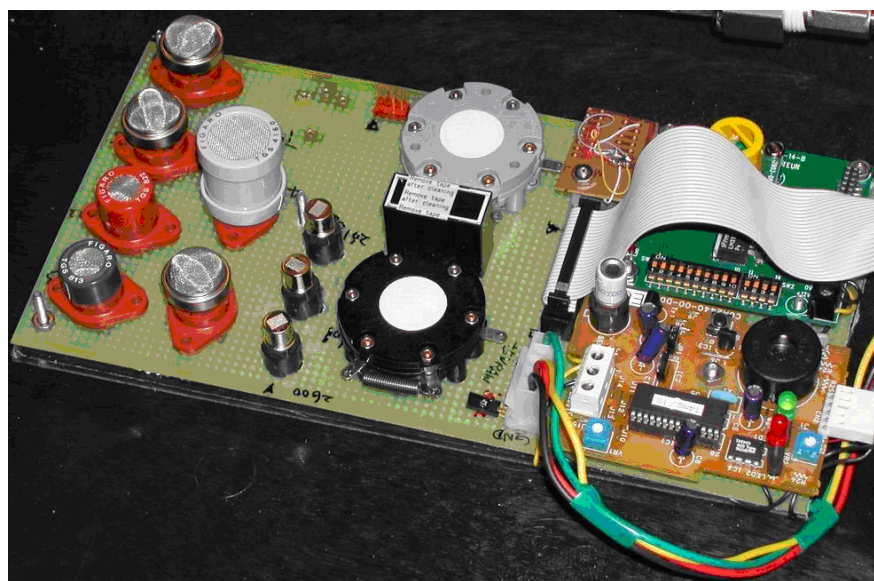


**Figure 1.** Photo of the electronic nose developed in our research laboratory.

## Typical gas sensors and their noise

### Resistive gas sensors

The resistive gas sensors we studied are of MOS (Metal-Oxide Semiconductor) such as tin dioxide. Figure 2 shows a typical sensor circuit and its interface diagram. Pins 2 and 5 are connected to the heater of the sensor, and the resistance between Pins 1 and 6 is designated as  $R_s$ . With pure air  $R_s$  is high. With the presence of detectable gases,  $R_s$  changes with the variation of gas concentration. Since  $V_C$  is a fixed voltage, by measuring the voltage on the resistor  $R_L$ , the change on  $R_s$  as well as the gas concentration can be calculated.

This type of sensor features largely in its heater power dissipation ranging from several hundreds of milliwatt to 1 watt. The working temperature is as high as 400 °C. This will result in higher resistor thermo-noise. Besides, there exist typical semiconductor noises such as Schottky noise, flicker noise etc. As the output signal of the sensor is large enough, the interface circuit uses only a voltage follower as a buffer between the sensor output and the A/D converter, which makes the system less sensitive to external interferences.

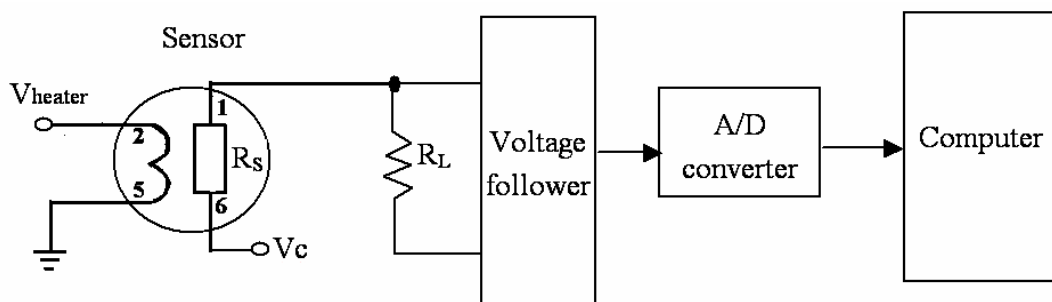


**Figure 2.** Resistive gas sensor and its interface circuit diagram.

### Gas sensors with electromotive output

Figure 3 shows the circuit of a gas sensor with electromotive output and its interface diagram. There is a heater between Pins 1 and 6. A thermometer for temperature compensation is between Pins 2 and 5. The electromotive VEMF between Pins 3 and 4 reflects the concentration of detectable gas. Lower capability of payload is the main feature of this type of sensor. It requires a pre-amplifier with extremely high input impedance at a value over  $10^{11}$  Ohm. As a result, it has the disadvantage of being vulnerable to external electromagnetic interferences in addition to the noise of the resistive gas sensor.

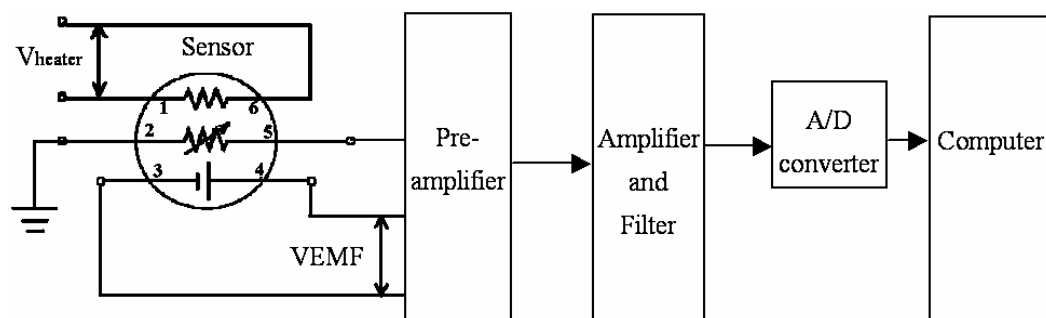


**Figure 3.** Electromotive gas sensor and its interface circuit diagram.

*Sensors with dynamic heating*

The above two types of sensors have a fixed voltage for their heaters, the current of which is constant, whereas the current of the sensor in Figure 4 is dynamic. The difference between this type of gas sensors and the one in Figure 2 lies in the voltage on the sensor heater. Here, the voltage on the heater is a pulse signal that results in a large dynamic current as well as electromagnetic interference to other sensors in the sensor array of the e-nose. The timing control circuit is used to control the voltage applied to the sensor heater and the sampling epoch. Figure 5 is an oscilloscope-recorded waveform about the interference before any noise cancelling measure is taken, where the upper channel is the voltage waveform of heater in Figure 4, which also indicates the current on the heater. The lower channel in Figure 5 is the output waveform of another electromotive gas sensor in pure air that should be a straight line without the interference.

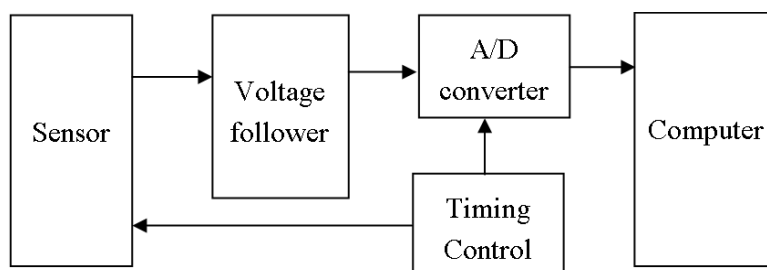


**Figure 4.** Schematic diagram of an odorant gas sensor with dynamic heating and its interface.

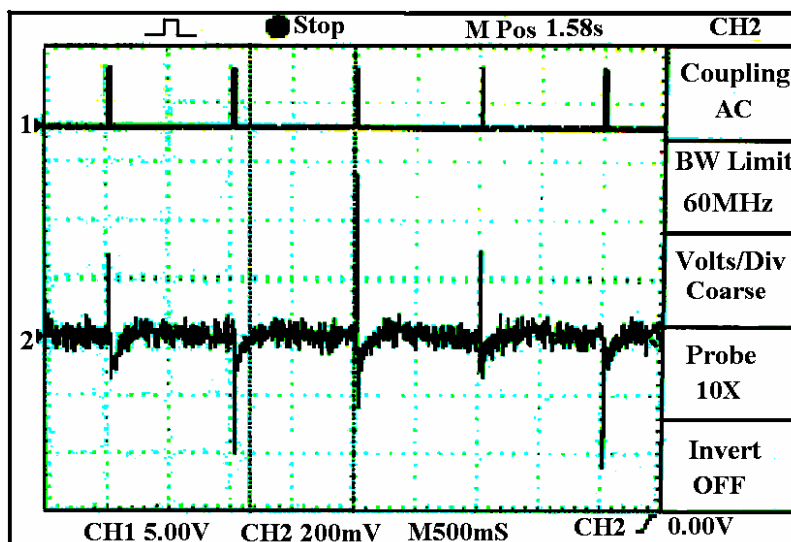


**Figure 5.** Interference on an odorant gas sensor with electromotive output.

*Gas sensors with current output*

Figure 6 shows a typical electrochemical gas sensor and its interface diagram. The working current and voltage of the circuit are low and do not produce interference to other sensor's output. Since the sensor's output current is extremely weak (only several micro amps), it requires the gain of the amplifying circuit be up to several thousands. Thus, the whole circuit is more sensitive to external

disturbances from other sensors than that of sensors with a lower amplifier gain. The noise is also amplified by several thousand times and it has stricter requirement on the equivalent input noise of the amplifier.

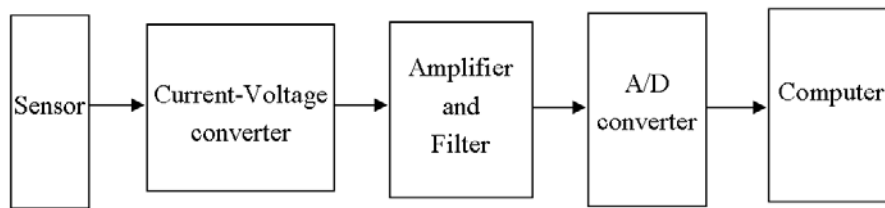


**Figure 6.** Gas sensor with current output and its interface circuit diagram.

### Probability distribution function (*pdf*) of noise

The histogram method, which has been proved to be an unbiased estimation for a random variable, is used to estimate the *pdf* of noise. The estimation error decreases at a rate of  $N^{-2/3}$  as a function of the total number  $N$  of the samples [10].

Let  $X_1, X_2, \dots, X_N$  be independent and identically distributed on  $[0,1]$  with  $N$  the total number of samples. Let  $m$  be an integer and  $h = 1/m$ . Define the bins as

$$B_1 = [0, h), B_2 = [h, 2h), \dots B_m = [(m-1)h, 1] \quad (1)$$

Let  $\hat{p}_j = v_j/N$  and let  $v_j$  be the number of observations in  $B_j$ . Then the histogram estimation of probability distribution function  $f(x)$  is given as:

$$\hat{f}_n(x) = \begin{cases} \hat{p}_1 / h & x \in B_1 \\ \hat{p}_2 / h & x \in B_2 \\ \dots & \\ \hat{p}_m / h & x \in B_m \end{cases} \quad (2)$$

The following two questions should be answered when the histogram estimation method is used:  
 1) How to measure the error between  $\hat{f}_n(x)$  and the real probability distribution function  $f(x)$ ?, and  
 2) What is the optimal  $h$  that makes the approximation of  $\hat{f}_n(x)$  to  $f(x)$  the best?

For the first question, we use the risk function or mean integrated squared error  $R(f, \hat{f})$  between the two functions to measure the error between  $\hat{f}_n(x)$  and the real probability distribution function  $f(x)$ . The function  $R(f, \hat{f})$  is given by:

$$R(f, \hat{f}) = \mathbf{E} \left\{ \int (f(x) - \hat{f}(x))^2 dx \right\} \quad (3)$$

where  $\mathbf{E}\{\cdot\}$  is to calculate the expected value (mean). For the second question, it is obvious that the smaller the  $R(f, \hat{f})$ , the more closer will be  $\hat{f}_n(x)$  and  $f(x)$  (with the exception of only some point sets with zero measure). When  $R(f, \hat{f})$  reaches its minimum, the best approximation of  $\hat{f}_n(x)$  to

$f(x)$  is obtained. Since  $f(x)$  is unknown,  $R(f, \hat{f})$  cannot be calculated directly, but its minimum can be reached by making  $\hat{J}(h)$  the minimum [10]. The function  $\hat{J}(h)$  is given by:

$$\hat{J}(h) = \frac{2}{(n-1)h} + \frac{n+1}{n-1} \sum_j^m p_j^2 \quad (4)$$

The optimal  $h$  that results in the minimum value of  $\hat{J}(h)$  can be obtained by increasing the value of  $m$  from 1. Here, the corresponding formula in [10] is improved by changing its minus sign between the first and the second item into a plus sign according to our experiments. Otherwise, it cannot converge.

### Power spectrum estimation of noise

The periodical graph and averaged segmenting periodical graph methods were used to obtain the power spectrum estimation of noise [11]. For a periodical graph, the power spectrum estimation is given as:

$$S(k) = \frac{1}{N} |\hat{X}(k)|^2 \quad k=0, 1, \dots, N-1 \quad (5)$$

where  $|\hat{X}(k)|$  is the modulus of the Discrete Fourier Transformation (DFT) of  $X_1, X_2, \dots, X_N$ , and  $N$  is the total number of data sets.

To highlight the feature of noise, the mean value of data is removed before the DFT. Otherwise, the d.c. component (zero frequency) will be too large to show other components. The variance of periodical graph is bigger than that of the averaged segmenting periodical graph, but it is useful in observing the baseline shifting of sensors (it corresponds to the lower frequency components near zero frequency).

The averaged segmenting periodical graph is obtained by segmenting the data  $X_1, X_2, \dots, X_N$  into  $K$  small non-overlapping sections. The length of each small section is  $M$  with  $KM = N$ . First, the power spectrum is estimated for each small section (also remove the mean of the small section before the DFT). Then, the power spectrum estimation will be the average of the  $K$  small sections. The disadvantage of this method lies in its losing of information on sensor's baseline shifting that is much smaller during the small section than that of the whole section. The advantage is its asymptotic consistent estimation of real power spectrum. With the increase of  $M$ , the variance of the averaged segmenting periodical graph approaches zero. By this manner, the power spectrum estimation of the small section  $j$  is given as:

$$S_j(k) = \frac{1}{M} |\hat{X}(k)|^2, \quad k=0, 1, \dots, M-1 \quad (6)$$

where  $\hat{X}(k)$  is the DFT of  $X_1, X_2, \dots, X_M$ . The total power spectrum estimation is given as:

$$S(k) = \frac{1}{K} \sum_{j=1}^K S_j(k), \quad k=0, 1, \dots, M-1 \quad (7)$$

## Experiment results

Four types of sensors are used in the test: (1) resistive gas sensors (such as TGS813); (2) gas sensors with electromotive output (such as TGS4160); (3) gas sensors with dynamic heating (such as TGS2442); (4) gas sensors with current output (such as 3ETO). The first three types of sensors are MOS sensors produced by Figaro Ltd., while the fourth ones are electrochemical gas sensors produced by City Technology Ltd.

Figure 7 depicts the response of the above sixteen sensors, each of which is sampled by a 12-bit A/D converter at 6.4 Hz sampling frequency. A charcoal filter (which results in pure air input) was used from epoch A. Since no detectable gas appears, the output of sensors is noise only. A pump was used to intake the pure air into a chamber within which the sensor array lies. After epoch C, the chamber was opened which resulted in the temperature dropping. To get the feature of noise, the stabilized data (from epoch B to C) was used to compute the power spectrum and *pdf* estimation. The number of data sets for each sensor used in calculation is 30,000. In averaged segmenting periodical graph method, the data were segmented into  $K=6$  small sections with the length of each one as  $M=5,000$ . In depicting the *pdf* curve, to highlight the non-zero part, without the loss of generality, we normalized the sensor's output data into  $[0,1]$ , i.e., let the maximum and minimum of sensor output data be  $X_{max}$  and  $X_{min}$ , respectively. Then the normalized data will be given as:

$$X = (X - X_{min}) / (X_{max} - X_{min}) \quad (8)$$

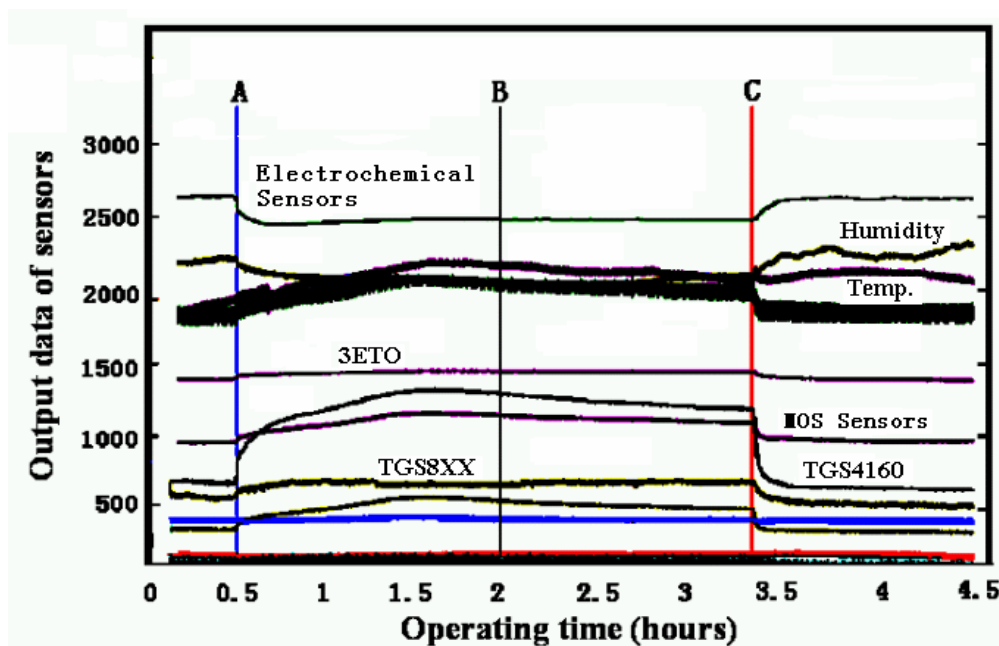


**Figure 7.** Power supply and response of the 16 sensors in e-nose.

Our experiments show that the sensors can be categorized into three types according to their noise power spectrum and *pdf* estimation (see Table 1). Here, a white noise means that its power spectrum magnitude keeps almost constant in the whole frequency range except the d.c. and its nearby

component, while a coloured noise contains considerable low frequency components besides that of the white noise.

**Table 1.** Category of sensors according to their power spectra and *pdf*.

<i>pdf</i> \ Power spectra	Single peak	Double peaks
Coloured noise	(1) TGS813 etc.	(3) TGS830 etc.
White noise	(2) 3ETO etc.	N/A

(1) For the case of coloured noise with a single peak *pdf*, Figures 8(a) and 8(b) show the time-domain curve and the power-spectrum estimation curve, respectively. It shows that the power spectrum of noise mainly consists of two parts: one is the almost constant-magnitude part filling the whole frequency band, and the other is composed of some lower frequency components that may be caused by some inherent feature of the sensor and its circuit. Some of them have the same frequency as signal; it cannot be filtered out by just a simple low-pass filter.

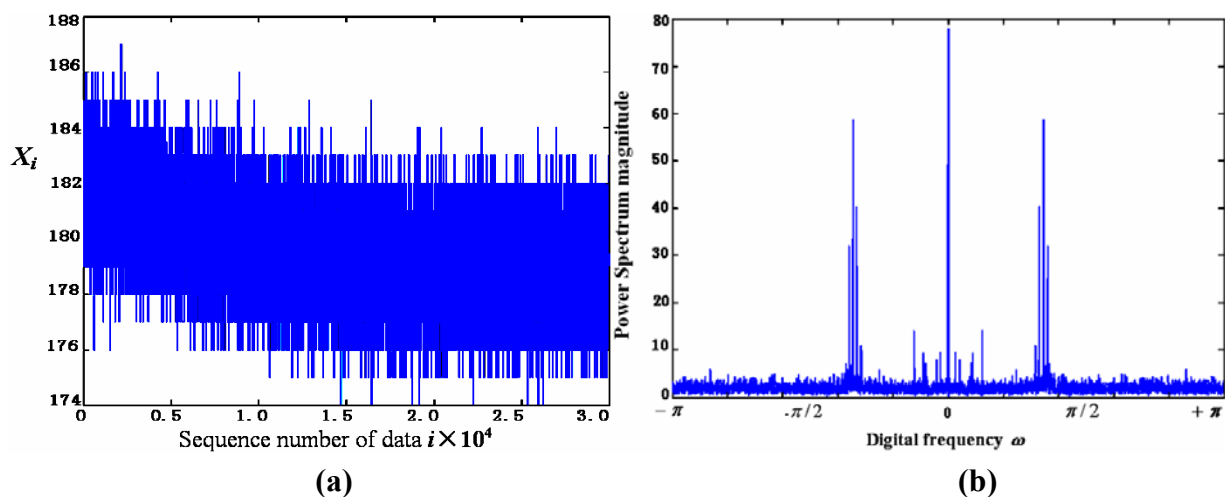


**Figure 8.** The noise (a) and its power spectrum estimation (b) of the first type of sensors in Table 1.

Figure 9 shows the curve of  $\hat{J}(h)$  from equation (4) with  $h = 1/m$ . It can be seen that when  $m = 10$ , i.e.,  $h = 0.1$ ,  $\hat{J}(h)$  reaches its minimum that makes the risk function  $R(f, \hat{f})$  minimum. The  $h$  value at  $h = 0.1$  makes the estimation of *pdf* to be optimal. Figure 10 gives the *pdf* estimation under this  $h$  value. It is close to a Gaussian distribution.

(2) In the case of white noise with single peak, the noise in time domain and its power-spectrum estimation curve are shown in Figures 11(a) and 11(b), respectively. The *pdf* estimation is shown in Figure 11(c) with the optimal value at  $h = 1/75$ . It is similar to a Gaussian distribution. The envelop of the noise power spectrum is almost constant in the whole band. Thus, it is reasonable to consider this type of noise as normal white noise. For the sensors 3SH (current output) and TGS4160 (electromotive), their output signals are too weak and the gain of amplifier has to be large enough (about 6,000), or the input impedance is too high (more than  $10^{11}$  Ohm). The noise energy of these sensors is much bigger than that of the first type in Table 1, which implies that the noise in this type of sensor cannot be ignored.

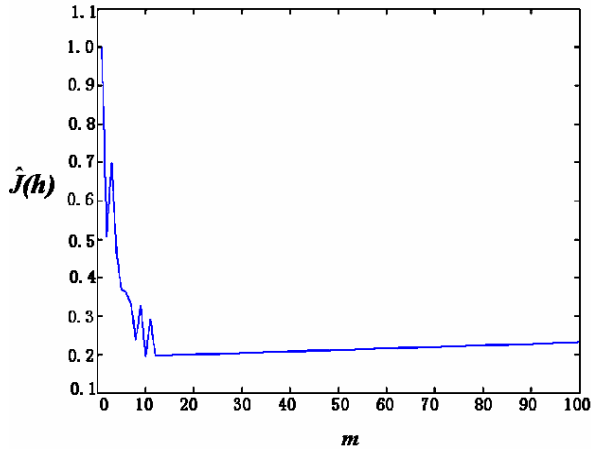


Figure 9.  $\hat{J}(h)$  as a function of  $m$ .

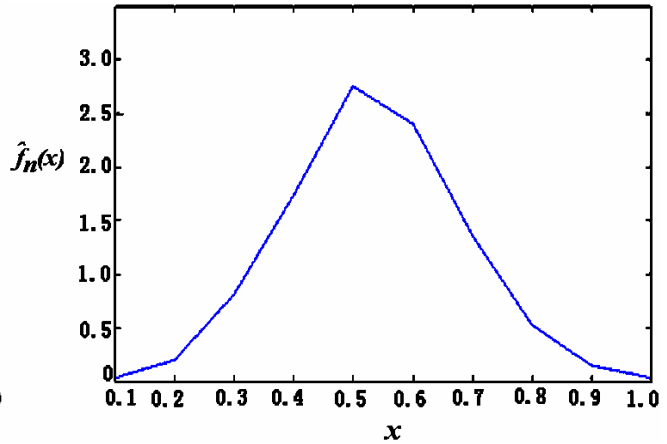
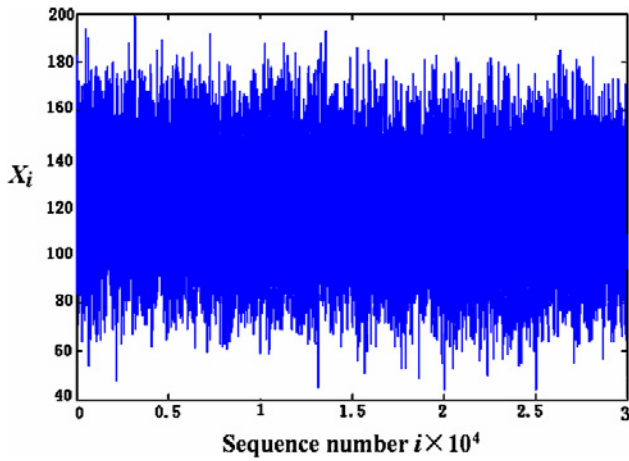
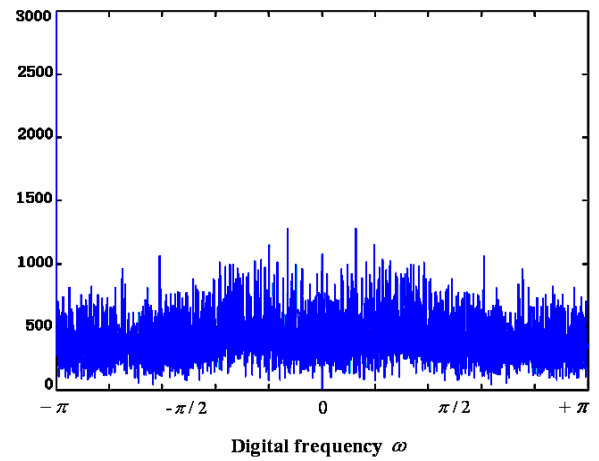


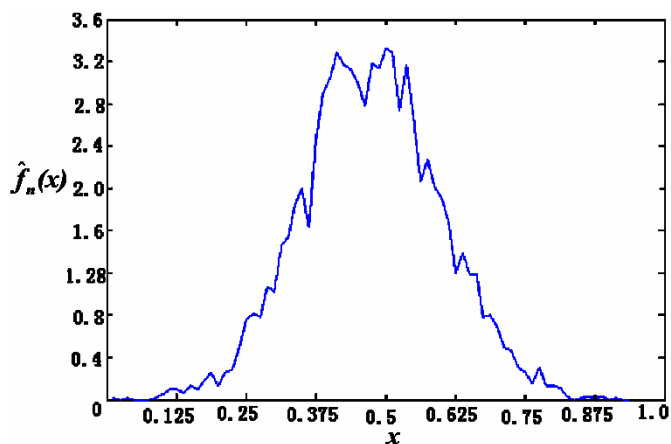
Figure 10. Histogram under the optimal value of  $h$ .



(a)



(b)



(c)

Figure 11. The noise (a), its power spectrum (b) and  $pdf$  estimation (c) of the second type of sensors in Table 1.

(3) For the coloured noise with double peak  $pdf$ , Figures 12(a) and 12(b) show the noise in time domain and its power spectrum estimation of sensor, respectively. Figure 12(c) is the estimation of  $pdf$  with the optimal value at  $h = 1/29$ . In comparison to the first type of sensors in Table 1, both have similar coloured noise power spectrum and many of their low frequency components have the same location in the frequency domain. This implies that the inherent features of the sensors are similar, as

they are produced by the same manufacturer. The only obvious difference here is that its *pdf* has double peaks, while the first type has only one. The double peaks in its *pdf* imply the high appearance frequency of these two types of noise magnitude.

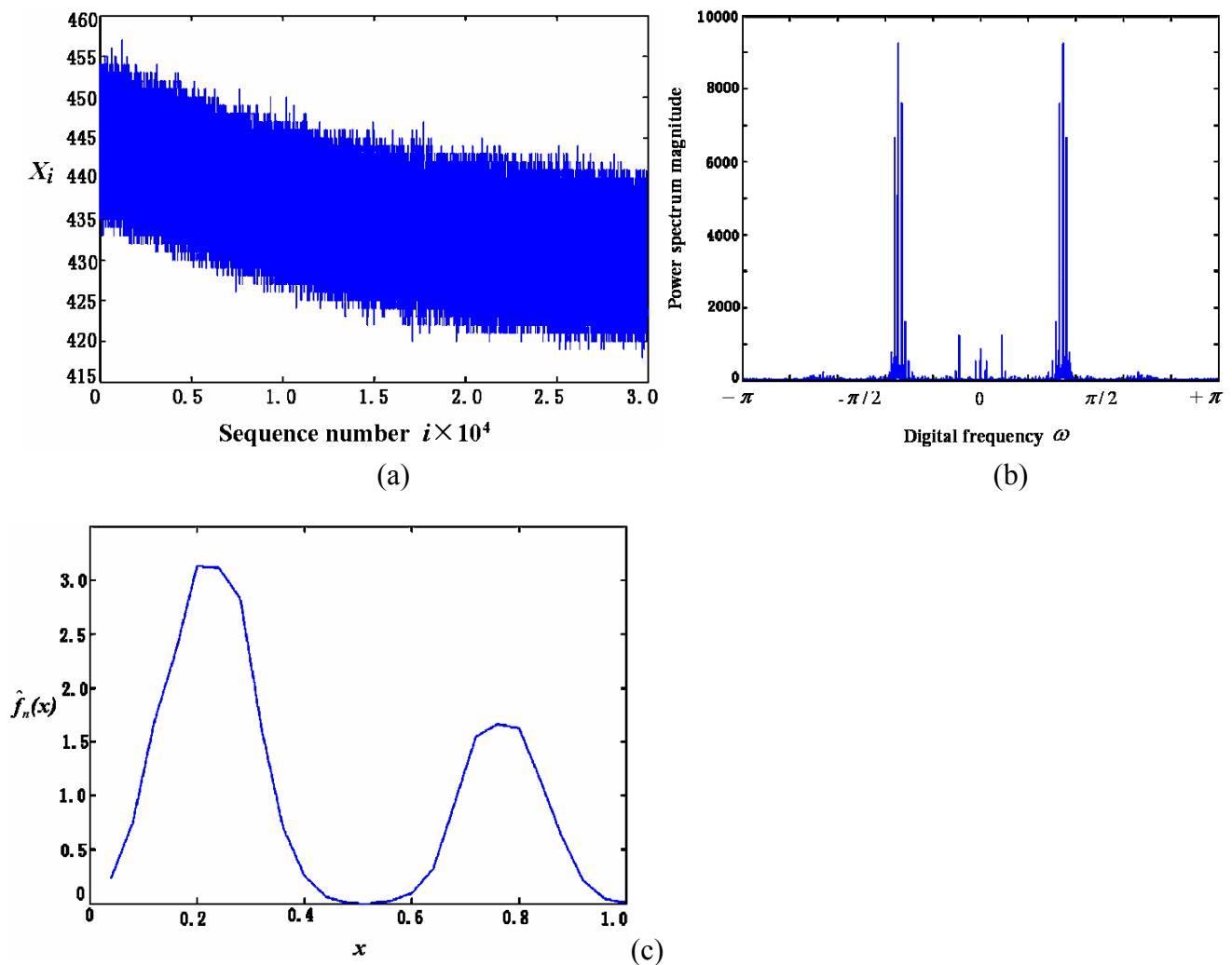


**Figure 12.** The noise (a), its power spectrum (b) and *pdf* estimation (c) of the third type of sensors in Table 1.

(4) For some sensors such as TGS830, TGS2600, the remarkable difference exists in their zero frequency component of noise power spectrum between the periodical graphs and averaged segmenting periodical graph methods. This can be observed when comparing Figure 12(b) and Figure 13. No peak appears in the nearby zero frequency of the averaged segmenting periodical graph in Figure 12(b), which is opposite to its counterpart in Figure 13. It is due to the fact that the sensor baseline shifts slowly within the whole time period (the total 30,000 data sets), although in both methods the mean is removed. Whereas in each small section (5,000 data sets) the baseline changes little and results in almost no nearby zero frequency component. That indicates, of all sensors tested, the three types of sensors can work more stably and have much smaller baseline shift than other sensors.

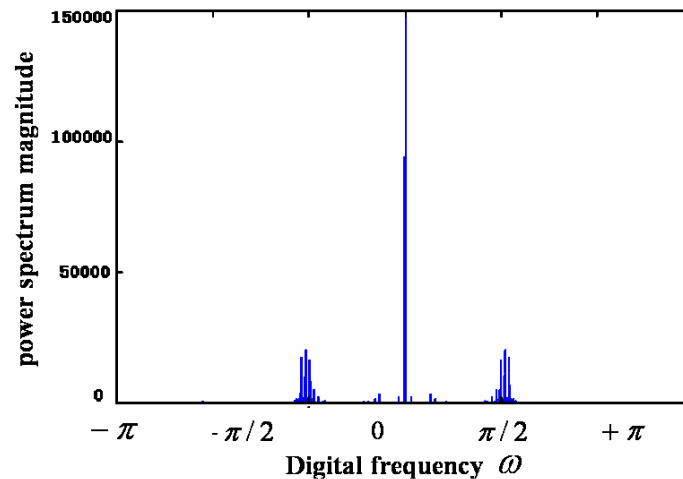


**Figure 13.** Power spectrum by periodical graph.

## Conclusions

The sensor and its interface circuit of four types of odorant gas sensors of an electronic nose are investigated and their noise features are analyzed. Several points are worth to be mentioned:

1. Since the sensors only work with its corresponding circuits as a whole, the sensor noise here means the whole noise from the sensor and its amplifying circuit. The noise is related to the art of manufacture, the input impedance of amplifier and its gain. In our experiment, the optimal operating circuits and devices recommended by the manufacturers are adopted. So it is reasonable to believe those e-noses which use the same type of sensors have similar circuit structure and noise feature as we give here.
2. The noise in the sensors of the e-nose can be categorized into coloured or white noise according to its power spectrum. The coloured noise can be regarded as the white noise plus some stronger low frequency components. The *pdf* of noise is of either single peak or double peaks.
3. The noise of resistive gas sensor is coloured one.
4. The white noise lies in either electromotive sensor or sensor with current output, which is due to either the weak signal or the high input impedance.
5. To estimate the *pdf* of noise, we have used the optimal width ( $h$ ) for bins in histogram that results in the closest estimation to the real *pdf* in the sense of smallest integrated mean squared error. The averaged segmenting periodical graph estimation of noise power spectrum is an asymptotic consistent estimator of the real power spectrum. The error of estimation is expected to be small enough considering the huge number of data sets.
6. The baseline shift of sensor can be observed through comparing the periodical graph and the averaged segmenting periodical graph of noise. Of all the sensors tested, the three sensors TGS830, TGS2600, TGS2602 can work more stably and have smaller baseline shift than others. They almost have no baseline shift in each small section of 5,000 data sets (corresponding to 13 minutes or so). But in the whole period of 30,000 data (corresponding to 1.5 hours), there is still baseline shift.

## References

1. Pearce, T.C. *Handbook of machine olfaction: electronic nose technology*, Wiley-VCH, Weinheim, **2003**, Chap. 5.
2. Gardner, J.W.; Bartlett, P.N. *Electronic noses principles and applications*, Oxford University Press Inc., New York, **1999**.
3. Hurst, J.W. Electronic noses and sensor array based systems: design and applications, *Proceedings of the 5<sup>th</sup> International symposium on Olfaction and the Electronic Nose*, Pennsylvania, **1999**.
4. Schiffman, S.S.; Bennett, J.L.; Raymer, J.H. Quantification of odours and odorants from swine operations in North Carolina, *Agricultural and Forest Meteorology*, **2001**, *108*, 213.
5. Goodner, K.L.; Dreher, J.G.; Rouseff, R.L. The dangers of creating false classifications due to noise in e-nose and similar multivariate analyses, *Sens. Actuators B*, **2001**, *80*, 261.
6. Wang, Y.; Zhang, C. A novel methodology to cancel the additive coloured noise for real-time communication application, *IEICE Transactions on Electronics*, **2002**, *85*, 480.
7. Biswal, B.; DeYoe, E.A.; Hyde, J.S. Reduction of physiological fluctuations in fmri using digital filters, *Magnetic Resonance in Medicine*, **1996**, *35*, 107.
8. Friedrichs, M.S. A model-free algorithm for the removal of baseline artifacts, *Journal of Biomolecular NMR*, **1995**, *5*, 147.
9. Solis, J.L.; Kish, L.B.; Vajtai, R.; Granqvist, C.G.; Olsson, J.; Shnurer, J.; Lantto, V. Identifying natural and artificial odors through noise analysis with a sampling-and-hold electronic nose, *Sens. Actuators B*, **2001**, *77*, 312.
10. Wasserman, L.A. *All of statistics: a concise course in statistical inference*, Springer, New York, **2004**.
11. Mulgrew, B.; Grant, P.; Thompson, J., *Digital signal processing*, Palgrave, New York, **1999**.

## **Application of Artificial Neural Networks in Multitouch-Sensitive Systems for the Detection of Nitrohydrocarbons in the Air**

**Andrew V. Kalach** \*

Physical Department, Institute of Ministry of Internal Affairs, Patriotov pr., 53, 394065 Voronezh, Russia

\* Author to whom correspondence should be addressed. Email: [andrey\\_kalach@mnogo.ru](mailto:andrey_kalach@mnogo.ru)

*Received: 30 August 2004 / Accepted: 03 December 2004 / Published: 28 February 2005*

---

**Abstract:** Artificial neural networks (ANN) were applied for use with electronic-nose generated analytical signals. The use of ANN as a sensor calibration means was evaluated. Piezoelectric quartz sensors array in addition to the ANN data allow recognition of aliphatic nitrohydrocarbons C<sub>1</sub>–C<sub>3</sub>.

**Keywords:** piezosensors array, nitrohydrocarbons, artificial neural network.

---

## Introduction

Touch-sensitive electronic-nose systems include nonselective sensors and methods of analytical signals processing based on the modern artificial intelligence development [1-2]. It is applied, for example, to pattern recognition methods and multiparametrical graduation. The multitouch-sensitive approach allows simultaneous qualitative and quantitative analysis of complex mixtures.

The use of artificial neural networks (ANN) seems to be very progressive for measuring information coming from separate sensors or their combination (the multitouch-sensitive system) [3-7].

## Experimental work

The main task of the qualitative analysis is the components recognition of aliphatic nitrohydrocarbons mixes (AN). The mixes of various mixtures were prepared in a thermostatic amalgamator. The analysis was done at  $25 \pm 0.5$  °C.

The quantitative analysis was carried out in a number of the multicomponent systems simulating possible applications of an "electronic nose". Modeling gas mixes containing AN in amount of  $5 \cdot 10^3 - 7.5 \cdot 10^2$  g/m<sup>3</sup> were analyzed.

Component concentration was measured simultaneously after the appropriate system training using the modeling mixes set (24-48), containing AN in various ratios. The "Electronic nose" consisted from 3 to 6 sensors depending on the task. To minimize the humidity influence, piezosensors were kept in the evaporator between the measurements. Before starting the analysis, the touch-sensitive block was blown by dried air up to the moment of the constant quartz plate fluctuations frequency. The duration of the analysis took 2-5 min.

The piezosensor analytical signals were processed using linear (principal component analysis) and nonlinear (ANN) methods.

The "electronic nose" application was investigated for the detection of widespread dangerous substances such as aliphatic nitrohydrocarbons (nitromethane, nitroethane, 1<sup>-</sup> and 2<sup>-</sup> nitropropane) in air. As piezosensors modifiers, we applied squalan, 1-apiezon, 1,2,3-tris(-cianoethoxy)propane, triton X - 100, triton X - 305, triethanolamine. The modifier solution was deposited onto the piezosensor electrode surface with the help of a microsyringe.

The use of piezosensors is a special case of more general touch-sensitive devices. Piezosensors are simple in use, compact and applicable for pollutant detection directly in gas emission. However in complex systems, their selectivity is insufficient; the outside components cause significant touch-sensitive function deviations from the theoretical (linear) dependence (Sauerbrey equation).

## Results and discussion

The circuit of the multitouch-sensitive gas-sorption system called the "electronic nose" (Figure 1) was developed. The sensor included in the system is characterized by a cross-sensitivity to the analyzed gas environments components and possess rather high signal reproducibility that is easily identifiable through AN. Moreover, the realization of an environment for on-line monitoring is possible; the

"electronic nose" is applicable both for chemical component recognition and foodstuff components [1, 8-10].

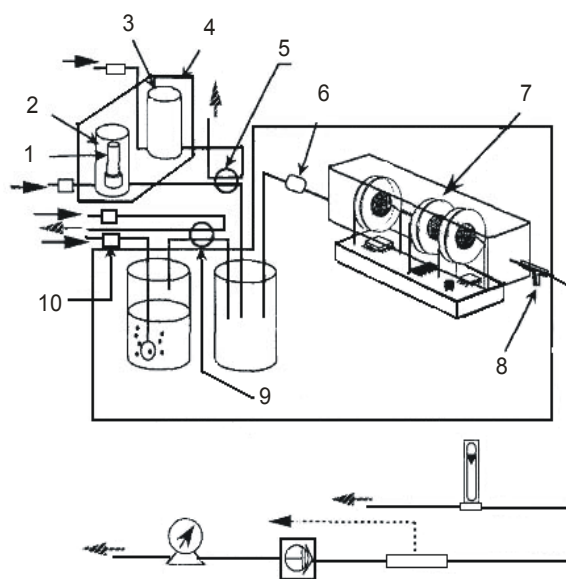


**Figure 1.** Circuit of gas-sorption experimental set: 1, 2 ampoules with compound; 3 intermediate buffer capacity; 4 thermostatic capacity; 5, 9 three-running crane; 6 buffer capacity; 7 cell of detecting; 8 two-running crane; 10 traps for impurity.

Formal ANN are made from artificial (formal) neurons. The most widespread variant is the MacCulloch and Pitts neuron [8], representing the elementary model of the biological neuron (Figure 2). Its functioning is described by the following equation:

$$Y = F\left(\sum_{j=1}^n w_j \cdot x_j\right) \quad (1)$$

where  $Y \in \mathbb{R}$  – a neuron output;  $x_j \in \mathbb{R}$ ,  $j$  – input neuron signals;  $w_j$  – weight factors;  $F$  – linear or nonlinear neuron activation function with the range of  $\mathbb{R}$  definition.

The following sigmoid functions are used as the function of activation:

$$F(t) = \frac{1}{1 + e^{-t}}, \mathbb{R} \rightarrow (0, 1) \quad (2)$$

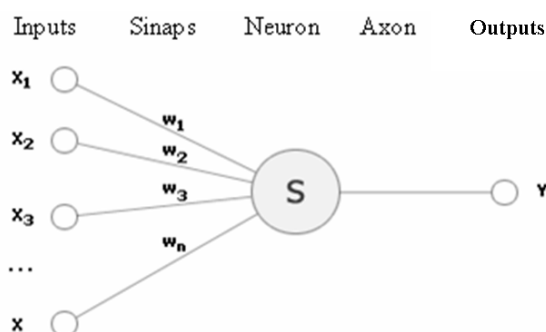


**Figure 2.** Artificial neuron.

For the effective decision of the qualitative or quantitative substances analysis, ANN should pass a training stage. In addition, the adjustment of topology, weight factors, and function parameters of activation or other network parameters are carried out by specially formed training selection.

At training, the artificial neural networks should have the correct output signals. To achieve, it the training sample is made from pairs  $(z_g, x_g)$ . The training is considered to be complete, when the criterion of the quality of training is stabilized at some level. By the way of such criterion residual dispersion is applied:

$$S_0^2 = \frac{1}{N} \sum_{g=1}^N (z_g - y_g)^2 \quad (3)$$

where  $y_g$  is a target signal of ANN.

At small dispersion, the accuracy of artificial neural networks approximation of the graduation characteristic is considered to be sufficient. Once the training comes to an end, if the accuracy is not achieved, the complexity of ANN must be increased, increasing  $k$  or passing larger number of layers to the network.

The training procedure is reduced to criterion function minimization on the set of possible values of  $w_j$ . For ANN training, the method of back-mistake propagation received the greatest attention and it is called the algorithmic version of the gradient method.

#### *Construction of the sensors graduation parameters*

The graduation of a sensor (gauge, measuring channel) consists in the measurement of the input value (factor) and the output signal of X sensor. As a result one has a set of values  $(Z_g, X_g)$ ;  $g=1, N$ , where  $N$  is a number of experiences. The unknown quantity is the graduation dependence  $Z=Z(X)$  found by the results of the experiment.

The task is reduced to the standard approximation and there are numerous methods and techniques to solve it. As the values  $Z_g$  and  $X_g$  can have measuring errors, then in order to obtain the dependence of graduation the statistical methods (regression or the confluent analysis) are used.

The principle of the use of the artificial neural network approach is based on the well-known theorem [8], according to which the continuous function, given on an individual cube, variable quantities can approximate with the given accuracy of formal three-layered neural networks. Such networks contain a layer of the input units representing input signal forks. One intermediate (latent) layer and output layer (last two layers) consist from formal neurons. In ANN structure, only the neuron number of the latent layer  $k$  needs solving. To calculate it we use the following ratio:

$$\frac{mN}{(n+m) \cdot (1 + \log_2 N)} \leq k \leq m \left( \frac{N}{n} + 1 \right) + \frac{m}{n+m} \left( \frac{N}{n} + 2 \right) \quad (4)$$

where  $n$  and  $m$  – are the number of inputs and outputs of neural network accordingly. It is recommended to choose the number  $k$  close to the top borders of values.

ANN provide the exact reproduction of the approximation function so it makes them effective, in contradistinction to the traditional methods.

The ANN advantages consist in the absence of the necessity of the detailed information of a priority concerning the approximation function (in the regress analysis at absence of such information function display on basic) and universality. The ANN restrictions are caused by the unusual form of the representation of a result as the program simulating the work of a trained network. At the neural network approach, the substantial interpretation of the received dependences is also complicated. For example, in multitouch-sensitive systems it is impossible to the separate sensors' level selectivity in relation to the determined substance or to the range on the information level.

The responses of multitouch-sensitive system to the influence of aliphatic nitrohydrocarbons  $C_1 - C_3$  vapors in a wide range of concentration ( $0.005-0.075 \text{ g/m}^3$ ) are studied. This interval includes their extreme admissible concentration in the air of the working zone ( $0.03 \text{ g/m}^3$ ). The ANN structure and its parameters are optimized to decrease the detection mistake. The accuracy of detection AN is 1.5-2.3 %, besides the array did not contain sensors, which were selective to the separate components of a mixture. The ANN property to be trained makes them more perspective in comparison with the algorithms of the information processing based on the use of the rigid system of the preconditions.

Thus, the solution of problems of the chemical analysis of complex environments is possible using the multitouch-sensitive approach. This approach consists of the simultaneous use of measurements of chemical sensor arrays in combination with the mathematical method of data processing, taking into account nonlinearity of the response or other distortions of the function of sensors in the multicomponent environment. With the multitouch approach it becomes possible to get the known accurate information about the compound concentration in the multicomponent environment. The selectivity of separate sensors used as a set does not have any meaning of principle. On the contrary, it is important that the sensors have sensitivity to the maximal compound number and differ in parameters of this sensitivity.

The combination of a matrix of non-selective piezoelectric sensors and the method of signal processing has resulted in the creation of an analytical device for the qualitative recognition of complex gas mixes, and the multicomponent analysis. As required, both operations can be carried out with one experimental measurement of an analytical signal from an "electronic nose".

## Acknowledgments

The author thanks Dr. Natalya Ezhova for her assistance in correcting the article translation into English.

## References

1. Vlasov, Yu.G.; Legin, A.V.; Rudnit'kaya, A.M. Electronic language multitouch system on the basis of a file of nonselective sensor controls and methods of recognition of images. *Gauges and systems*, **1999**, *6*, 3.
2. Rudnitskaya, A., Ehlert A.; Legin, A.; Vlasov, Y.; Büttgenbach, S. Multisensor system on the basis of an array of non-specific chemical sensors and artificial neural networks for the determination of inorganic pollutants in a model groundwater. *Talanta*, **2001**, *2*, 425.

3. Lu, Y.; Bian, L.; Yang, P. Quantitative artificial neural network for electronic noses. *Anal. Chim. Acta*, **2000**, *417*, 101.
4. Mahfouz, I.A. Drilling wear detection and classification using vibration signals and artificial neural network. *Int. Journal of Machine Tools & Manufac.*, **2003**, *43*, 707.
5. Kuo, R.J. Multi-sensor integration for on-line tool wear estimation through artificial neural networks and fuzzy neural network. *Engin. Appl. of Art. Intel.*, **2000**, *13*, 249.
6. Sriyudthsak, M.; Teeramongkolrasamee, A; Moriizumi, T. Radial basis neural networks for identification of volatile organic compounds, *Sens. Actuators B*, **2000**, *65*, 358.
7. Zhang, H.; Balaban, M.O; Principe, J.P. Improving pattern recognition of electronic nose data with time-delay neural networks. *Sens. Actuators B*, **2003**, *96*, 385.
8. Wasserman, F. *Neurocomputing engineering: the theory and practice*. Moscow: World, **1992**.
9. Filaretov, G.F.; Zhitkov, A.N. Application of artificial networks in touch systems. *Gauges and systems*, **1999**, *5*, 2.
10. Semenov, L.A.; Siraya, T.N. *Methods of construction of the graduation characteristics of means of measurement*. Moscow: Standards, **1986**.

## **Environmental Studies with the Sensor Web: Principles and Practice**

**Kevin A. Delin**<sup>1,\*</sup>, **Shannon P. Jackson**<sup>1</sup>, **David W. Johnson**<sup>1</sup>, **Scott C. Burleigh**<sup>1</sup>, **Richard R. Woodrow**<sup>1</sup>, **J. Michael McAuley**<sup>1</sup>, **James M. Dohm**<sup>2</sup>, **Felipe Ip**<sup>2</sup>, **Ty P.A. Ferré**<sup>2</sup>, **Dale F. Rucker**<sup>2</sup> and **Victor R. Baker**<sup>2</sup>

<sup>1</sup> NASA / Jet Propulsion Laboratory, 4800 Oak Grove Drive, Pasadena, California 91109-8099

<sup>2</sup> Department of Hydrology and Water Resources, University of Arizona, Tucson, AZ 85721

\* Author to whom correspondence should be addressed. Email: [kevin.delin@jpl.nasa.gov](mailto:kevin.delin@jpl.nasa.gov)

*Received: 04 October 2004 / Accepted: 05 December 2004 / Published: 28 February 2005*

---

**Abstract:** In 1997, the Sensor Web was conceived at the NASA/Jet Propulsion Laboratory (JPL) to take advantage of the increasingly inexpensive, yet sophisticated, mass consumer-market chips for the computer and telecommunication industries and use them to create platforms that share information among themselves and act in concert as a single instrument. This instrument would be embedded into an environment to monitor and even control it. The Sensor Web's purpose is to extract knowledge from the data it collects and use this information to intelligently react and adapt to its surroundings. It links a remote end-user's cognizance with the observed environment. Here, we examine not only current progress in the Sensor Web technology, but also its recent application to problems in hydrology to illustrate the general concepts involved.

**Keywords:** Sensor Web, network, wireless, hydrology, flood.

---

## Overview of the Sensor Web

In its most general form, the Sensor Web is a macro-instrument comprised of spatially-distributed sensor platforms [1]. As shown in Figure 1, these platforms, or pods, can be orbital or terrestrial, fixed or mobile. Coordinated communication and interaction among the pods provides a local fusion of the dispersed data and results in a spatio-temporal understanding of the environment. Specific portal pods provide end-user access points for command and information flow into and out of the Sensor Web. The NASA/JPL Sensor Webs Project is currently focused on *in-situ* Sensor Webs, with the resulting instrument accessible, in real-time, via the Internet.

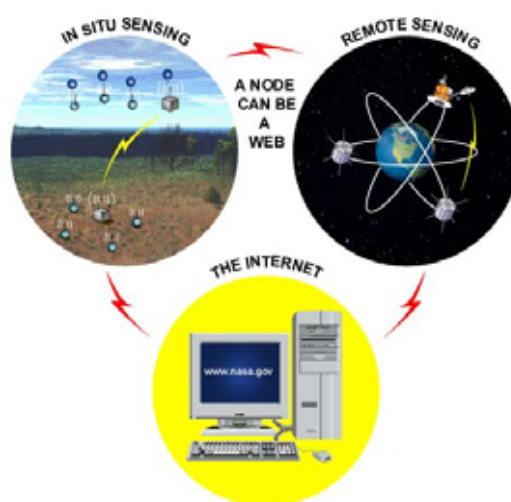


**Figure 1.** Generalized concept of the Sensor Web, including both orbital and terrestrial platforms.

The Sensor Web's capabilities are useful in a diverse set of outdoor applications ranging from precision agriculture to perimeter security to effluent tracking. Wireless networks of sensors are often marketed as replacements for running wire to sensing points. Naturally this holds true for the Sensor Web as well, with the individual pods communicating among themselves wirelessly. However, it is more significant that the Sensor Web, with its unique global information sharing protocol, forms a sophisticated sensing tapestry that can be draped over an environment. This Sensor Web approach allows for various complex behaviors and operations such as on-the-fly identification of anomalous or unexpected events, mapping vector fields from measured scalar values and interpreting them locally, and single-pod detection of critical events which then triggers changes in the global behavior of the Sensor Web.

Wireless networks are not a new approach to environmental monitoring and it is common to find systems where remote sensors in the field communicate to central points for data processing in a star-network formation. The Sensor Web, however, is a temporally synchronous, spatially amorphous network, creating an embedded, distributed monitoring presence which provides a dynamic infrastructure for sensors. By eschewing a central point on the network, information flows everywhere throughout the instrument (see Figure 2).

So far, this sounds like a typical *ad hoc*, self-configuring, mesh network. Often, the ideas of hopping information around such a network are framed in terms of the power advantage gained by

doing so. While this advantage certainly exists, the Sensor Web concept goes one step further: the individual pods comprising a Sensor Web are not just elements that *can* communicate with one another; they are elements that *must* communicate with one another. Whereas wireless networks are typically discussed as confederations of individual elements (like computers connected to the Internet), the Sensor Web is a single, autonomous, distributed instrument. The pods of a Sensor Web are akin to the cells of a multi-cellular organism; the primary purpose for information flow over a Sensor Web is not about getting data to an end-user, but rather to the rest of the Sensor Web itself.

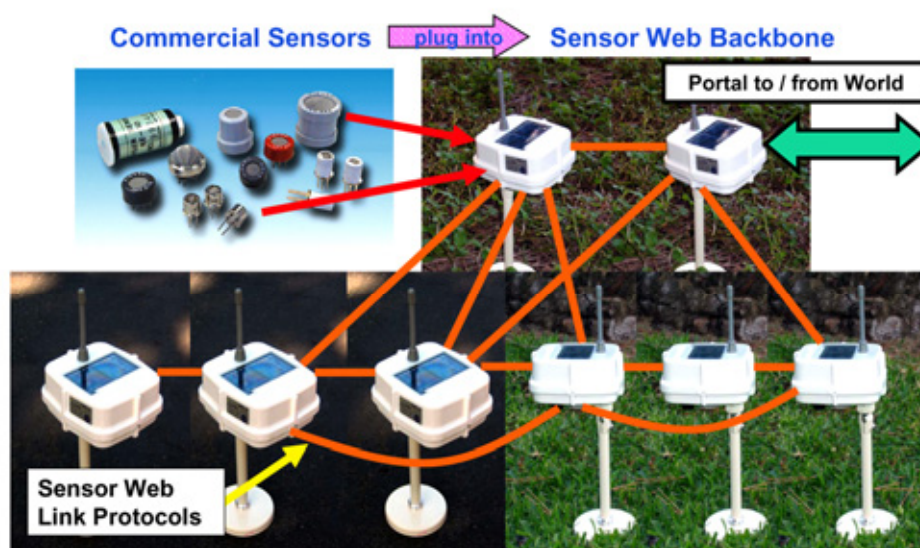


**Figure 2.** The Sensor Web forms an informational backbone that creates a dynamic infrastructure for the sensors in the Sensor Web pods.

By design, the Sensor Web spreads collected data and processed information throughout its entire network. As a result, there is no design criterion for routing as in more typical wireless systems. Routing, by definition, is a focused moving of information from one point to another. In contrast, information collected by a Sensor Web is spread everywhere, rendering meaningless the concept of routing on it. Instead, the communication protocol on a Sensor Web is relatively simple and is structured for both omni- and bi-directional information flows. Omni-directional communication implies no directed information flow, while bi-directional communication lets individual pods (and end-users) command other pods as well as receive information from them. Consequently, information on the Sensor Web can result from four types of data: (a) raw data sensed at a specific pod, (b) post-processed sensed data from a pod or group of pods, (c) commands entered into the distributed instrument by an external end-user, and (d) commands entered into the distributed instrument by a pod itself. The Sensor Web processes this internal information, draws knowledge from it, and reacts to that knowledge.

Since there is no specific routing of information, all pods share everything with each other. After each measurement is taken, both raw and processed information from each pod are moved throughout the Sensor Web to all other pods before the next measurement is taken. Because the Sensor Web is a single, distributed instrument, its internal operations are synchronous from pod to pod (again in contrast to more common wireless networks). In this way, the total snapshot associated with that

instant in time is available to all pods on the Sensor Web. This global data sharing allows each pod to sense phenomena beyond its specific location. Pods may therefore, combine data across the Sensor Web to identify a moving front and determine its speed and direction, a task that a single-point measurement can not accomplish. Pods may also use neighbours to examine the stochastic nature of their local measurements to determine whether or not the data collected are well-behaved. Such macroscopically coordinated data processing would not be as straightforward if each pod were semi-autonomous on the network, as in typical wireless sensor systems. There is a degree of stiffness to the information flow over the Sensor Web compared to the individually directed node-to-node information threads on more typical wireless systems. The Sensor Web pods may be thought of as individual, synchronized pixels in a much larger instrument that can take snapshots at regular intervals of the entire environment in which it is embedded and each pixel is simultaneously aware of the overall picture as well as its local readings.

### Sensor Web pods

A Sensor Web pod consists of five basic modules:

- (1) The radio, which links each pod to its local neighborhood. The NASA/JPL Sensor Web pods use radios operating in the 900 MHz license-free Industrial, Science and Medical (ISM) band with an upper range of ~200 m or more. (Implicitly, we assume none of the *in-situ* Sensor Webs discussed here are deployed underwater, where acoustic modems severely limit bandwidth and communication range relative to these ISM radios.)
- (2) The microcontroller, which contains the system's protocols, communicates with the attached sensors, and carries out data analysis as needed.
- (3) The power system. The NASA/JPL system uses a battery pack with solar panels to keep the batteries charged. The combination of solar panels and micropower electronic design have kept Sensor Web pods operating in the field for years without requiring maintenance.
- (4) The pod packaging. This key module is often overlooked, especially for Sensor Web applications in the wild. The package must be light, durable, inexpensive, and sealed against such elements as rain, snow, salty sprays, dust storms, and local fauna. In addition, it must provide for easy and rapid mounting.
- (5) The sensor suite. This module is completely determined by the specific application. Ideally, the sensor suite will, in fact, be the prime-determining factor for the size, cost, and power requirements of a Sensor Web pod, making the Sensor Web infrastructure attractive for any application. What is considered an inexpensive or small Sensor Web pod in one application may not be viewed as such in another.

We have been conditioned by decades of experience with Moore's Law (and the technology revolution associated with it) to think that smaller is always better. There are certainly practical reasons for limiting the size of a Sensor Web pod. In an outdoor environment, smaller and lighter pods are easier to deploy since more can fit into, say, a backpack. However, shrinking pods to infinitesimal sizes is undesirable for a typical outdoor Sensor Web system. Consider the impact of size with respect to three key Sensor Web pod design issues: power, antenna size, and transducers.

An important design requirement for typical outdoor Sensor Webs is pod longevity. In many cases, deployment is only practical during certain seasons and therefore, intra-season maintenance must be avoided. As a result, maximizing the available power, by cleverly using batteries and/or energy harvesting, is critical. Batteries are often rated in terms of their energy density (watt-hours per unit volume). This is because cells can be added serially to increase total available voltage. The larger the volume of the Sensor Web pod, the more volume is available for power from any particular battery technology.

There are only two ways to maintain a given amount of battery power level available while allowing the pod volume to shrink: improve the battery technology or reduce energy use within the pod. While there are numerous efforts to provide higher energy-density power sources than are typically available (e.g., lithium ion batteries), none are yet commercially available for consumer use. In addition, many experimental batteries have limited lifetimes. Moreover, any suitable battery technology must be essentially zero-maintenance and environmentally robust (especially to changes in temperature, both seasonal and diurnal). As for improving energy efficiency, the laws of physics require a certain power output to broadcast a given distance. Therefore, although one can lower the energy per bit involved in computation, the wireless communication puts a hard limit on how much energy will be required for the system to operate for a given pod-to-pod distance.

Now, consider energy harvesting which is typically accomplished via solar power charging secondary batteries. Here, too, the smaller the platform, the smaller the solar panels used to re-energize the system, and the smaller amount of energy that can be harvested for a given panel. Clearly, beyond a certain size, the smaller one designs a Sensor Web pod for a given set of operating parameters, the more one gives up in terms of longevity with respect to available power.

Antennas are also directly related to platform size. Again, the laws of physics dictate the appropriate antenna geometry for a given operating frequency to ensure a proper impedance match into the radiated space. As a result, while the on-board processor and radio electronics may shrink, the antenna may not if a particular communication range is required. Without proper coupling, radiation efficiency is reduced and power must be increased to the radio to maintain range. We therefore find that since most outdoor Sensor Webs required pod-to-pod ranges of at least tens of meters, indiscriminate shrinking of the individual antennas clearly compromise the telecommunication subsystem.

Lastly, consider the sensors themselves. many sensors used in outdoor field applications, though compact and inexpensive, are not micro-electromechanical system (MEMS) devices and therefore cannot be integrated into the Sensor Web pod at the chip level. As a result, for a wide variety of Sensor Web applications in an outdoor environment, the sensors will be additional components added to the basic pod platform. Clearly, there is little to be gained by continually shrinking the platform if the sensors themselves remain the limiting size element. Moreover, shrinking the platform may actually complicate the design if it becomes difficult to integrate the sensors into the pod.

As shown in Figure 3, the NASA Sensor Web pods have been developed in several sizes, including that of a gumball and that of a couple of decks of playing cards. Significantly, the gumball-sized pod dates back to 1998 [1], demonstrating, even then, that it was relatively easy to make small platforms so long as only simple measured parameters (i.e., temperature, humidity, etc.) and short pod-to-pod communication distances (i.e., order of meters) were required. Such small pods are ideal for building

or factory monitoring, but less practical for outdoor environments for reasons discussed above. From this discussion, it is apparent that, while smaller pods are desirable, shrinking pods beyond a certain point leads to diminishing returns.

### Fielding a Sensor Web

With the objective to do real *in-situ* environmental work, the NASA/JPL Sensor Webs Project has been aggressive about fielding instruments. Sensor Webs have been deployed in a large variety of demanding real-world locations for many months or even years. For example, Sensor Webs have been at the Huntington Botanical Gardens in San Marino, CA, starting with the deployment of Sensor Web 2.0 in June 2000 and continuing with Sensor Web 3.0, the first permanent wireless sensor network system to provide continuous real-time streaming data to users over the Internet, in October 2001. The Gardens continue to remain a significant test site for Sensor Web technology [1]. Information about other deployments in a variety of environments as well as real-time, streaming data from several present deployments, is available on the Internet [2].

From the experience of deploying the Sensor Web in a multitude of environments with varying conditions, it is apparent that the ease with which the system is deployed is just as critical for acceptance by end-users as are its technological aspects. With the exception of applications in battlefield theaters, most outdoor Sensor Web applications require the system to be deployed in manner that does not harm the monitored environment. For example, end users have expressed concerns that if Sensor Web pods are too small, local fauna may try to ingest them and choke. End-users also want to avoid littering their environment with hundreds of pieces of microelectronic gear.

Most applications require tracking specific pod location and it is therefore highly unlikely that pods will simply be sprinkled over large areas. In addition, coupling sensors into the environment will usually prevent such a passive deployment. For example, neither subterranean nor seismic sensors can be deployed by a sprinkling technique, as both require laborious efforts for appropriate sensor mounting. Consequently, the mounting and placement of Sensor Web pods will be an active operation and likely to be done by hand in most instances.

The methods used to mount the Sensor Web pods depend not only on the application but also the particular field site. Pod placement very close to the ground can limit transmission distance. Nevertheless, while the Huntington Garden pods are within 10 inches of the ground, they have sufficient communication power to keep an adequate pod-to-pod distance. Often, for logistical reasons, the Sensor Web pods tend to be mounted higher off the ground with the attendant benefit of increasing the wireless distance. Local terrain is rarely level which also tends to increase transmission distances. We have typically used posts (for horizontal surfaces) and brackets (for vertical surfaces) to mount the pods. These types of mounts are both small enough and light enough to bring into the field yet are sturdy enough for fixing the Sensor Web pods rigidly in place for long durations.

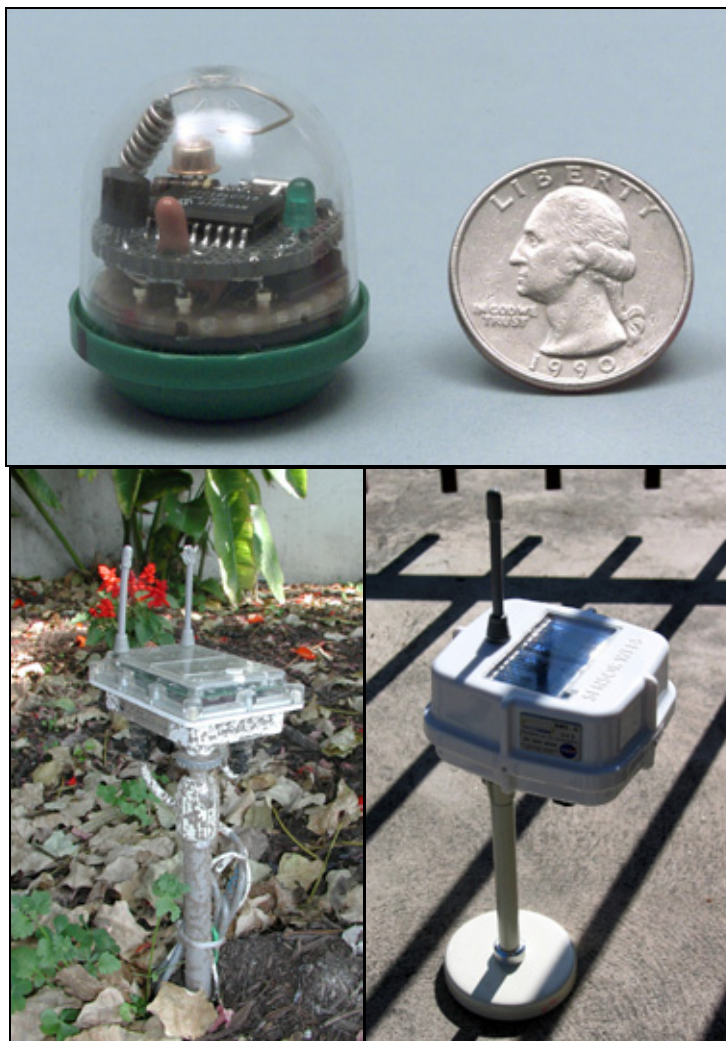


**Figure 3.** Various Sensor Web pods. Top: Functioning Sensor Web 1.0 pod, circa 1998. Note the small size which includes antenna, battery, and temperature and light sensors. Bottom Left: Sensor Web 3.1 pod deployed at the Huntington Botanical Gardens, circa 2002. It is about the size of two decks of playing cards. The pod is mud spattered from rain and watering and has a chewed antenna. Subterranean sensors (soil moisture and temperature) can be seen going into the ground. Bottom Right: A Sensor Web 5.0 pod, circa 2004. This new generation of Sensor Web pods is more compact and more power efficient than previous ones, a direct result of exploiting Moore's Law in its design.

### **Sensor Web deployment at a recharge basin facility**

Each year, large-scale flooding affects millions of people around the world with attendant losses of property and life. A major limitation in the mapping and characterization of catastrophic floods is an inability to monitor them in real-time. For instance, it has been historically difficult to study transient hydrologic phenomena such as storm-induced flooding, surface water movements, water infiltration, and soil moisture conditions. This limitation has had a direct impact on accurate flood prediction systems. The Sensor Web can address this deficiency by providing real-time detection and monitoring of both surface water conditions and water infiltration.

We have deployed a Sensor Web at the Central Avra Valley Storage and Recovery Project (CAVSARP) facility located west of Tucson, AZ [2,3] and shown in Figure 4. The facility is located in a desert environment of the semi-arid Southwest United States where the artificial recharge basins experience repeated flood cycles. The controlled flooding conditions at the CAVSARP facility are ideal for the investigation of various hydrologic processes. Common geomorphologic features related to flood inundation observed at the site are analogous to features often found in ancient paleolakes on both Earth and Mars and include wave-cut terraces, polygonal-patterned ground, and ridges related to drying of basin floor materials. Algal mats are also visible in some of the basins during the drying period of the flood cycle. Thus, the flood-related phenomena at the facility are of great interest to both hydrologists and terrestrial and planetary geologists.

There are several technology-related reasons for this site choice as well. The CAVSARP facility, with its controlled flood conditions, allows us to continue our efforts to develop the Sensor Web as a tool for the study of spatio-temporal phenomena. For example, the Sensor Web can track the moving flood front, follow the infiltration of water into the ground, and provide information to map and characterize the lateral and vertical extent of the floodwaters. Moreover, the extreme temperature variations of the Arizona desert (both diurnal and seasonal) provide yet another test of the Sensor Web's robustness. The deployed Sensor Web had essentially identical hardware to those of previous installations [4] and no special provisions were made for the new environment.

The recharge basins are operated cyclically to allow for routine maintenance of the surface conditions. These operations lead to periodic infilling, with a water front progressing across the basin. Once the inflow of water is shut off, the floodwaters continue to infiltrate into the ground and the drying portion of the cycle begins with the drying front reversing the original flood pattern. The basins were constructed to have a smoothly varying elevation, which declines from south to north. As a result, the north ends of the basins fill first during flooding and dry last during draining. Existing instruments in each basin provide for continuous monitoring of inflow rate at the inlet pipe and water height at the deep end. These instruments are connected to a Supervisory Control And Data Acquisition System (SCADA), allowing for remote monitoring of basin operations. A visual staff gauge is regularly read to confirm the accuracy of the water level sensors.

A single basin (102), measuring approximately  $700 \times 2400$  ft<sup>2</sup>, was strategically outfitted with 13 Sensor Web 3.2 pods, the number and placement of pods being determined by science requirements, rather than technological limitations. As shown in Figure 5, the pods were mounted on stakes to elevate them above the flood waters which can rise as high as 7 ft. (While the pods themselves are water-tight, pod-to-pod radio communication would not be possible if they were submerged.) Each pod, in addition to collecting air temperature, humidity, and light levels also collects two soil moisture readings (one at the surface and one 0.5 m below) and a surface soil temperature reading. This is accomplished by wires that run from the pod into the ground. Measurements are made at 5 minute intervals with the results being fed to the Internet in real-time (via the portal pod 0). Figure 6 shows the deployed Sensor Web during a flooding event.

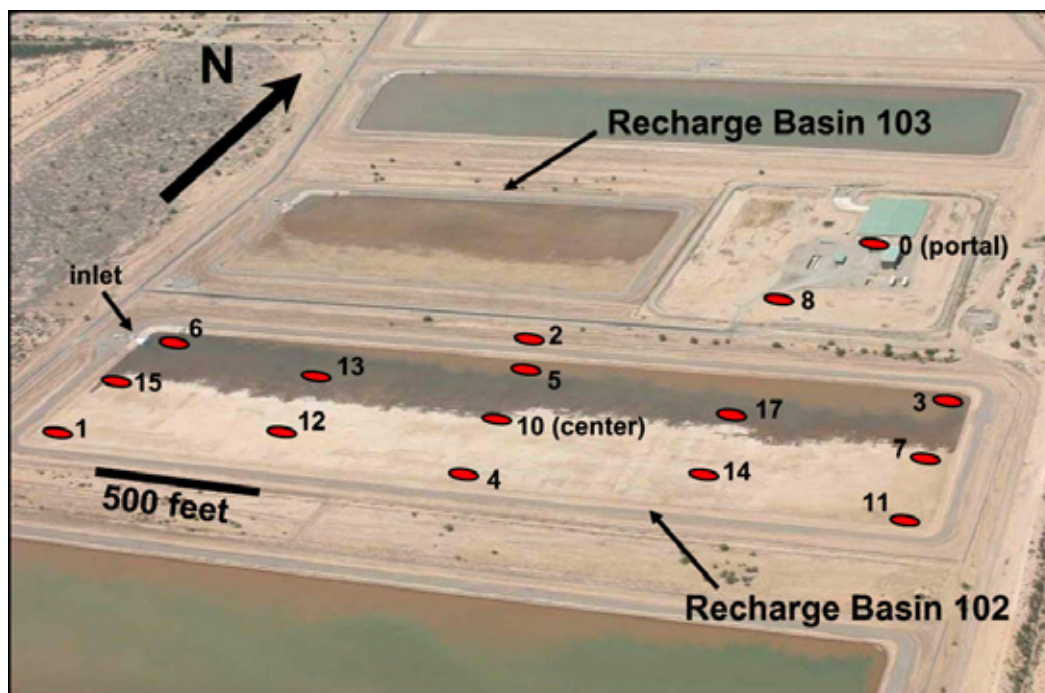


**Figure 4.** Aerial view of a portion of CAVSARP facility showing the location of the Sensor Web pods in recharge basin 102. The portal pod (pod 0) is connected to a computer which transfers the data to the Internet. In this photograph, recharge basin 103 is drying out, with the wetter soil in the northern portion of the basin. In contrast, basin 102 is being flooded with the moving water advancing southward. The basins immediately north of 103 and south of 102 are fully flooded.

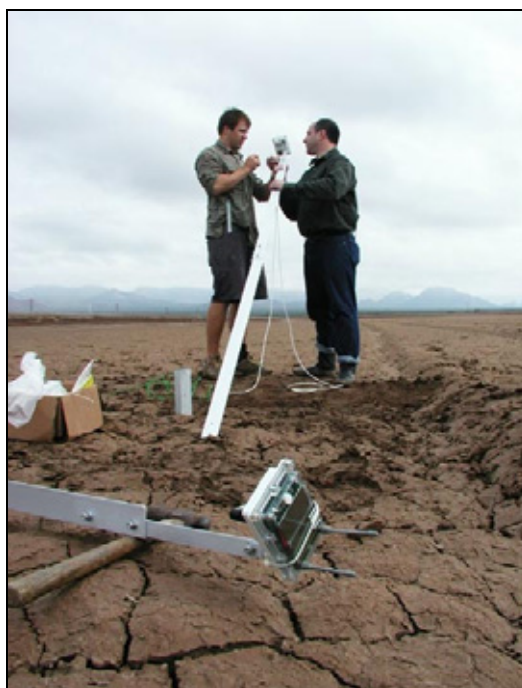


**Figure 5.** NASA/JPL team members deploy a Sensor Web 3.2 pod in recharge basin. Extended stands allow the pods to stay operational above water during a flooding event. Note polygon patterns in soil, indicative of previous flooding/drying cycles.



**Figure 6.** View looking north with recharge basin 102 fully inundated. Pod 11 is clearly visible above the rising water.

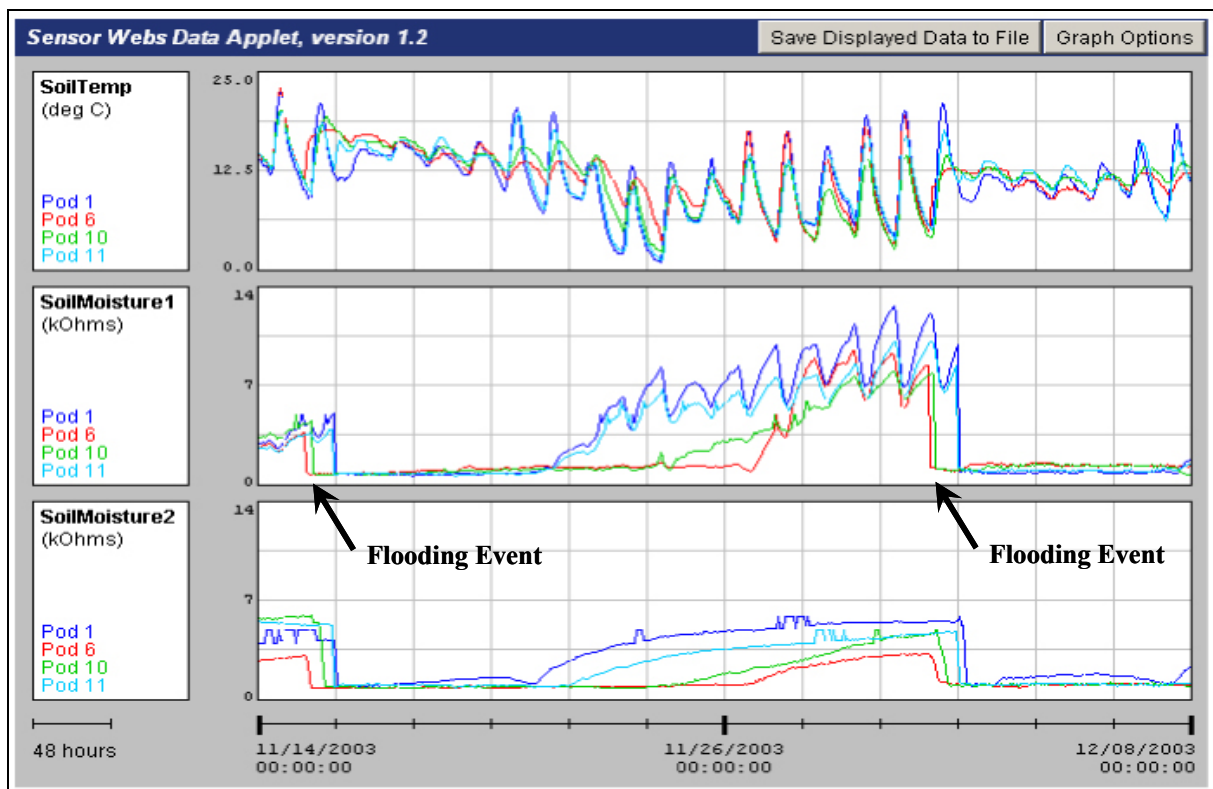


**Figure 7.** Screen-capture of Internet data from CAVSARP facility. Graphs (top to bottom): surface temperature ( $^{\circ}\text{C}$ ), surface moisture, and soil moisture at 0.5 m depth (relative units; lower values imply wetter soil). Diurnal cycles in soil water potential measurements are largely artifacts that can be corrected using the soil temperature at the same location and depth. Sensor Web pod 1 (southwest basin corner) is in blue, pod 6 (basin inlet, northwest corner) in red, pod 10 (basin center) in green, pod 11 (southeast basin corner, diagonal from pod 6) in light blue. Data correlate with water discharge into basin, inundation, infiltration, drying, and the beginning of another cycle.

### Preliminary use of Sensor Web in hydrologic studies

This Sensor Web has been collecting data since its deployment in November 2003. The real-time, streaming output from this system was made available via the Internet; a sample screen-capture is shown in Figure 7. Unlike remote techniques, which can only observe the basins for relatively short durations on finite schedules, the Sensor Web's data stream provides continuous information for tracking surface water motion and ground infiltration. The spatial and temporal patterns of wetting and drying can thus, be fully monitored and results incorporated into hydrological models and compared with space- and airborne-based investigations [5]. This analysis is ongoing. As a result, this Sensor Web can both augment and ground-truth the remote data traditionally used in hydrologic studies.

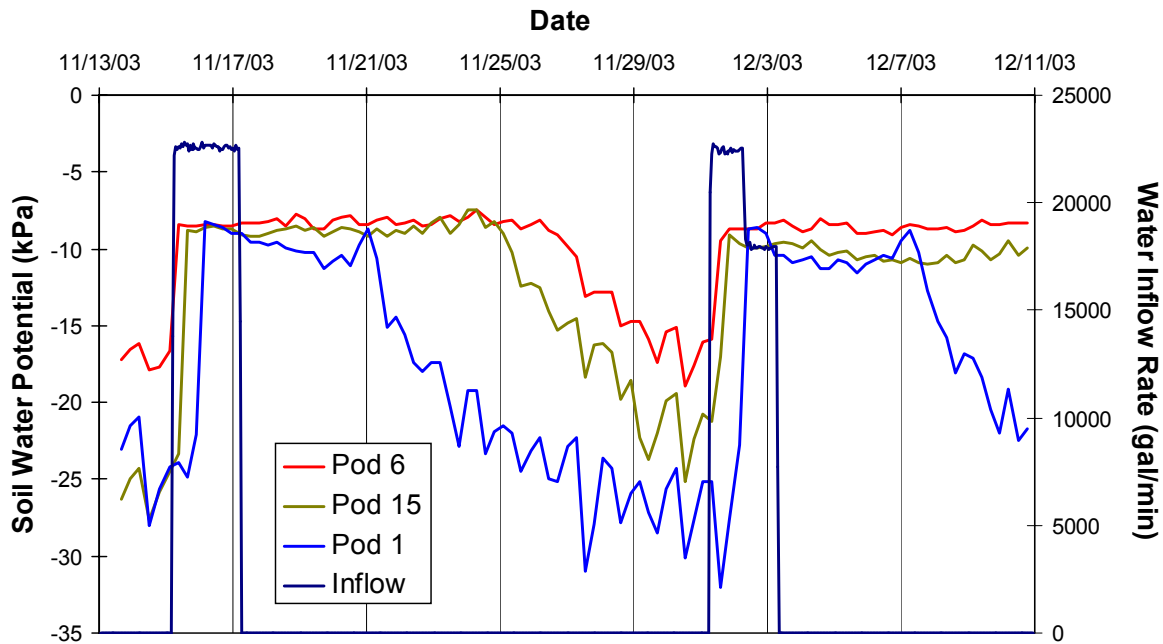
The repeatable nature of the flooding/drying dynamics is apparent in Figure 7. The soil moisture measurements are made with Watermark sensors [6], where electrodes embedded in a granular matrix yield a lower resistance when the surrounding soil is wetter. As a result, the raw data reveals the motion of the flooding water as sharp drops in resistance. (The diurnal cycles seen in the raw data are sensor artifacts and can be corrected with soil temperature measurements [7].) It only takes a few hours for the flood front to traverse the basin from the inlet in the northwest corner to the basin center but a much longer time (about 20 hours) to reach the basin's southwest and southeast corners. Note, too, that the water reaches the southern border relatively evenly (as indicated by pods 1 and 11), which is expected from both basin construction and the photographic evidence shown in Figure 4. Moreover, it is also clear from Figure 7 that the drying front traverses the reverse route, albeit at a much slower speed. Not surprisingly, the surface dries more thoroughly than the deeper portions of the ground.

The raw data can be downloaded using the Sensor Web's graphical user interface so that these initial observations can be further refined into more meaningful hydrologic terms. Soil moisture can be described in terms of the forces that retain the water in the soil. At equilibrium, the energy status of the water in the sensor's granular matrix is equal to the energy status of the water in the surrounding soil. The electrical resistance measured is then related to the soil water potential by the sensor-specific calibration:

$$\text{SoilWaterPotential}(kPa) = -\frac{4.093 + 3.213 \times R}{1 - 0.009733 \times R - 0.01205 \times T} \quad (1)$$

where  $R$  is the sensor resistance in  $k\Omega$  and  $T$  is the soil temperature in  $^{\circ}\text{C}$  [7].

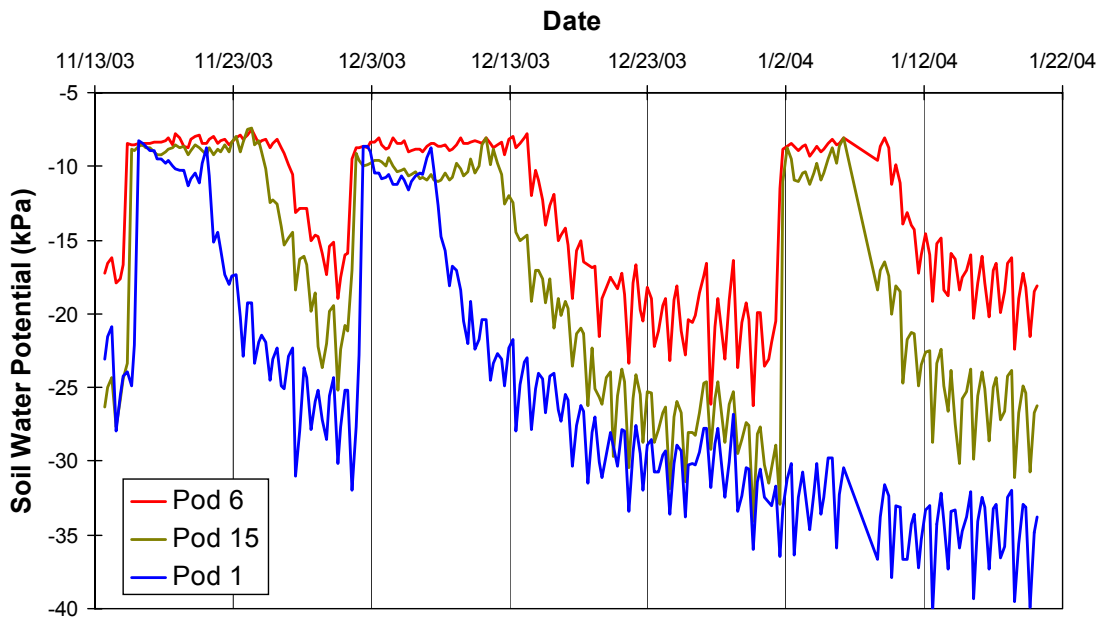
Figure 8 shows the same two flooding events of Figure 7 at a depth of 0.5 m, but with the raw data interpreted in this manner. The inlet flow is also plotted. The maximum inflow rate was approximately 22800 gal/min with the water rising, in this case, to 5.7 ft. The pods examined are on the basin's western border and, again, it is clear that a finite time is required for the moving water front to travel south from the inlet (pod 6) to the near corner (pod 1). In contrast, note how rapidly the soil moisture at depth increases at pod 6. The slight difference in the temporal aspects of soil wetting between the two flood events (most notably at pod 6) is attributable to the fact that the soil moisture sensors were planted just prior to the first flood event and therefore, the surrounding soil was disturbed and not as compacted as before sensor insertion. The second flooding event therefore, provides data for more accurate modeling. Again, the Sensor Web provides a continuous embedded monitoring presence which leads to a more refined picture of events.



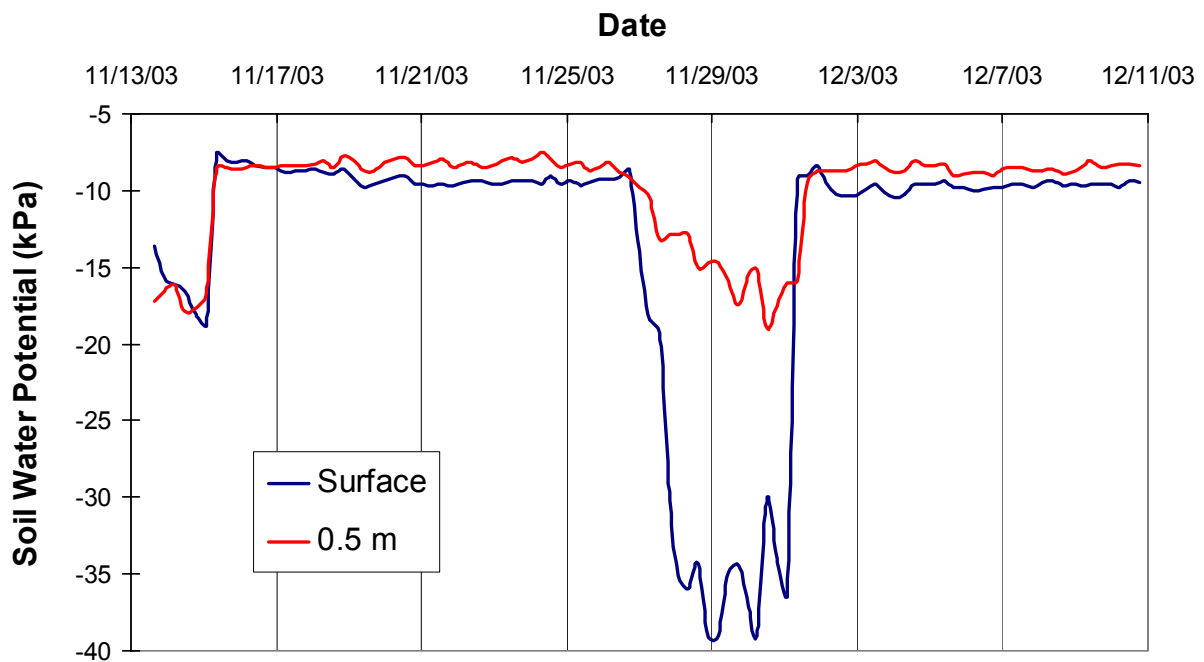
**Figure 8.** Soil water potential at 0.5 m deep along the west basin border during the first two flooding events after deployment. Traveling from north to south, the pods are positioned: 6 (inlet), 15, and then 1. Also shown is the inlet water rate.

Figure 9 increases the time-scale of observation. Included now is a third flooding event occurring late on January 1, 2004. Notice, however, that this time the inflow is not left on long enough to allow the water front to reach the southern side of the basin and the soil at pod 1 continues to dry out. Figure 10 reveals that, in general, soil water potential at the surface is more responsive than that at depth. This type of subterranean measurement, the inferred vertical tracking of water movement and soil drying as a function of time, is not possible using remote measurement techniques. Coupled with the large spatial extent of the Sensor Web, this temporal vertical tracking will provide a powerful tool for understanding transient hydrologic phenomena.

These preliminary results clearly demonstrate several new methodologies for hydrology created by the Sensor Web. Both transient and subterranean hydrologic phenomena can be captured to better model and understand percolation in different soil types, and can be captured in native environments on a long-term basis. Unlike the information obtained by remote measurements, the data from the Sensor Web are continuous and not restricted by orbital paths, flight schedules, or local weather conditions. Moreover, the *in-situ* Sensor Web data can also be compared to remote measurements to provide ground-truth. The Sensor Web deployed in the recharge basin is therefore more than just a functioning technological test. It is a functioning scientific instrument for hydrologic use.



**Figure 9.** Soil water potential at 0.5 m deep along the west basin border. Note that the third flooding event did not last long enough to affect pod 1.



**Figure 10.** Comparison of pod 6 soil water potential at two depths.

## Summary

The primary focus of Sensor Web development thus far has been to demonstrate that the technology is stable, robust, and attractive to potential end-users. For a user community to adopt it, however, the Sensor Web needs to be more than just well-engineered; it must also be easily deployed and

maintained and provide valuable output. The overall simplicity of the Sensor Web system as an operational instrument is demonstrated by the fact that most Sensor Webs are deployed and operated in a variety of environments (including Antarctica [8]) without requiring assistance from the NASA/JPL team.

As shown by our case study, the Sensor Web can provide important spatio-temporal data needed to track transient phenomena. In our hydrology example, these phenomena include flooding and infiltration. The simultaneous measurements of temperature and soil moisture at different locations and depths make it possible to monitor the changes in soil moisture in different strata. The results also provide an excellent opportunity to develop a mechanism for the study of flood dynamics in a controlled and well-instrumented environment. The Sensor Web, therefore, has a great potential to change our way of monitoring and understanding hydrologic processes on Earth and beyond. Similar examples can be found in other environmental studies.

Having demonstrated many of the Sensor Web's core capabilities with a myriad of deployments, we are now moving Sensor Web development into a new phase, focusing as much on applications as technology. The continuous, virtual monitoring and reacting capabilities have wide ranging uses for resource management, pollutant tracking, and perimeter monitoring. This step requires us to take full advantage of the large-scale awareness already built into the Sensor Web protocols. In this way, the output of the hydrologic Sensor Web, for example, would not consist of a collection of scalar measurements (soil moisture) but rather a single vector (water motion) with pod-to-pod data fusion occurring within the Sensor Web itself. This will truly give the Sensor Web the capacity to make sophisticated, autonomous decisions. Indeed, we anticipate that future hydrologic Sensor Webs could provide early-stage triggers for satellite monitoring systems to focus on developing flood conditions and alerts for downstream communities. As awareness of this unique distributed instrument and its capabilities spreads into other user communities, the Sensor Web is expected to become an important wireless sensor network architecture.

### Acknowledgements

We are grateful to the City of Tucson and Tucson Water for their critical cooperation in this activity. The Sensor Webs Project team is also indebted to the following JPLers for their many and varied contributions: Alan Kleinsasser, Lonnie Lane, Loren Lemmerman, Philip Moynihan, Peter Robles, and Amy Walton. The Sensor Webs described here were constructed at the Jet Propulsion Laboratory, California Institute of Technology, under a contract with NASA.

### Reference

1. Delin, K.A. The Sensor Web: A macro-instrument for coordinated sensing, *Sensors*, **2002**, *2*, 275.
2. <http://sensorwebs.jpl.nasa.gov/>
3. Delin, K.A.; Jackson, S.P.; Johnson, D.W.; Burleigh, S.C.; Woodrow, R.R.; McAuley, M.; Britton, J.T.; Dohm, J.M.; Ferré Felipe Ip, T.P.A.; Rucker, D.F.; Baker, V.R. Sensor Web for spatio-temporal monitoring of a hydrological environment. *Proceeding of the 35th Lunar and Planetary Science Conference*, League City, TX, March **2004**.

4. Delin, K.A.; Jackson, S.P.; Burleigh, S.C.; Johnson, D.W.; Woodrow, R.R.; Britton, J.T.; The JPL Sensor Webs project: Fielded technology. *Proceeding of Space Mission Challenges for Information Technology*, Pasadena, CA, July **2003**.
5. Rucker, D.F.; Dohm, J.M.; Ferré F. Ip, T.P.A.; Baker, V.R.; Davies, A.G.; Castano, R.; Chien, S.; Cichy, B.; Doggett, T.C.; Greeley, R.; Sherwood, R. Central avra valley storage and recovery project (CAVSARP) site, Tucson, Arizona: Floodwater and soil moisture investigations with extraterrestrial applications. *Proceeding of the 35th Lunar and Planetary Science Conference*, League City, TX, March **2004**.
6. Available from Irrrometer Co., <http://www.irrometer.com/>
7. Shock, C.C. Soil water potential measurement by granular matrix sensors. in *The Encyclopedia of Water Science*. Stewart, B.A.; Howell, T.A. (Eds.), Marcel Dekker, 899, **2003**.
8. Delin, K.A.; Harvey, R.P.; Chabot, N.A.; Jackson, S.P.; Adams, M.; Johnson, D.W.; Britton, J.T. Sensor Web in Antarctica: Developing an intelligent, autonomous platform for locating biological flourishes in cryogenic environments. *Proceeding of the 34th Lunar and Planetary Science Conference*, Houston, TX, March **2003**.

© 2005 by MDPI (<http://www.mdpi.net>). Reproduction is permitted for non-commercial purposes.